PB97-163950

DETERMINATION OF PILE DRIVEABILITY AND CAPACITY FROM PENETRATION TESTS. VOLUME 3 LITERATURE REVIEW, DATA BASE, AND APPENDIXES

GOBLE, RAUSCHE, LIKINS AND ASSOCIATES, INC., CLEVELAND, OH

MAY 97

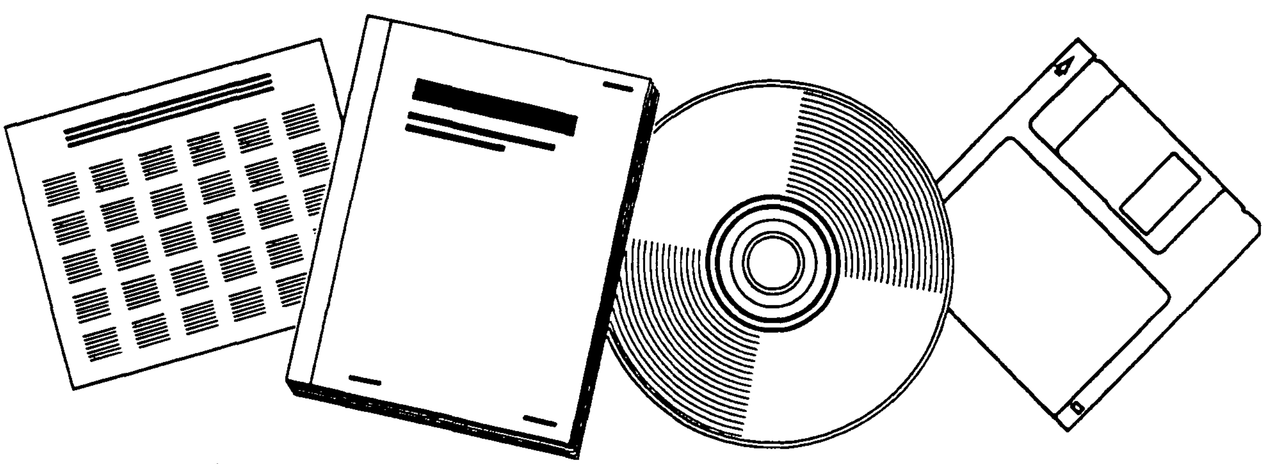

U.S. DEPARTMENT OF COMMERCE
National Technical Information Service

Determination of Pile Driveability and Capacity From Penetration Tests

Volume III: Literature Review, Data Base, and Appendixes

PUBLICATION NO. FHWA-RD-96-181

MAY 1997

U.S. Department of Transportation
Federal Highway Administration

Research and Development
Turner-Fairbank Highway Research Center
6300 Georgetown Pike
McLean, VA 22101-2296

FOREWORD

This report, *Determination of Pile Driveability and Capacity from Penetration Tests*, is comprised of three volumes. Volume III (FHWA-RD-96-181), contained here, documents the results of a literature study and summarizes available information on dynamic soil models and their parameters. Volume I (FHWA-RD-96-179) summarizes the design and experimental use of a method that extracts dynamic soil resistance parameters as the Standard Penetration Test is being performed. Extensive correlations with full scale load tests were made based on these results. Volume II (FHWA-RD-96-180) of the series describes the data bank that has been assembled as part of the study and contains dynamic and static load test data.

Charles J. Nemmers, P.E.
Office of Engineering
Research and Development

NOTICE

Technical Report Documentation Page

1. Report No.	2.	3. Recipient's Catalog No.
FHWA-RD-96-181	PB97-163950	

4. Title and Subtitle	5. Report Date
DETERMINATION OF PILE DRIVEABILITY AND CAPACITY FROM PENETRATION TESTS Volume III: Literature Review, Data Base and Appendixes	May 1997
	6. Performing Organization Code
7. Author(s) Rausche, F., Thendean, G., Abou-matar, H., Likins, G.E., Goble, G.G.	8. Performing Organization Report No. 3E3A-0193
9. Performing Organization Name and Address Goble Rausche Likins and Associates, Inc. 4535 Renaissance Parkway Cleveland, Ohio 44128	10. Work Unit No. (TRAIS) 11. Contract or Grant No. DTFH61-93-C-00047
12. Sponsoring Agency Name and Address Office of Engineering R&D Federal Highway Administration 6300 Georgetown Pike McLean, Virginia 22101-2296	13. Type of Report and Period Covered Final Report October 1991 - September 1994 14. Sponsoring Agency Code

15. Supplementary Notes

FHWA Contracting Officer's Technical Representative: Carl Ealy, HNR-30
FHWA Technical Consultant: Jerry DiMaggio, HNG-31

16. Abstract

Research has been conducted on the potential improvement of dynamic wave equation analysis methodology using in-situ soil testing techniques. As a basis for this investigation, the literature was reviewed and a summary was compiled of efforts made to date on the development of models and associated parameters for pile driving analysis. Furthermore a data base was developed containing more than 150 cases of test piles with static load tests, dynamic restrike tests, soil information, driving system data and installation records. One hundred data base cases were subjected to correlation studies using both wave equation and CAPWAP. This work yielded dynamic soil model parameters which did not indicate a specific relationship with soil grain size.

The in-situ soil testing device utilized was a Modified SPT which yielded data from both static and dynamic measurements. Either static uplift or torque tests yielded static ultimate shaft resistance, and uplift tests also indicated a shaft resistance quake. Static compressive tests on a special tip indicated ultimate end bearing and associated toe quake. Indirectly, by signal matching, soil damping parameters were calculated. These quantities were then used for the prediction of full-scale pile behavior. Data from the Modified SPT were gathered and analyzed on six sites with previous full-scale static pile tests and on three sites where static load tests were to be performed at a later date.

Recommendations derived from these tests pertain to the current soil model and to proposals for future changes. In general, the current approach was found to yield, on the average, very reasonable results for end of installation situations. For restrike tests, standard parameters may be misleading. Any necessary modifications to the current approach, for example, the use of particularly large toe quakes or low toe damping factors should be based on Modified SPT measurements. Differences between prediction and full-scale pile field behavior were attributed to soil strength changes over relatively small distances which cannot be detected with standard SPT spacings of 5 ft (1.5 m).

This volume is the first in a series. Other volumes in the series are:
FHWA-RD-96-179 Volume I: Final Report
FHWA-RD-96-180 Volume II: Appendixes

17. Key Words	18. Distribution Statement
Pile driving, foundation, pile foundation, wave equation, CAPWAP, standard penetration test, in-situ test, pile capacity, pile driveability, pile data base, energy, static load test, dynamic load test, soil damping.	No restrictions. This document is available to the public through the National Technical Information Service, Springfield, Virginia 22161.

19. Security Classif. (of this report)	20. Security Classif. (of this page)	21. No. of Pages	22. Price
Unclassified	Unclassified	166	

Form DOT F 1700.7 (8-72)
(PF V2.1, 12/13/93)

SI* (MODERN METRIC) CONVERSION FACTORS

APPROXIMATE CONVERSIONS TO SI UNITS

Symbol	When You Know	Multiply By	To Find	Symbol
		LENGTH		
in	inches	25.4	millimeters	mm
ft	feet	0.305	meters	m
yd	yards	0.914	meters	m
mi	miles	1.61	kilometers	km
		AREA		
in^2	square inches	645.2	square millimeters	mm^2
ft^2	square feet	0.093	square meters	m^2
yd^2	square yards	0.836	square meters	m^2
ac	acres	0.405	hectares	ha
mi^2	square miles	2.59	square kilometers	km^2
		VOLUME		
fl oz	fluid ounces	29.57	milliliters	mL
gal	gallons	3.785	liters	L
ft^3	cubic feet	0.028	cubic meters	m^3
yd^3	cubic yards	0.765	cubic meters	m^3
NOTE: Volumes greater than 1000 l shall be shown in m^3.				
		MASS		
oz	ounces	28.35	grams	g
lb	pounds	0.454	kilograms	kg
T	short tons (2000 lb)	0.907	megagrams (or "metric ton")	Mg (or "t")
		TEMPERATURE (exact)		
°F	Fahrenheit temperature	5(F-32)/9 or (F-32)/1.8	Celcius temperature	°C
		ILLUMINATION		
fc	foot-candles	10.76	lux	lx
fl	foot-Lamberts	3.426	candela/m^2	cd/m^2
		FORCE and PRESSURE or STRESS		
lbf	poundforce	4.45	newtons	N
lbf/in^2	poundforce per square inch	6.89	kilopascals	kPa

APPROXIMATE CONVERSIONS FROM SI UNITS

Symbol	When You Know	Multiply By	To Find	Symbol
		LENGTH		
mm	millimeters	0.039	inches	in
m	meters	3.28	feet	ft
m	meters	1.09	yards	yd
km	kilometers	0.621	miles	mi
		AREA		
mm^2	square millimeters	0.0016	square inches	in^2
m^2	square meters	10.764	square feet	ft^2
m^2	square meters	1.195	square yards	yd^2
ha	hectares	2.47	acres	ac
km^2	square kilometers	0.386	square miles	mi^2
		VOLUME		
mL	milliliters	0.034	fluid ounces	fl oz
L	liters	0.264	gallons	gal
m^3	cubic meters	35.71	cubic feet	ft^3
m^3	cubic meters	1.307	cubic yards	yd^3
		MASS		
g	grams	0.035	ounces	oz
kg	kilograms	2.202	pounds	lb
Mg (or "t")	megagrams (or "metric ton")	1.103	short tons (2000 lb)	T
		TEMPERATURE (exact)		
°C	Celcius temperature	1.8C + 32	Fahrenheit temperature	°F
		ILLUMINATION		
lx	lux	0.0929	foot-candles	fc
cd/m^2	candela/m^2	0.2919	foot-Lamberts	fl
		FORCE and PRESSURE or STRESS		
N	newtons	0.225	poundforce	lbf
kPa	kilopascals	0.145	poundforce per square inch	lbf/in^2

* SI is the symbol for the International System of Units. Appropriate rounding should be made to comply with Section 4 of ASTM E380.

(Revised September 1993)

TABLE OF CONTENTS

TABLE OF CONTENTS (Continued)

TABLE OF CONTENTS (Continued)

TABLE OF CONTENTS (Continued)

LIST OF FIGURES

Volume I: Final Report

LIST OF FIGURES (continued)

Volume I: Final Report

LIST OF FIGURES (continued)

Volume I: Final Report

LIST OF FIGURES (continued)

Volume I: Final Report

Figure | Page

LIST OF FIGURES (continued)

Volume II: Appendixes

LIST OF FIGURES (continued)

Volume II: Appendixes

LIST OF FIGURES (continued)

Volume II: Appendixes

LIST OF FIGURES (continued)

Volume II: Appendixes

LIST OF FIGURES (continued)

Volume II: Appendixes

Figure		Page

LIST OF FIGURES (continued)

Volume II: Appendixes

LIST OF FIGURES (continued)

Volume II: Appendixes

LIST OF FIGURES (continued)

Volume II: Appendixes

LIST OF FIGURES (continued)

Volume II: Appendixes

LIST OF FIGURES (continued)

Volume II: Appendixes

Figure		Page

LIST OF FIGURES (continued)

Volume II: Appendixes

LIST OF FIGURES (continued)

Volume II: Appendixes

LIST OF FIGURES (continued)

Volume II: Appendixes

LIST OF FIGURES (continued)

Volume II: Appendixes

LIST OF FIGURES (continued)

Volume II: Appendixes

LIST OF FIGURES (continued)

Volume II: Appendixes

LIST OF FIGURES (continued)

Volume II: Appendixes

LIST OF FIGURES (continued)

Volume III: Literature Review, Data Base and Appendixes

LIST OF FIGURES (continued)

Volume III: Literature Review, Data Base and Appendixes

LIST OF TABLES

Volume I: Final Report

LIST OF TABLES (continued)

Volume I: Final Report

LIST OF TABLES (continued)

Volume II: Appendixes

LIST OF TABLES (continued)

Volume III: Literature Review, Data Base and Appendixes

LIST OF SYMBOLS

Volume I: Final Report

A	-	cross section area or setup parameter
A3	-	average of the three highest shaft resistance per unit length
A_s	-	pile soil contact area
A_{toe}	-	toe area
B	-	pile width
Cl	-	circumference of the pile
c	-	velocity of wave propagation
E	-	modulus of elasticity
F1	-	loading toe quake multiplier (hyperbolic model)
F2	-	unloading toe quake multiplier (hyperbolic model)
$F_m(t)$	-	force measured near the top of drill string
$F^{\downarrow}(t)$	-	downward traveling force wave
$F^{\uparrow}(t)$	-	upward traveling force wave
$\bar{f}_s$	-	average unit sleeve friction
J or J_c	-	Smith damping constant
J_s	-	shaft damping
J_t	-	Toe damping
L	-	pile length below gauges
MS	-	shaft support soil mass
NFac	-	ratio of number of pile segments to soil segments
K	-	ratio of unit pile friction to unit sleeve friction
k	-	cushion stiffness
m	-	mass constant
N	-	SPT N-value
N_{60}	-	SPT N-value corrected to 60 percent transfer efficiency
n	-	damping exponent
q	-	quake
Q_p	-	pile toe resistance
Q_s	-	pile shaft resistance or shaft quake
Q_t	-	toe quake
q_{c1}, q_{c2}, q_{c3}	-	average cone tip resistance
R	-	total measured toe resistance
R(t)	-	toe resistance force
R_a	-	inertia or acceleration dependent resistance
R_{cT}	-	total calculated toe resistance
R_d	-	dynamic or velocity dependent resistance

Volume I: Final Report

R_s	-	static or displacement dependent resistance
R_u	-	ultimate static capacity
SK	-	shaft radiation damping parameter
$u(t)$	-	displacement at the toe
$\dot{u}(t)$	-	velocity of soil
$\ddot{u}(t)$	-	acceleration
$\dot{u}_m$	-	measured velocity
v_{impact}	-	SPT hammer impact velocity
Z1	-	impedance of the very top pile segment
ϕ_a	-	toe radiation damping constant
τ_o	-	soil shear strength at time t_0
$\tau(t)$	-	soil shear strength at time t
Δ_i	-	final displacement

Volume III: Literature Review, Data Base and Appendixes

A	-	setup factor
C_1	-	frequency dependent parameter for toe soil stiffness (Mitwally and Novak, 1988)
C_2	-	frequency dependence parameter for toe soil damping (Mitwally and Novak, 1988)
c_H	-	damping factor at toe (Holeyman, 1988)
c_s	-	frequency dependent shaft damping (Mitwally and Novak, 1988)
c_t	-	frequency dependent toe damping (Mitwally and Novak, 1988)
c_u	-	undrained shear strength
E	-	elastic modulus
E'	-	modulus of viscosity (Holeyman, 1988)
E_i	-	initial tangent modulus (Holeyman, 1988)
f_s	-	cone shaft friction or unit shaft resistance
G	-	soil's shear modulus
G_b	-	toe soil shear modulus (Mitwally and Novak, 1988)
I_p	-	influence coefficient (Hussein, 1992)
J	-	Smith damping factor
J_c	-	Coyle-Gibson exponent damping factor
J_G	-	toe damping prior to failure (Lee et al., 1988)
J_G'	-	toe damping during failure (Lee et al., 1988)

LIST OF SYMBOLS (continued)

Volume III: Literature Review, Data Base and Appendixes

J_L'	-	shaft damping prior to failure (Lee et al., 1988)
J_M	-	purely viscous damping factor (Middendorp and Brederode, 1984)
$J_{R,toe}$	-	toe damping value (Randolph and Simons, 1986)
J_s	-	shaft damping
J_t	-	toe damping
k	-	soil stiffness
k_H	-	soil stiffness at toe (Holeyman, 1988)
k_s	-	shaft soil stiffness
k_t	-	soil stiffness (Randolph and Simons, 1986)
m_S	-	soil mass
n	-	Coyle-Gibson damping exponent
p_c	-	cone tip pressure
p_y	-	yield pressure (Liang and Sheng, 1992)
q	-	quake
q_r	-	ultimate strength at the base (Holeyman, 1988)
q_s	-	shaft quake
q_t	-	toe quake
q_{ut}	-	unit toe resistance
r_o	-	pile radius
r_H	-	cone bottom radius (Holeyman, 1988)
r_m	-	radius of zone of soil deformation (Nguyen et al., 1988)
R_d	-	total dynamic soil resistance
R_f	-	failure load (Lee et al., 1988)
R_t	-	total shaft resistance (Middendorp and Brederode, 1984)
R_s	-	total static soil resistance
R_u	-	ultimate resistance
R_{t1}	-	failure load at time t_1
R_{t2}	-	failure load at time t_2
S_1	-	frequency dependent parameter for shaft soil stiffness (Mitwally and Novak, 1988)
S_2	-	frequency dependent parameter for shaft soil damping (Mitwally and Novak, 1988)
t_i	-	time to failure
u	-	displacement of pile segment
$\dot{u}$	-	velocity of pile segment
$\ddot{u}$	-	acceleration of pile segment

LIST OF SYMBOLS (continued)

Volume III: Literature Review, Data Base and Appendixes

u_p	-	pore water pressure
v_1	-	pile velocity (Briaud and Garland, 1984)
v_2	-	pile static reference velocity (Briaud and Garland, 1984)
v_s	-	shear wave velocity
σ	-	stress
ϵ	-	strain
ϵ_l	-	average volumetric locking strain (Liang and Hussein, 1992)
ρ	-	soil mass density
τ_{max}	-	maximum shear strain (Nguyen et al., 1988)
τ_o	-	soil shear strength (Liang and Hussein, 1992)
τ_u	-	ultimate shear stress
ν	-	Poisson's ratio
ϕ	-	friction angle of soil
ω	-	frequency

CHAPTER 1

INTRODUCTION

This is the third volume of the report on a research contract entitled "Determination of Pile Driveability and Capacity from Penetration Tests." It contains results of a literature study, description of a data base generated as a part of the research, and, in several appendixes background information on the dynamics of pile driving and testing methods.

The most important part of this volume is the literature review contained in chapter 2. It was an essential part of the Interim Report, submitted to the Federal Highway Administration in 1992. The literature review primarily dealt with aspects of soil modeling for dynamic analyses of piles and methods for determining dynamic resistance parameters for the representation of the pile-soil interface. Even though some other publications may have treated this general area of research since 1992 no major changes or updates have been made to this chapter. However, it is believed that the report is still representative of the State-of-the-Art of 1995.

The third chapter describes the data base entries, statistically summarizes the data base contents by major groups and by title, pile type and other major parameters. A discussion of the value of the data base is also contained in chapter 2 of volume 1.

The appendixes of this volume combine a variety of background information for pile dynamic testing and analysis methods. Appendix A explains the travelling wave concept on which the wave equation approach is based. Appendix B discusses soil damping models of pile analysis methods. Appendix C summarizes the mathematical models of the wave equation approach. Appendix D describes the Case Method and the CAse Pile Wave Analysis Program (CAPWAP) which are based on dynamic pile measurements. Ground surface measurements had been hoped to help in the dynamic analysis of piles in the early phases of this project. They are described in appendix E, even though their value for pile driveability and capacity determination appears to be very limited at this time. Appendix F gives a brief description of the results of a study dealing with the sensitivity of wave equation solutions to variations in dynamic soil parameters. Appendixes G and H, finally, based on a study of the data base presented in chapter 3 of this volume, summarizes cases with large toe quakes and damping factors, respectively.

2. LITERATURE REVIEW ON DYNAMIC PILE ANALYSIS MODELS

2.1 INTRODUCTION

This report examines and summarizes findings of published research works in the area of soil modeling for pile driveability and bearing capacity predictions. This study does not concern itself with the derivation and solution of the partial differential equation (wave equation) which describes the propagation of stress waves along the pile. It may suffice to say that we are capable of solving that equation either by means of a lumped mass model, or a finite element analysis or by the characteristics method. The latter may also be thought of as assembling the solution for a complete pile from that for individual uniform and continuous pile segments. Furthermore, we may assume that the current hammer and driving system model is adequate or is replaced by the measurement of forces and velocities during pile driving. For this reason, we now can concentrate on the study of the soil representation.

The following literature review has three goals. The first goal is to investigate publications in the area of large strain, dynamic soil modeling for the description of soil behavior during pile driving. The second goal is to accumulate data published in the literature on the damping and quake factors to be used for Smith-type wave equation analyses. Finally, for the development of potential future test methods, a review will be made of available in-situ, dynamic test methods that could be useful for estimating dynamic soil parameters.

2.2 REVIEW OF LITERATURE ON DYNAMIC SOIL MODELS

It is probably reasonable to start with the Smith model itself since earlier work has either been very basic (*e.g.*, the derivation of the differential "wave equation" by d'Alembert in 1747 or the closed form solutions which were summarized by St. Venant in 1867 - see Timoshenko and Goodier (1951) and appendix A). This work, although extremely important for an understanding of wave propagation in a pile, does not deal with the more complex problem of soil resistance behavior during static and dynamic loading. Of course, this earlier work does not relate to discrete solutions of the wave equation. Furthermore, studies performed to improve simple dynamic driving formulas are also ignored as insignificant for wave equation technology.

In 1960, Smith published a summary of findings from 12 years of wave equation applications. He clearly stated his elasto-plastic and linearly viscous soil resistance model and he made resistance parameter recommendations. According to this model, the total dynamic soil resistance acting on a pile segment can be calculated from:

$$R_d = R_s\,(1 + J\,\dot{u}) \tag{2.1}$$

where R_s is the static soil resistance that is calculated based on the displacement, u, and $\dot{u}$ is the velocity of the pile segment on which R_d acts and J is the "Smith" damping factor (figure 2.1). Thus:

$$R_s = ku \quad \text{for } u < q \tag{2.2a}$$

and:

$$R_s = R_u \quad \text{for } u > q \tag{2.2b}$$

The value q is called quake, and R_u is the ultimate resistance at an individual pile segment (shaft or toe). During unloading (when the pile rebounds and displacements decrease), the static resistance, R_s, will decrease along a line given by the soil stiffness, k. In equation (2.1), a "Smith" damping factor, J, multiplied by the pile segment velocity, $\dot{u}$, increases (or decreases) the shear resistance. The total dynamic resistance, R_d, may be considered a dynamic soil property which depends on both pile displacements and velocities (as defined by Smith). However, it is important to realize that the velocity dependent component is linear once R_s has reached ultimate and rebound has not yet started. Figure 2.2 shows: (a) the static and damping resistances as a function of pile displacement, (b) also plotted *vs* time, and (c) *versus* velocity. Obviously, the damping force behaves linearly with velocity only during a short time after the quake has been reached. Once the quake is reached, the velocity is usually decreasing and relatively small.

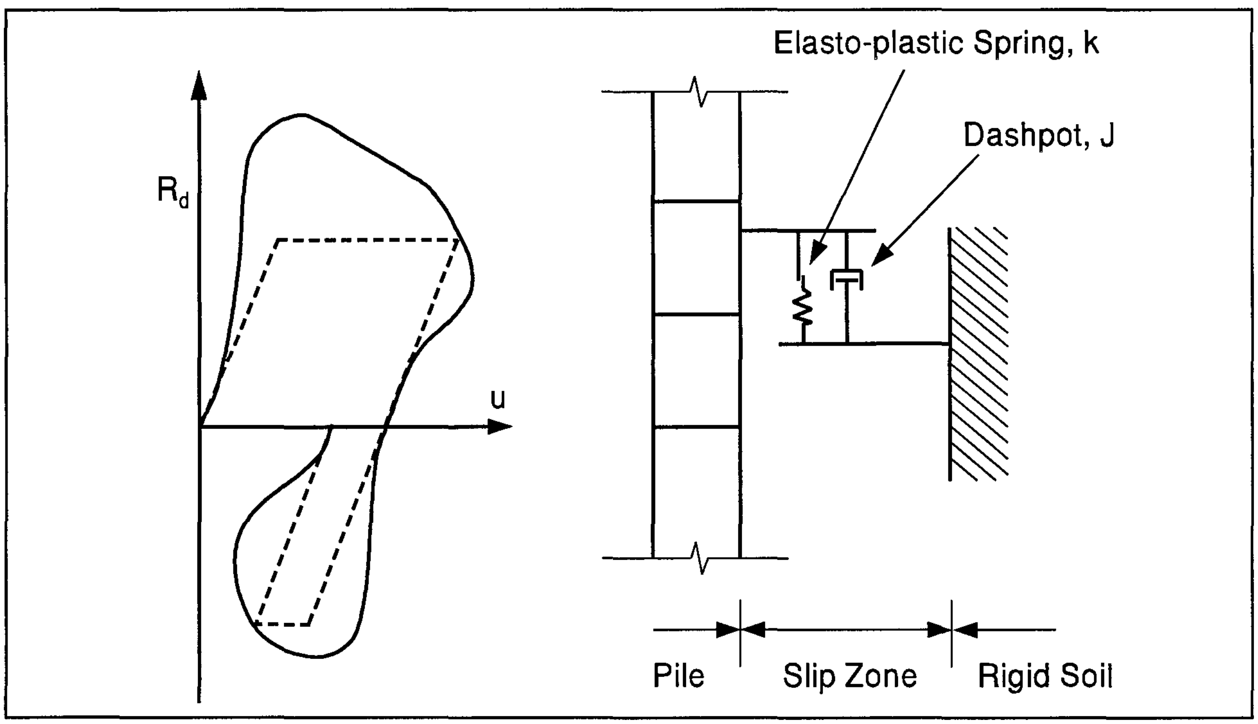

Figure 2.1: Smith Soil Resistance Model

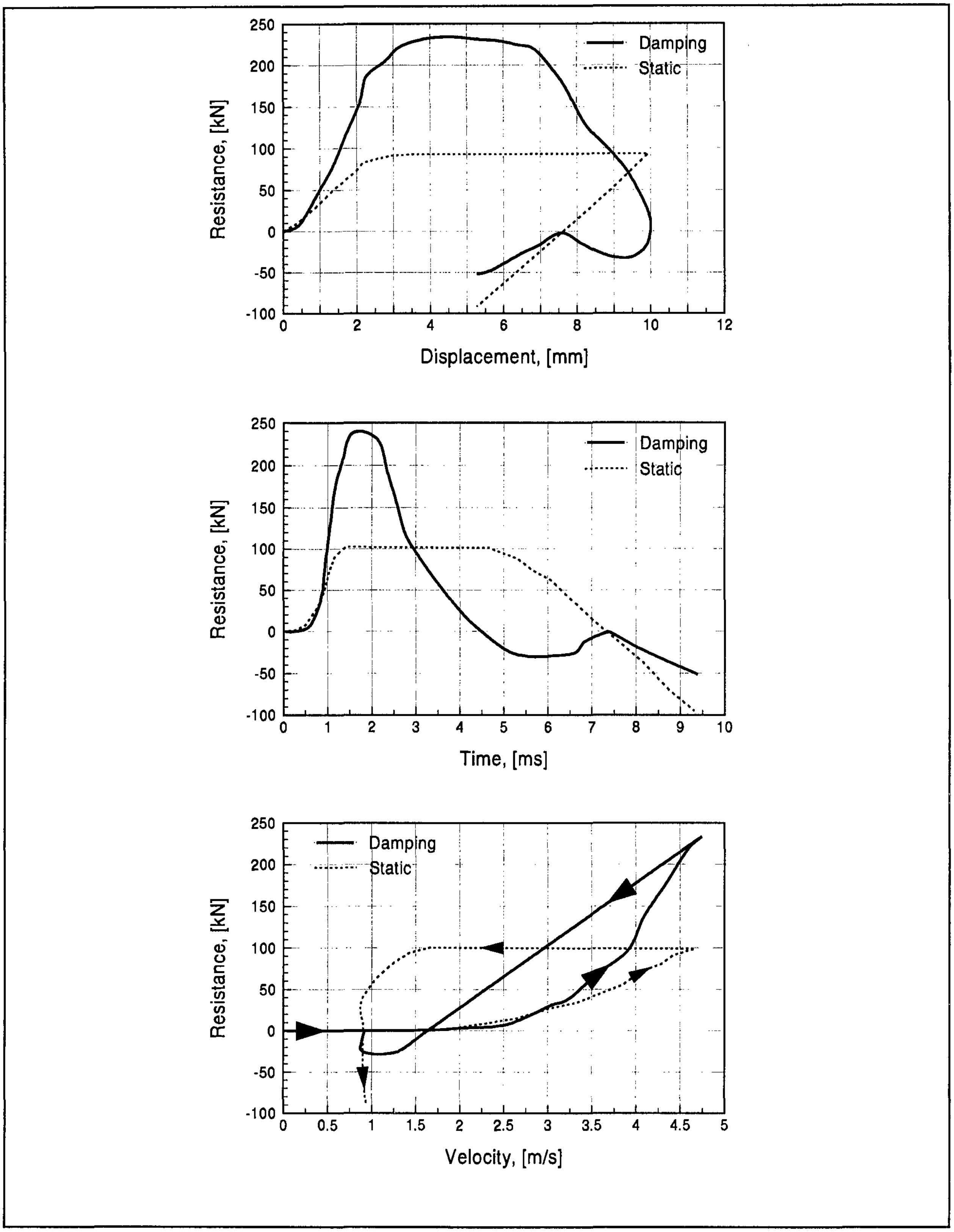

Figure 2.2: Smith Resistance Components Plotted versus Displacement (Top), Time (Middle), and Velocity (Bottom)

A series of correlation papers followed the original work of Smith. For example, Forehand and Reese (1964) compared wave equation with load test results from 24 cases. They had difficulties in determining soil model parameters by matching wave equation and load test capacities because of the variety of possible solutions, *i.e.*, the results were not uniquely defined.

In the late 1960's, the Federal Highway Administration and the Texas Transportation Institute supported research at Texas A&M University which resulted in a series of findings and publications all supporting the finding that Smith's approach had merit and only needed minor refinements. One series of experiments, conducted by Coyle and Gibson (1970), was particularly instructive. The researchers tested triaxial, unconsolidated, undrained samples to failure under a variety of loading velocities. They then plotted the ratio R_d/R_s as a function of loading velocity (figure 2.3) and found that a best fit of the data would be achieved, if the Smith resistance were expressed in a modified form as follows:

$$R_d = R_s(1 + J_c\dot{u}^n) \tag{2.3}$$

with n was approximately equal to 0.2.

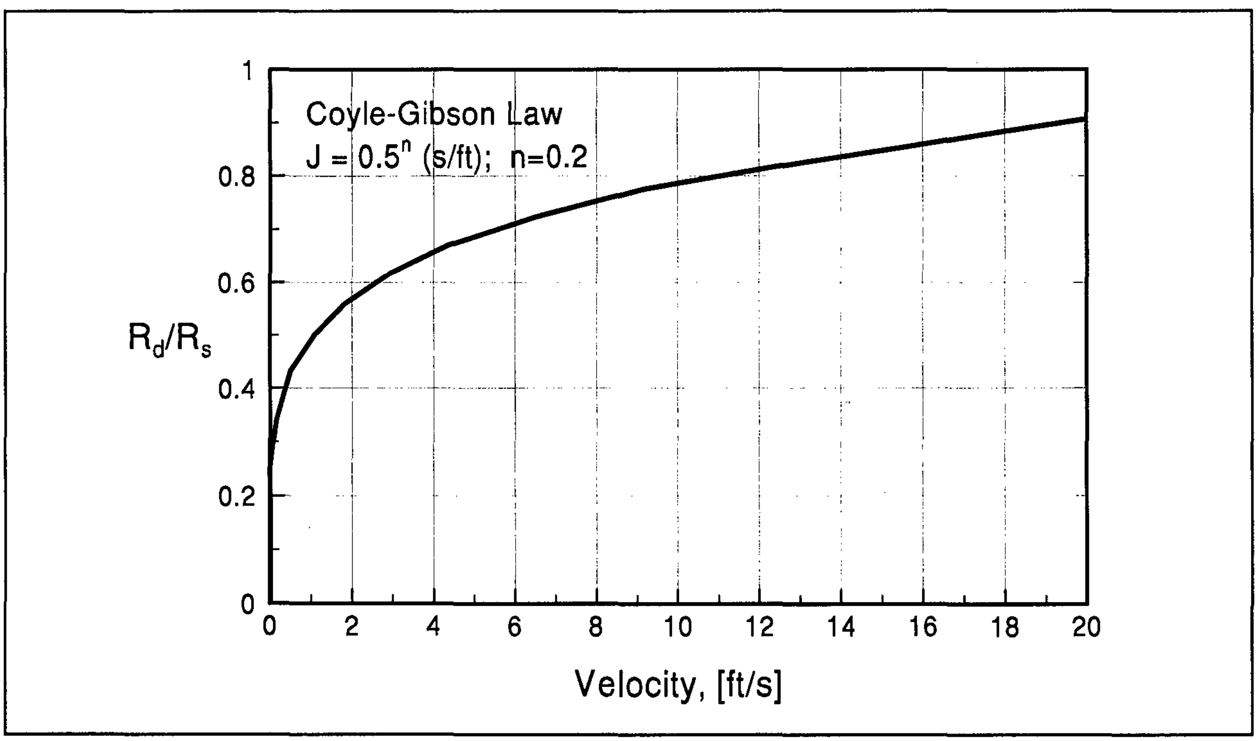

Figure 2.3: The Coyle-Gibson Resistance versus Velocity Plot

Coyle and Gibson also found that the J_c-values could be related to the Liquidity Index of clay, and the effective friction angle of sand. Unfortunately, later research did not support this contention. For example, Coyle et al. (1972) concluded after a series of tests on miniature piles in various soils that Smith's original equation held fairly well for the tip resistance and that J_t = 0.15 s/ft (0.49 s/m) would be acceptable. On the other hand, the modified resistance equation yielded fairly constant shaft damping parameters with n = 0.35 and J_s = 1.25 s/ft$^{0.35}$ (1.89 s/m$^{0.35}$). Note that the Smith notations of J_s and q_s for shaft damping and shaft quake, and J_t and q_t for toe damping and toe quake, respectively, have been adopted in this report.

The results obtained by Coyle and Gibson (1970) have often been referenced or supported by further research. For example, similarly important work was reported by Dayal and Allen (1975), who tested penetrometers at various rates and concluded that rate effects were small in sands and significant in clays. They reported a very pronounced effect of friction increases in clays for penetration velocities above 150 mm/s (0.5 ft/s); toe resistance increases were not as strong. Litkouhi and Poskitt (1980) performed additional laboratory tests and so did Heerema (1979) and Heerema (1981). Their findings were generally interpreted as indicating that the damping behavior during a hammer blow should not be linearly related to pile velocity. Sometimes, however, contradictions were found. For example, Heerema (1979) wrote that shaft resistance in sand was not velocity dependent (J_s = 0). Additional considerations concerning the exponential damping law are included in appendix B.

The FHWA also supported the development of program and documentation packages for routine wave equation applications. The resulting TTI (Hirsch et al., 1976) and WEAP (Goble and Rausche, 1976) packages included recommendations for quake and damping parameters which have been used with good success in the U.S. and many other countries.

A completely different approach for pile analysis was proposed by Novak (1977) and Novak et al. (1978) based on work done by Baranov (1967). Their purpose was an analysis of pile foundations under dynamic loads. These researchers, therefore, assumed an infinite, homogeneous, isotropic and viscoelastic soil medium and no separation between pile and soil. Their approach is, therefore, only valid for applications with small strains in the soil and zero pile set. Clearly, these assumptions do not apply to most pile driving conditions. These solutions were adopted by several researchers (*e.g.*, Simons and Randolph, 1985, Corte and Lepert, 1986, Randolph and Simons, 1986) for the representations of low strain shaft friction, *i.e.*, in the early part of pile penetration before plastic deformations occurred at the soil-pile interface.

An approach, independent of the Novak, or Coyle and Gibson procedures was adopted by Briaud and Garland (1984, 1985) when they examined the effect of increasing loading rates. This approach was derived based on the behavior of laboratory tests. Detailed data listings on both laboratory soil and pile tests which were the basis of this work were in Briaud and Garland, (1984). They expressed the failure load in terms of a time to failure, t_i:

$$R_{t1}(t_1)^n = R_{t2}(t_2)^n \tag{2.4}$$

R_{t1} and R_{t2} are failure loads with respective times to failure t_1 and t_2. For example, the index 2 could refer to a static and the index 1 to a dynamic test. However, even for the static test a certain time to failure should be calculated. The exponent, n, seems to be related to the soil's water content and varies from 0.02 for stiff clay to 0.10 for soft clay. (In personal communication, Briaud suggested n = 0.001 for sand). The Briaud and Garland law produces a linear relationship between dynamic resistance and penetration velocity on a log-log plot. Considering that the static and dynamic failure would be reached at equal deformations, equation (2.4) could also be rewritten in terms of pile velocity:

$$R_{t1} = R_{t2}(v_1/v_2)^n \tag{2.5}$$

In this form, the similarity with Coyle and Gibson's approach becomes apparent, particularly, since the static reference velocity v_2 may be considered a constant. It is believed that this law is valuable for explaining rate effects on failure load (*e.g.*, cone penetration tests, differences between maintained and constant rate of penetration load tests, *etc.*). Briaud and Garland also combined the exponential failure law with a hyperbolic shear stress-strain model for a calculation of load-set curves of piles.

As mentioned earlier, Randolph and Simons (1986) devised a model (practically an elastic spring and a linear dashpot as shown in figure 2.4) which again included the Novak's approach for small displacements (or the initial loading) of the shaft . The shaft soil stiffness is assumed to be 2.9G, where G is the soil's shear modulus. The model also includes a spring and dashpot for radiation damping. Once the soil-pile interface slips plastically, the soil resistance is modeled only by a slider with an additional dashpot in parallel with the slider to represent viscous damping. Thus, radiation damping is switched off at that time. For the toe, the authors practically adopt the Smith model. However, they model soil stiffness, k_t, (from which the quake can be calculated, given the ultimate toe resistance) and toe damping value, $J_{R,toe}$ both as functions of the soil shear modulus:

$$k_t = 4G(r_o)/(1 - \nu) \tag{2.6}$$

and:

$$J_{R,toe} = 3.4(r_o)^2 G\rho/(1 - \nu) \tag{2.7}$$

where r_o is the pile radius, ν is Poisson's ratio and ρ is the soil mass density. Interestingly, the authors suggest a purely viscous (not a Smith or modified Smith) damping approach.

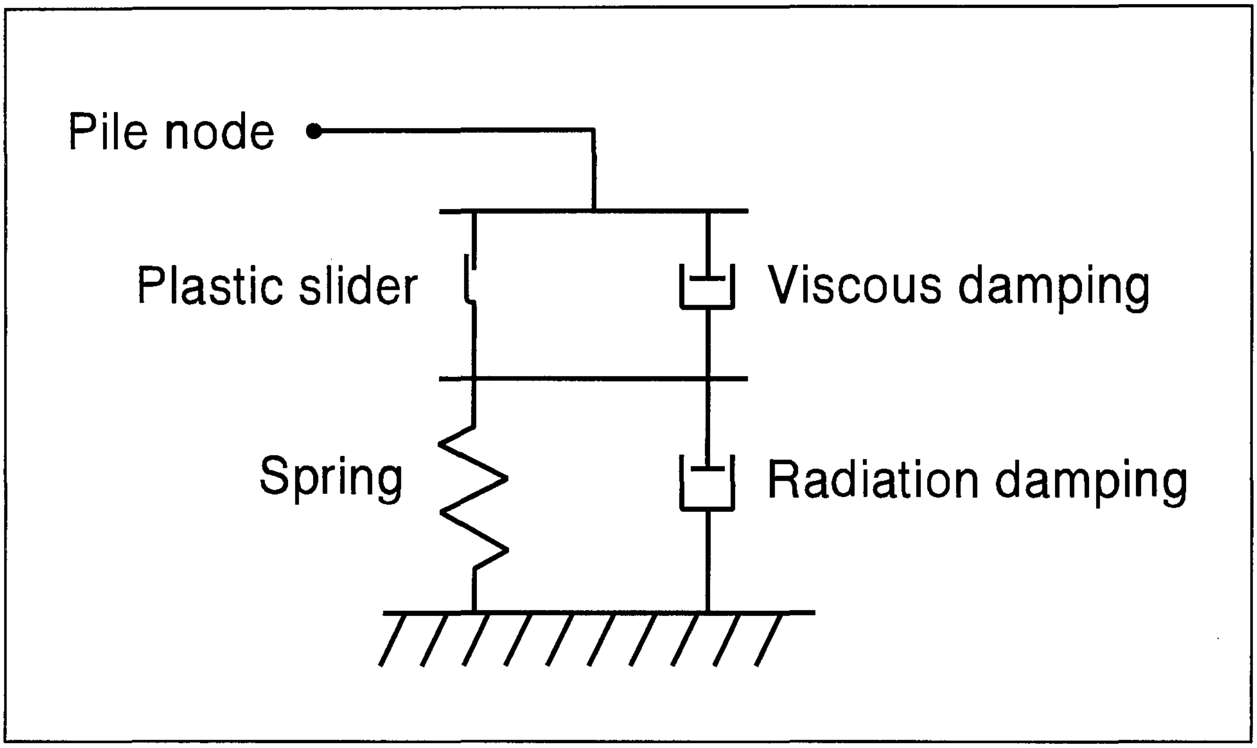

Figure 2.4: The Randolph Simon Shaft Soil Model

Corte and Lepert (1986) proposed a simple model for shaft resistance which would model the plastified soil by a slider which rested on a spring dashpot element representing the non-plastified soil away from the slip zone. The authors concluded that Smith's model was a practical approach which was only lacks a rational way of soil resistance parameter selection.

Mitwally and Novak (1988) responded to the efforts of others who wanted to use Novak's low strain approach in their study of the Smith model, and investigated two soil models. Shaft Model I, included an elasto-plastic spring and a linear dashpot. The soil stiffness on shaft and toe were, respectively, given by:

$$k_s = G\, S_1 \tag{2.8a}$$

$$k_t = G_b r_o C_1 \tag{2.8b}$$

where S_1 and C_1 are frequency dependent parameters; G and G_b are the soil's shear modulus at shaft and toe, respectively. Frequency dependent damping parameters may be calculated from:

$$c_s = G\, S_2/\omega \tag{2.9a}$$

and:

$$c_t = G_b r_o C_2/\omega \tag{2.9b}$$

Again, S_2 and C_2 are frequency dependent quantities, and ω is the frequency of the pile motion. This first model limits the static shaft resistance component by means of a quake where the Smith recommendation of 0.1 in (2.5 mm) is accepted. This is interesting since most followers of Novak's approach calculate the quake based on the soil shear modulus. On the other hand, the Model I of Mitwally and Novak implies that the ultimate resistance at a segment can be calculated by multiplying the soil stiffness (given by the soil shear modulus) by 0.1 in (2.5 mm).

Second model of Mitwally and Novak consists of an elasto-plastic spring on top of spring-dashpot arrangement which represents the soil motion. Stiffness and damping values appear to be the same as in Model I. However, rather than using a quake, *i.e.*, a deformation, to limit the shaft resistance, the ultimate shear stress, τ_u, is introduced. Also, the spring stiffness of the radiation damping model is only generally described as "sufficiently high so that the connection almost behaves as rigid when the interface force is less than the ultimate." The toe resistance is modeled as by Smith.

Nguyen et al. (1988) proposed to use a standard Smith model for the plastifying soil together with an additional dashpot representing radiation damping which separates from the model when the soil plastifies. The same model had been discussed by Randolph and Simons (1986) and Corte and Lepert (1986). Nguyen et al. showed how the four soil parameters could be calculated based on the soil's shear modulus which was calculated as a function of shear strain magnitude. For example, the toe quake is:

$$q_t = (r_o\, \tau_{max})(\ln(r_m/r_o) + 2)/2G \tag{2.11}$$

where $r_m = 2.5\ L\ (1 - \nu)$ representing a zone over which soil deformation occurs, τ_{max} is the maximum shear strain, and ν is Poisson's ratio.

Based on both Novak et al. (1978) and Simons and Randolph (1985), Lee et al. (1988) developed "A rational wave equation model for pile driving analysis." This work also includes the Coyle-Gibson approach, *i.e.*, the modified Smith damping law. In summary, Lee et al. propose to calculate the shaft quake from:

$$q_s = R_f/(2.75G) \tag{2.12}$$

where R_f is the failure load which is calculated according to Coyle and Gibson, 1970 (presumably with the maximum velocity at impact for $\dot{u}$ in equation (2.3)). Thus:

$$R_f = R_u(1 + J_c\dot{u}^n). \tag{2.13}$$

Obviously, the term 2.75G in the expression for q_s is the shaft soil stiffness. For the shaft damping prior to failure, Lee et al. (1988) calculate:

$$J_L' = 2\,\pi\,r_o\,\sqrt{\rho}\,G \tag{2.14}$$

For the toe, other expressions are chosen to calculate soil stiffness and damping based on the soil's shear modulus. It is noteworthy that this model does not employ a viscous or radiation damping term during soil failure, and it appears that discontinuities will develop in the resistance *vs* time behavior. This model, therefore, requires the knowledge of G, ρ and ν for the prefailure analysis, and J_G', J_G and n for the analysis during failure. Lee at al. give recommendations for the calculation of these quantities which makes their approach more complete than others.

Holeyman (1988) described an approach for the dynamic modelling of the pile base. (This subject is particularly important for large displacement piles and may be the most important area of necessary improvement for the dynamic pile models.) Holeyman added a truncated cone divided into additional segments, representing soil mass and soil stiffness underneath the pile toe. He based the properties of this cone (both geometric and elastic) on the soil's shear modulus, G, and its Poisson's ratio, ν. The cone has a bottom radius r_H and rests on a spring with stiffness, k_H, and dashpot with damping factor, c_H:

$$k_H = 4\;G\;r_H/(1-\nu) \tag{2.15}$$

and:

$$c_H = 3.4 r_H^2 (\rho G)^{1/2}/(1-\nu) \tag{2.16}$$

The elastic and dynamic behavior is modeled with a hyperbolic stress-strain relationship and a linearly viscous behavior. Thus, the stress in the cone is written as:

$$\sigma = E\epsilon + E'\,d\epsilon/dt \tag{2.17}$$

and:

$$\epsilon = \frac{q_r}{E_i}\,\frac{q}{q_r - q} \tag{2.18}$$

in which E' is the modulus of viscosity (damping factor for the truncated cone material), q_r is the ultimate strength at the base, and E_i is the initial tangent modulus. The hyperbolic law has the advantage of allowing for prediction of an ultimate strength even where only partial resistance activation occurs. Furthermore, the ultimate strength is scaled up as a function of the velocity based on Coyle and Gibson (1970) with a fixed n_G = 0.2 and a reference ultimate strength (determined at a loading rate of 0.79 in/s or 20 mm/s). In this approach, the truncated cone is divided into several segments. Its base rests on the spring and dashpot described earlier with parameters k_H and c_H, respectively. The forces against the pile base and between the soil segments are then calculated based on the hyperbolic stress and linearly viscous laws. The example given by Holeyman shows that the hyperbolic extrapolation of the ultimate capacity potentially introduces considerable uncertainty.

In summary, most researchers agree, that there is a static and a dynamic failure load. A static failure load may be defined at failure velocities less than 0.012 in/s (0.3 mm/s). Although this rate is approximately 1/10,000 of the maximum pile velocity under a pile driving hammer blow, it is also 10 to 100 times faster than a typical pile load test. In contrast, Constant Rate of Penetration load tests are typically conducted at penetration speeds of 0.00016 in/s (0.004 mm/s) or approximately 100 times slower than suggested in the literature as a static reference velocity on which the exponential calculation of the dynamic failure load would be calculated. Such high "static" loading rates make the laboratory data collected to date rather questionable. The dynamic resistances may be 2 to 3 times (1.5 to 2 times) greater at the shaft (toe) than the static ones. The general consensus is, therefore, that rather than damping resistance, an increased static resistance is calculated and later reduced by an appropriate factor. It is the authors' experience, however, that this approach will not provide the necessary model components for successful matching of pile dynamic signals unless radiation or viscous damping is also included during the time of slippage.

2.3 REVIEW OF LITERATURE ON EXPERIMENTAL STUDIES

In addition to tests confirming the Coyle-Gibson approach, discussed earlier, several researchers have conducted laboratory tests in an attempt to relate static to dynamic shaft and point resistance. For example, Meynard and Corte (1984), investigated the resistance effect of dry fine sand in a tank on a suddenly moving rod (0.8 in or 20 mm diameter, 40 ft or 12 m length) passing through the tank. They suggested correlations of the sands dynamic stiffness according to Novak et al. (1978) with the soil's shear moduli calculated from pressuremeter tests. They did not demonstrate a relationship between velocity and dynamic shaft resistance (both velocities and displacements varied).

Middendorp and Brederode (1984) used an experimental setup (rod diameter 0.79 in or 20 mm, length 32.8 ft or 10 m) which was very similar to that of Meynard and Corte. They suggested a shaft resistance of the form:

$$R_t = R_s + J_M\dot{u} + m_s\ddot{u} \tag{2.19}$$

where R_s is the static resistance as proposed by Smith, J_M is a purely viscous damping factor and m_s is a soil mass value. The variables $\dot{u}$ and $\ddot{u}$ are the pile's velocity and acceleration at a point, respectively. Although details of the results were not given, it is interesting that the authors observed that the velocity dependent resistance component remained constant at lower velocities (the velocities apparently were often in the neighborhood of 2.3 ft/s or 0.7 m/s). In fact, they proposed a constant dynamic resistance which only varied with the sign with velocity and which was 24 percent of the static ultimate resistance. Assuming the traditional model and using their reported velocity values, the Middendorp-Brederode test results suggested a Smith damping factor J_s = 0.11 s/ft (0.37 s/m). Furthermore, the dynamically calculated quake was 0.006 in or 0.15 mm *versus* a statically measured one of 0.12 in (2.8 mm).

Beringen and van Koten (1984) apparently used the Middendorp-Brederode tests and plotted shaft resistance of wet and dry sand as a function of loading velocity (between 0.009 and 0.98 ft/s or 0.003 and 0.3 m/s). The log-log plot did not indicate a change of skin friction with velocity over the plotted range.

Model pile tests (L = 31.5 in or 800 mm, diameter = 0.43 in or 11 mm) were also performed by van Koten et al. (1988) in a modified triaxial cell filled with saturated sand. Pile head force was measured both during dynamic and static loading. The piles carried approximately 2/3 of their load in shaft resistance and a 25 percent higher dynamic than static soil resistance was measured.

2.4 PARAMETERS FOR SMITH'S SOIL MODEL

Based on the literature study, recommendations of various researchers for damping constants have been summarized in tables 2.1a and 2.1b. Recommendations for both the standard (n = 1) and the modified Smith (exponential) approach were listed with the n-exponent identifying the approach. Similarly, recommendations found in the literature for quakes were listed in table 2.2. Unfortunately, these tables are not very complete. For example, the pile type is important for recommended quake values, but it is often not identified in the literature.

Note that quantities q_s and q_t, and J_s and J_t pertain to toe and shaft properties, respectively. Note also that conversion of J values from one unit system to another should be done using the following formulas:

$$J(s/ft) = J(s/m)\ (3.28)^n \tag{2.20a}$$

and:

$$J(s/m) = J(s/ft)\ (.3048)^n \tag{2.20b}$$

Smith's famous recommendations quakes of 0.1 in (2.5 mm), and damping factors of 0.05 and 0.15 s/ft (0.17 and 0.50 s/m) for shaft and toe, respectively, still present a good initial estimate. Smith chose these values independent of soil type and he concluded that the solutions would be relatively insensitive to small variations in these parameters.

Table 2.1a: Damping Values from Literature with n = 1					
Soil Description	Shaft Damping J_s s/m	Shaft Damping J_s s/ft	Toe Damping J_t s/m	Toe Damping J_t s/ft	Reference
All Types	0.170	0.050	0.500	0.150	Smith, 1960
Coarse Sand	0.500	0.150	0.500	0.150	Forehand and Reese, 1964
Sand - Gravel	0.500	0.150	0.500	0.150	Forehand and Reese, 1964
Fine Sand	0.500	0.150	0.500	0.150	Forehand and Reese, 1964
Loam over Sand, 50 percent Sand	0.660	0.200	0.660	0.200	Forehand and Reese, 1964
Silt, Fine Sand over Hard Strata	0.660	0.200	0.660	0.200	Forehand and Reese, 1964
Sand + Gravel over Hard Strata	0.500	0.150	0.500	0.150	Forehand and Reese, 1964
Non-Cohesive	0.170	0.050	0.500	0.150	Goble and Rausche, 1976
Cohesive	0.660	0.200	0.500	0.150	Goble and Rausche, 1976
Sand	0.170	0.050	0.500	0.150	Hirsch et al., 1976
Silt	0.330	0.101	0.500	0.150	Hirsch et al., 1976
Clay	0.660	0.201	0.033	0.010	Hirsch et al., 1976
London Clay, c_u = 15 kPa	1.300	0.396	0.570	0.174	Litkouhi and Poskitt, 1980
London Clay, c_u = 35 kPa	1.700	0.518	0.590	0.180	Litkouhi and Poskitt, 1980
London Clay, c_u = 60 kPa	0.900	0.274	0.530	0.162	Litkouhi and Poskitt, 1980
Forties Clay, c_u = 5 kPa	1.200	0.366	0.610	0.186	Litkouhi and Poskitt, 1980
Forties Clay, c_u = 45 kPa	0.800	0.244	0.590	0.180	Litkouhi and Poskitt, 1980
Magnus Clay, c_u = 5 kPa	1.600	0.488	0.870	0.265	Litkouhi and Poskitt, 1980
Magnus Clay, c_u = 40 kPa	2.400	0.732	0.590	0.180	Litkouhi and Poskitt, 1980
Magnus Clay, c_u = 80 kPa	0.900	0.274	0.360	0.110	Litkouhi and Poskitt, 1980
Sand	0.167	0.051	0.330	0.101	Soares et al., 1984
Silt	0.340	0.104	0.300	0.091	Soares et al., 1984
Clay	0.000	0.000	0.009	0.003	Soares et al., 1984

Table 2.1b: Damping Values from Literature with $n \neq 1$						
Soil Description	Note: Dimension of J_s and J_t Depends on N					Reference
	Shaft Damping J_s	Shaft Exponent n_s	Toe Damping J_t	Toe Exponent n_t	Units	
Sand, ϕ=30°			1.300	0.200	$(s/ft)^n$	Coyle and Gibson, 1970
Sand, ϕ=35°			1.000	0.200	$(s/ft)^n$	Coyle and Gibson, 1970
Sand, ϕ=40°			0.800	0.200	$(s/ft)^n$	Coyle and Gibson, 1970
Clay, LI=0.3			1.150	0.180	$(s/ft)^n$	Coyle and Gibson, 1970
Clay, LI=0.0			0.750	0.180	$(s/ft)^n$	Coyle and Gibson, 1970
Fine Grained Soils	1.250	0.350			$(s/ft)^n$	Coyle and Gibson, 1970
Medium Stiff Clay			1.000	0.200	$(s/ft)^n$	Dayal and Allen, 1975
London Clay, c_u = 15 kPa	1.499	0.210	0.689	0.220	$(s/ft)^n$	Litkouhi and Poskitt, 1980
London Clay, c_u = 35 kPa	2.068	0.160	0.710	0.210	$(s/ft)^n$	Litkouhi and Poskitt, 1980
London Clay, c_u = 60 kPa	1.094	0.170	0.648	0.190	$(s/ft)^n$	Litkouhi and Poskitt, 1980
Forties Clay, c_u = 5 kPa	1.382	0.200	0.788	0.170	$(s/ft)^n$	Litkouhi and Poskitt, 1980
Forties Clay, c_u= 45 kPa	1.027	0.260	0.659	0.370	$(s/ft)^n$	Litkouhi and Poskitt, 1980
Magnus Clay, c_u = 5 kPa	1.827	0.450	1.006	0.330	$(s/ft)^n$	Litkouhi and Poskitt, 1980
Magnus Clay, c_u = 40 kPa	2.677	0.360	0.726	0.280	$(s/ft)^n$	Litkouhi and Poskitt, 1980
Magnus Clay, c_u = 80 kPa	1.104	0.570	0.440	0.370	$(s/ft)^n$	Litkouhi and Poskitt, 1980
Sand, Little Silt, ϕ=30°			2.000	0.200	$(s/ft)^n$	Heerema, 1981

Table 2.2: Quake Values from Literature

Soil Description	Shaft Quake q_s mm	Shaft Quake q_s in	Toe Quake q_t mm	Toe Quake q_t in	Pile Dia. mm	Pile Dia. in	Pile Type	Reference
All Types	2.50	0.10	2.50	0.10			All	Smith, 1960
Coarse Sand	2.50	0.10	2.50	0.10				Forehand and Reese, 1964
Sand - Gravel	2.50	0.10	2.50	0.10				Forehand and Reese, 1964
Fine Sand	3.80	0.15	3.80	0.15				Forehand and Reese, 1964
Loam, 50 percent Sand	5.00	0.20	5.00	0.20				Forehand and Reese, 1964
Silt, Fine Sand,	5.00	0.20	5.00	0.20				Forehand and Reese, 1964
Sand, Gravel,	3.80	0.15	3.80	0.15				Forehand and Reese, 1964
Non-Cohesive	2.50	0.10	D/120	0.00			All	Goble and Rausche, 1976
Cohesive	2.50	0.10	D/120	0.00			All	Goble and Rausche, 1976
Sand	2.50	0.10	2.50	0.10			All	Hirsch et al., 1976
Silt	2.50	0.10	2.50	0.10			All	Hirsch et al., 1976
Clay	2.50	0.10	2.50	0.10			All	Hirsch et al., 1976
Very Dense Sandy Silty Glacial Till			20	0.79	324	12.8	CEP	Authier and Fellenius, 1980
Dense Clayey Silty Glacial Till			8/20	0.31/0.79	305	12.0	PSC	Authier and Fellenius, 1980
Hard Silty Clay Till			10.70	0.42	610	24.0	PSC	Likins, 1983
Dense Sand			18.00	0.71	610	24.0	PSC	Likins, 1983
Dense Fine Sand			13.00	0.51	458	18.0	CEP	Likins, 1983
Hard Silty Clay, End of Drive			10.00	0.39	305	12.0	H-Pile	Hannigan, 1984
Hard Silty Clay, Begin Restrike			2.5/4.5	0.10/0.18	305	12.0	H-Pile	Hannigan, 1984
Sand	0.25	0.01	0.25	0.01			All	Soares et al., 1984
Silt	0.26	0.01	0.26	0.01			All	Soares et al., 1984
Clay	0.17	0.01	0.17	0.01			All	Soares et al., 1984

Soares et al., 1984, summarized the quake and damping values from 28 different publications. Their findings are also included in tables 2.1a and b, even though they may repeat results from other authors. Several papers describe case studies where unusually large toe quakes (large skin quakes have not been reported in the literature) have been identified by CAPWAP, a high strain signal matching method described in appendix D. The publication by Authier and Fellenius (1980) includes two of the earliest, CAPWAP calculated, large toe quake cases. Before using the CAPWAP analysis, large quakes could only be identified using a set-rebound record. Even then magnitude and origin of the large quake were not clearly identifiable. Likins (1983) described three large quake cases of displacement piles with 18 to 24 in (400 to 600 mm) diameter. Soils were described as hard silty clay in one case, and dense sands in the other two cases. CAPWAP analysis was used to determine quakes both during the end of driving and at the beginning of restriking. Hannigan (1984) presented a case study where a 12-in (305 mm) H-pile was driven into very hard, silty clay. Ordinarily, one would assume that an H-pile is of the non-displacement type and, therefore, one would not expect large quakes at the toe of such a pile. However, in this case, the pile obviously plugged and a 0.4 in (10 mm) toe quake was indicated at the end of driving. During restriking, the toe quake was lower at 0.1 to 0.18 in (2.5 to 4.5 mm), *i.e.*, it was then nearly normal.

Thompson (1980) discussed the results of Fellenius (1980) paper and suggested that knowing too much may not be advantageous. He meant that the large quake problem only occurred during driving. Wave equation analyses, performed with large quakes, would indicate very low capacities; however, during static application the quakes would be smaller and the capacities would conceivably be much higher than indicated by the dynamic analysis. This contention is reasonable if the blow count was very high during driving and therefore not all capacity would be activated during the test driving. This argument does, however, not hold in all cases. Although, it has been often observed that the large quake occurs only during driving and not during the static load test, the bearing capacity in the static situation is not necessarily higher than indicated by the wave equation performed with the correct dynamic quake.

Tschebotarioff (1973) gives an example of such a difficult soil and recalls how bearing capacity was overpredicted because of an initially ignored bouncy pile behavior (a difficult soil is here one for which it is difficult to predict their static behavior from standard soil sampling and analysis methods, or from dynamic observations.) The data base also contains cases which document the fact that the pile bearing capacity would be overpredicted if the existence of large quakes would not be recognized. The data base's large toe quake cases are discussed in detail in appendix G. Another argument against Thompson's "ignorance is bliss" statement is the fact that the large quake situation might pose great difficulties for pile installation and bear the potential for contractor claims.

Using Coyle and Gibson's exponential damping law requires the determination of new damping factors either empirically or analytically (conversion of the standard Smith damping parameters to Coyle - Gibson factors is approximately possible; see appendix B). Coyle and Gibson (1970) laboratory tests yielded specific recommendations for damping parameters. Coyle et al. (1972) paper which included field tests on small piles (2.5 in or 63 mm diameter, 24 in or 600 mm length) supported somewhat different conclusions. These field-model pile tests produced inconclusive results for shaft damping in coarse grained soils. However, it is interesting to note that their measured shaft resistance *versus* time curves indicated early unloading behavior which we now would attribute to radiation damping. This soil model detail will be further discussed in appendix D of this volume and chapter 3 of volume I.

Wu et al. (1989) calculated quake and shaft damping factors for clay by using a finite element approach and matching results with a Smith type analysis. They assumed certain force pulse shapes and durations for their analyses. This analytical study again confirmed that the original Smith damping factors would not be constant when velocity varied.

2.5 SOIL CONSTANTS FROM CAPWAP

CAPWAP calculates damping, quake and other soil resistance values from measured pile top force and velocity curves. The CAPWAP approach has been described by Rausche et al. (1972), Mure et al. (1983), Goble and Rausche (1980) and most extensively in the CAPWAP manual (GRL and Associates, Inc., 1995). A summary of the CAPWAP model and its computational procedure is included in appendix D.

Rausche (1977) recommended the calculation of wave equation soil constants using CAPWAP and gave examples of good correlation. Indeed, CAPWAP should provide, for each instrumented test, soil resistance parameters which would lead to a perfect correlation between CAPWAP capacity and ordinary wave equation results. Unfortunately, several difficulties and differences between CAPWAP and the standard wave equation approach exist. The most important differences are the following:

- Hammer and driving system are obviously not modelled in the same manner by the two approaches. CAPWAP uses measured data at the pile top thereby eliminating the need to model the hammer. The hammer model of GRLWEAP or any program cannot possibly produce pile top conditions which are identical to the measurements. In the GRLWEAP correlations of this study, it was required that the force peak value and the maximum transferred energy to be made agreeable with the measurements within 10 percent. Naturally, this condition allows for significant differences between the measurements used by CAPWAP and the calculated impact effects of the wave equation approach.

- The pile analysis model of the two approaches differs. CAPWAP uses a continuous model while GRLWEAP uses the original Smith model. Significant differences occur where slacks or splices must be represented. The Smith approach is then more realistic. However, in most instances, the differences in pile model will not be the reason for noticeable differences in analysis results.

- The soil models of CAPWAP and Smith were originally identical. However, to match actual measurements it became necessary to make the CAPWAP model much more flexible and to add a significant number of variables. Table 2.3 compares the soil model of both methods. Appendixes C and D discuss the GRLWEAP and CAPWAP soil models in detail. Figures C.1 and D.7 show the GRLWEAP and CAPWAP soil model.

- The analysis procedure of both methods is completely different. Whereas CAPWAP attempts to match the measured curves as accurately as possible- -thereby neglecting to match the blow count exactly, the wave equation approach (for bearing capacity calculations) matches exactly the blow count and neglects the pile top boundary conditions. Actually, the wave equation only approximately calculates the blow count by subtracting a quake value from the maximum toe displacement under normal circumstances. Only the residual stress analysis employs a more realistic blow count calculation by comparing the pile penetration from blow to blow.

It is believed that this last difference is the most significant. However, even if the calculated blow count plus all damping values and loading quakes in CAPWAP and wave equation were identical, significant differences between the results of both methods must be expected because of the differences in hammer, driving system and soil model.

Even though CAPWAP calculated dynamic soil parameters may not exactly match those from wave equation analyses, these values would be good first approximations and indicate trends, as long as the CAPWAP model did not include radiation damping. Results from the correlation study will be discussed in chapter 3 of volume I.

2.6 SOIL CONSTANTS FROM IN-SITU TESTS

In-situ testing is commonly accepted for soil identification. In the United States, the Standard Penetration Test has been most widely used and because of the general familiarity with SPT blow counts, this technique is probably here to stay. The SPT also has the added advantage of providing a soil sample, even though it is disturbed and therefore only suitable for very basic laboratory tests. The SPT also has the advantage that it can penetrate deeper than other penetrometers since holes are predrilled before the test is conducted. Disadvantages are that

Table 2.3: Comparison of GRLWEAP with CAPWAP Soil Models			
Soil Parameter	CAPWAP	WEAP	Remarks - Significance
Ultimate Resistance	Yes	Yes	Identically used in both.
Loading Quakes	Yes	Yes	Identically used in both.
Unloading Quakes	Yes	No	Probably only important for long friction piles and as long as the blow count calculation relies on the maximum toe displacement (see below).
Unloading Level	Yes	No	Only important for shaft resistance. Similar significance as unloading quakes.
Reloading Level	Yes	No	Significance as for unloading quakes.
Toe Gap	Yes	No	Would be included in toe quake in GRLWEAP.
Plug mass	Yes	Yes	Although not explicitly available in GRLWEAP, plug can be easily modeled.
Soil Damping	Yes	Yes	CAPWAP uses linear approach, GRLWEAP uses Smith damping model. Significance has been discussed in appendix B. For toe CAPWAP offers both approaches.
Radiation Damping	Yes	No	May have very strong effect on results. It is known that this effect exists, however, general recommendations for dashpot and mass parameters are not available.
Capacity Activation	Full	Partial	For different quakes, wave equation analysis may not have all capacity activated, but still considers it associated with the calculated blow count. This makes wave equation predict higher than CAPWAP.

the "N" values often do not accurately reflect soil properties. For example, energy variations may produce errors. Also, the predrilling may cause some soil disturbance and gravel may plug the sampler thereby causing unusually high blow counts. SPT data interpretation requires empirical relationships between engineering soil properties and N-values. Fortunately, the N-value is always augmented by a soil description from samples, which at least yields an indication of soil type grain sizes.

Because of the importance of the SPT in several countries, most notably in the United States, published investigation results dealt with various effects. For example, Brown (1978) and Morgano and Liang (1992) concluded that there is no real influence of rod length on the SPT N-value. Many attempts have been made to improve the accuracy of soil strength predictions based on the SPT. In fact, a very large body of publications deals with the following issues.

1. Measurement of energy in the drive rod or evaluation of error sources of the SPT blow count results, *e.g.*, Schmertmann and Palacios (1979), Kovacs and Salomone (1982), ASTM D4633-86 (1986), and Skempton (1986).

2. Influence of rod size (diameter and length) on SPT N, Brown (1978) and Matsumoto and Matsubara (1982), McLean et al. (1975).

3. Correlation of the SPT blow count with soil friction angle, undrained shear strength, density, pile shaft resistance, pile end bearing, elastic modulus, shear modulus, *e.g.*, Meyerhof (1976), Schmertmann (1978) and Schmertmann (1979), Wrench and Novatzki (1986), Gazetas (1991).

4. Correlations between SPT N and Dutch Cone penetrometer q_c results , Mohan et al. (1970), Sanglerat (1972), Schmertmann (1979)

5. Dynamic measurements and analyses of the SPT driving process (though to a lesser degree than other topics, *e.g.*, Schmertmann and Palacios (1979), Bosscher and Showers (1987), Ellstein (1988), Morgano and Liang (1992).

Most pile designs in the United States are based on SPT results. Design methods extend from a very basic visual inspection of the SPT log and intuitive interpretations, or very simple SPT N-values to f_s (unit shaft resistance) and q_{ut} (unit toe resistance) conversions to an assessment of traditional soil strength parameters, and the more sophisticated α, β, or λ design methods. Sophisticated static analysis procedures often hide the fact that the design results are really based on very shaky assumptions in the soil strength assessment.

Other penetrometers usually follow the original Dutch Cone design (CPT). They may have a sleeve with enlarged diameter for a limited distance above the penetrometer bottom (cone). Friction over the sleeve and end bearing at the cone can be measured independently while the penetrometer is either slowly pushed or driven (dynamic penetrometer, DCPT). The electric penetrometer reads the two resistance values through strain measurements in the rod, a mechanical cone allows an independent loading of sleeve and point. An important result for soil classification is the friction ratio, *i.e.*, the ratio of friction on the sleeve to resistance on the cone. Robertson et al. (1989) showed how this friction ratio can be used to assign Case damping values. In this manner, the often qualitative soil classification by grain size is replaced by a quantitative, less intuitive method. Additional information can be gained by installing a piezometer in the tip of the cone. The resulting pore water pressure measurements are invaluable to the prediction of loss of friction during driving or setup and relaxation effects.

The interpretation of cone strength values naturally is more direct than the interpretation of the SPT N-values. In addition, the CPT records are nearly continuous while SPT results generally are obtained only at intervals of 5 ft (1.5 m). However, uncertainties still exist with CPT results because of the scale effect. Therefore, some adjustment factor has to be estimated that allows for the calculation from the cone to the pile unit toe resistance value. Briaud and Tucker (1988) discussed various methods of penetrometer and SPT interpretation and correlates the predictions with load test results on 98 piles tested in Mississippi.

A CPT with static and dynamic features is the Seismic Cone described by Campanella et al. (1986). The cone penetrometer is pushed statically into the ground and measurements of shaft friction (f_s), cone pressure (p_c), pore water pressure (u_p), and shear wave velocity (v_s) are measured. The shear wave velocity is measured by means of a seismometer located some distance above the cone. After the SCPT has been advanced to a measurement depth, and after all standard CPT measurements have been taken, horizontal impacts are applied to some loaded bearing plate at ground surface. The wave travel time is then measured and the cone is again advanced to the next level (probably 3.3 ft or 1 m deeper). The difference in wave travel times between two successive measurements is used to identify the shear wave velocity at a soil segment. The authors demonstrate that remarkably consistent results can be obtained.

Depending on the size of the cone, the depth of soil investigation under static load applications is often limited to soil layers with modest strengths. In hard layers, damage to the penetrometer may result if excessive forces are applied or the penetrometer cannot be retrieved. Different from the SPT, however, whose drive rod is not laterally supported and which is inserted in a drilled and potentially cased or slurry supported hole, both static and dynamic penetrometer (SCPT) may be loaded statically in compression with a reduced danger of rod buckling, under most circumstances. On the other hand, where the upper soil layers are too strong for rod penetration, predrilling may be required. In that case the penetrometer also may buckle.

Erickson (1992) summarized important work done with SPT and dynamic penetrometers for the direct or indirect (*e.g.*, the SPT blow count requires indirect interpretation to convert N to unit end bearing; the Dutch Cone result, q_c, can be used directly for end bearing calculations) determination of dynamic soil parameters. Of particular interest is the Swedish HfA penetrometer which is driven with a 140 lb (63.5 kg) ram and a fall height of 20 in (500 mm). It consists of a 1-1/4 to 1-3/8 in (32 to 36 mm) diameter drive rod and a 1-3/4 in (45 mm) diameter, 3.5 in (90 mm) long toe section with cone shaped tip. According to Erickson, this HfA cone falls between the internally standardized DPH and DPSH dynamic penetrometer standards. Also, the Swedish penetrometer has the same ram weight as the SPT. A second, smaller cone which is actually a drive rod with uniform cross section was also used in this study.

Erickson took dynamic measurements on two piling construction sites both on HfA and HsA Swedish dynamic penetrometers both at the end of driving and after 3 to 4 days of waiting and analyzed the dynamic data using Case Method and CAPWAP. He then performed static tests on the penetrometer. Next, precast concrete piles were driven and tested, unfortunately reaching sometimes relatively high blow counts like 10 mm/10 blows (300 blows/ft). GRLWEAP analyses were both based on manual and probe dynamic parameters. Actually, the manual values gave better correlations with real pile driving records.

Erickson's work included an effort to define a scaling procedure of such directly calculated results. In a first approach, he used the critical depth concept (Vesic, 1967) which states that unit shaft resistance and unit end bearing remain constant below a depth equal to 20 diameters. Since the penetrometer has a very small diameter, it reaches its critical depth already at a relatively shallow depth. A full-scale pile reaches critical depth at a much greater depth. Below the critical depth of the pile, the scale factor will be constant and equal to the ratio of pile diameter to penetrometer diameter. Above 20 penetrometer diameters (39.4 in or 1000 mm) the scale factor is unity. Between 20 penetrometer diameters and 20 pile diameters, the scale factors can be linearly interpolated. In a second conceptual model, the scale factor is related to the scale factor of the shaft resistance and can be calculated from different horizontal pressures on pile and penetrometer. Because of its significant soil displacement, the pile is assumed to experience a soil resistance which is proportional to the passive earth resistance. The penetrometer's soil resistance is only a function of the earth pressure at rest. For friction angles between 20 and 45°, the shaft resistance scale factor then varies between 3 and 20.

Liang and Hussein (1992) studied the current state of the art of dynamic pile analysis and used projectile theory to analyze a dynamic cone penetrometer test (DCPT). The goal of this study was the determination of Smith type soil parameters from DCPT. For the pile toe, the projectile theory has the advantage over Novak's approach that it is designed for large soil strains, utilizing the so-called "locking strain." Expressions for toe quakes and damping factors were derived:

$$q_t = 2\tau_o \ln(1/\epsilon_l) r_o (1 - \nu) I_p / E \tag{2.21}$$

where ϵ_l is the average volumetric locking strain (given by Liang and Hussein and based on cavity expansion theory), τ_o is the soil shear strength and I_p is an influence coefficient (between 0.5 and 0.75). Liang and Hussein also proposed a manner in which the soil's elastic modulus, E, may be found. His expression for toe damping, J_t is also a function of ϵ_l and τ_o, and, in addition, depends on the toe velocity and toe acceleration. It is somewhat complex and therefore not repeated here. He includes examples from three sites where the DCPT and full-scale piles were driven. He indicates good correlations between the measured blow count and those predicted based on the DCPT data.

Liang and Sheng (1992) also used cavity expansion theory to calculate the dynamic force at the toe of a penetrating pile. Based on this expression, the toe damping factor becomes an expression that involves the mass density of the soil (ρ), the toe radius (r_o), the acceleration ($\ddot{u}$), and velocity ($\dot{u}$), of the soil:

$$J_t = (\rho/3R_s)\,[2r_o(\ddot{u}/\dot{u}) + 3\dot{u}] \tag{2.22}$$

The division by the static resistance R_s was necessary in order to follow Smith's basic approach. The authors also derived a toe quake as:

$$q_t = r_o(1 + \nu)p_y/2E \tag{2.23}$$

The yield pressure, p_y, of the soil under the toe is related to the static resistance. The authors also present expressions for shaft quake (based on Kraft (1981) and shaft damping (a logarithmic expression based on Peck, 1962) which are not repeated here.

2.7 SOIL SETUP AND RELAXATION BEHAVIOR

The most accurate wave equation analysis, at best, would predict either the static bearing capacity at the time a hammer blow is applied (and its set is accurately measured) or the set of the pile under a hammer blow given its temporary static resistance. It is well known that the static resistance of the soil changes during the dynamic load application. A prediction of these changes based on soil type is therefore essential for successful wave equation predictions. Unfortunately, the literature does not contain much information or even an analytical model of soil strength changes due to pile driving (actually, engineers involved in drilled shaft construction also observe time dependent soil strength changes with time after construction). The reasons for soil setup are of course a loss of resistance during pile driving. This loss is usually attributed to thixotropy or soil remolding during driving, pore water pressure increases during driving (with associated loss of effective pressure) and other reasons for loss of effective stress. Relaxation, a more worrisome phenomenon, also appears to have various causes among them are negative pore water pressure with an artificially increased effective stress and what is generally described as creep.

The literature contains various case studies (and most case studies on pile installations deal with soil setup or relaxation). A summary of four case studies has been presented by Skov and

Denver (1988). They also formalized the manner in which the pile bearing capacity, R_u, can be calculated as a function of the time ratio t/t_o where t is the elapsed time since the end of installation, and t_o is a reference time that is also measured since the time of installation, and the factor A which is dependent on the soil type:

$$R_u = R_o[1 + A \log_{10}(t/t_o)] \tag{2.24}$$

For sand, clay and chalk, the authors recommend t_o values of 0.5, 1.0 and 5.0 days, and A values of 0.2, 0.6 and 5.0, respectively.

Other results were described by Fellenius et al. (1989). They reported, on tests in glacial deposits, setup factors (long-term capacity divided by end of driving capacity) of up to 4. Both bearing capacity values and their behavior over time varied widely in these heterogeneous glacial deposits. Preim et al. (1989) reported on dynamic and static pile test in silty and clayey sands. They concluded that shaft resistance increased practically linear over time while toe resistance remained constant. Camp and Hussein (1992) observed a different setup behavior in copper marl depending on the type of overburden soil. For a particular type of soil, however, setup gains appeared to occur linearly as a function of the logarithm of time.

3. DESCRIPTION OF DATA BASE

3.1 DATA BASE REQUIREMENTS

Chapter 2 of volume I contains a discussion of the requirements for data that would be considered complete and acceptable for the driven pile data base. These requirements, briefly stated, were:

1. A load test had to be performed to a capacity which would reach the Davisson limit. Extrapolation of the load test curve would be allowed if the bearing thus determined would not exceed the maximum applied load by more than 10 percent. The load test curve was entered in digital form in the data base.

2. An instrumented restrike test had to be performed with waiting times between end of drive and restrike comparable to the wait time between end of drive and load test. The restrike had to result in a blow count which was low enough for resistance activation. These blow count rules were relaxed where activation of dynamically determined load test capacities was not an issue. The dynamic tests had to be evaluated by Case Method and CAPWAP.

3. Soil borings, extending at least to the load test pile's toe elevation, had to be available. The soil boring results had to include some strength test results from in-situ tests such as SPT or CPT, or from laboratory tests performed on undisturbed samples. Soil boring results, including distance from load test pile, were completely entered into the data base.

4. Pile driving log from installation and restrikes, including hammer stroke, fuel setting or other hammer performance indicators, date of installation and date of restrike(s).

5. Complete description of pile material and cross section, hammer make and model, and driving system components including cushions and helmet details.

It was pointed out in chapter 2 of volume I that the above requirements limit the generality of the data base. However, it is extremely valuable as a research tool.

The data was entered in several spreadsheets thereby allowing for some calculations, statistical analysis and plotting. Tables 3.1 through 3.8 summarize the individual spreadsheet contents. One spreadsheet (table 3.7) was included for the listing of correlation results from GRLWEAP analyses.

To give the reader an appreciation of the contents of the data files, several columns of the General Information spreadsheet, further explained in table 3.1, are presented in table 3.9.

Preceding page blank

3.2 DATA BASE STATISTICS (January 1996)

Total number of entries (driven piles):	201
Meeting Data Base Requirements	133
Some criteria problems	17
Insufficient data	51
Pile breakdown	
PSC	88
Steel-H	50
Steel Pipe, Closed ended	44
Steel Pipe, open ended	11
Monotube	2
Reinforced Concrete	1
Spun Cylinder	1
Timber	3
Mandrel	1
Hammer breakdown	
Open end diesel	99
Closed end diesel	27
Single acting air/steam	64
Double acting air/steam	4
Rope driven	1
Hydraulic	6

Table 3.1: General and Pile Data Information

Col. No.	ENTRY NAME	EXPLANATION
1	ID #	Reference number. Entries are not organized in any systematic manner. In this way, adding additional data sets is a very simple matter.
2	Location/Site	A site identifying name.
3	Pile Name	A pile identifying name.
4	Data Source	An identifying name of the firm or agency submitting the data to the contractor.
5	Units	The unit system in which data is entered. Unit = 0 - SI system; forces in kN, length units in m and mm. Unit = 1 - English unit system; forces in kips, length units in in and ft.
6	Mat.	Pile material with code given in the header of the sheet.
7	Type	Pile type with code given in the header of the sheet.
8	Uniform Y/N	Uniformity of pile cross section.
9	Size	Major, identifying cross sectional dimensions.
10	Cross Sect. Size	A code for outside pile dimensions; see header of sheet.
11	Void Dia.	Primarily for concrete piles, the diameter of voids in the pile, if any.
12	Prestress	For prestressed concrete piles the effective prestress of the piles.
13	Strength	Yield strength of steel, compressive strength of concrete or timber.
14	El. Modulus	The dynamic modulus of the pile material.
15	Specific weight	The specific weight of the pile material.
16	Top Area	The cross sectional pile top area.
17	Gauge Area	The cross sectional area where transducers for dynamic measurements were attached.
18	Bottom Area	The cross sectional area of the pile at the pile bottom only different from top for non-uniform piles.
19	Circ.	Effective circumference of pile for unit shaft friction calculations.
20	Bottom Bg Area	Effective pile bottom area for unit end bearing calculations.

Note: Entries 13 through 16 pertain to pile top. For complex pile geometries or multi material piles, additional information is included in the Driving Log sheet.

Table 3.2: Driving Data

Col. No.	ENTRY NAME	EXPLANATION
1, 2, 3, 4		see table 3.1
5	Grade Elevation	Ground elevation during pile installation and restrike.
6	Driving Record	Y .. a spreadsheet with the driving log is available, N ... no data other than final or restrike blow counts are available.
7	Dyn. Data	Form in which dynamic data was available; for code see header of spreadsheet.
8	Date	Date of pile installation; it is important that the date is the date of end of driving (EOD).
9	Time	Time of EOD.
10	Pile Tip Elev.	Pile tip elevation at EOD.
11	Pile Length	Pile length at EOD.
12	Ham'r Stk/F.S.	Hammer stroke or fuel setting at EOD.
13	Obsv'd Stroke	Observed stroke may be visual or from blows per min for open end diesels, bounce chamber pressure for closed end diesels, or energy setting for hammers with internal velocity monitoring.
14	Blow Count	(Equivalent) blow count at EOD.
15	Dyn. Data	As for Col. 7 but at Beginning of 1st Restrike (BO1R).
16	Date	As for Col. 8 but at BO1R.
17	Time	As for Col. 9 but at BO1R.
18	Pile Length	As for Col. 11 but at BO1R.
19	Ham'r Stk/F.S.	As for Col. 12 but at BO1R.
20	Obsv'd Stroke	As for Col. 13 but at BO1R.
21	BOR Pile Tip	Pile Tip Elevation at BO1R.
22	Blow Count	As for Col. 14 but at BO1R.
23	EOR Pile Tip	Pile Tip Elevation at End of Restrike (EOR).
24	Blow Count	As for Col. 22 but at EOR.
25-34		As for Col. 15-24 but for 2nd restrike.
35-44		As for Col. 25-34 but for 3rd restrike.

Note: For additional restrikes, additional columns may be added to spreadsheet.

Table 3.3: Hammer and Driving System Information

Col. No.	ENTRY NAME	EXPLANATION
1, 2, 3, 4		see table 3.1
5	Hammer Name	The hammer used at EOD or BOR; if different hammers were used a remark should be made in "Comments" with additional information.
6	Ham'r Type	Hammer type as per code list in heading of spreadsheet.
7	WEAP Num.	The WEAP hammer file ID number.
8	Helmet Weight	The weight of helmet, inserts, hammer cushion.
9	Ram Weight	The hammer's ram weight.
10	Rated Energy Max	Usually the manufacturer's rated energy.
11	- EOD	The rated hammer energy pertaining to stroke or fuel setting at EOD.
12	- BOR	The rated hammer energy pertaining to stroke or fuel setting at BOR; if more than one restrike occurred with different settings, comments were appended in the "Comments" column.
13	Hammer Cushion Material	The hammer cushion material description as per code in header of spreadsheet.
14	- Area	The hammer cushion cross sectional area.
15	- Thick	The hammer cushion thickness.
16	Pile Cushion Material	The pile cushion material description as per code in header of spread sheet
17	- Area	The pile cushion cross sectional area.
18	- Th. EOD	The pile cushion thickness during EOD.
19	- Th. BOR	The pile cushion thickness during Restrike.
20	Comments	Since it is virtually impossible to provide individual entries for all possible combinations of driving and restriking equipment, particularly where there is more than 1 restrike, room for additional information is given in this "Comment" column.

Table 3.4: Dynamic Analysis Summary Information

Col. No.	ENTRY NAME	EXPLANATION
1, 2, 3, 4		see table 3.1
5	Field Meas.	Indicates for which test situations dynamic measurements are available as per code in header of spreadsheet.
6	Rec. Type	Form in which dynamic data was available; for code see header of spreadsheet.
7	Wave Speed	Wave speed used in the evaluation of the data.
8	Pile Impedance	Elastic modulus times cross sectional area divided by wave speed, all at the pile top; used in the data evaluation.
9	EOD PDA data - Pile length	Pile length below gauges during EOD.
10	- FMX	Maximum measured force at sensor location.
11	- VMX	Maximum velocity from measured acceleration.
12	- DMX	Maximum pile top displacement from measured acceleration.
13	- EMX	Maximum transferred energy at sensor location from measured force and acceleration.
14	- Cap. Code	Code for Case method as per header of spreadsheet.
15	Cap	Case Method capacity from measured force and acceleration evaluated as per cap. code.
16-22	BOR-1 data	Corresponds to columns 9-15 but for first restrike.
23-29	BOR-2 data	Corresponds to columns 9-15 but for second restrike.
30-36	BOR-3 data	Corresponds to columns 9-15 but for third restrike.

Table 3.5: CAPWAP Results (one spreadsheet each for EOD and all restrikes)

Col. No.	ENTRY NAME	EXPLANATION
1, 2, 3, 4		see table 3.1
5	Static Capacity - Total	The CAPWAP predicted pile bearing capacity.
6	- Skin	The CAPWAP predicted shaft resistance.
7	- Toe	The CAPWAP predicted toe resistance.
8	Soil Damping - Skin	The CAPWAP predicted Smith-type damping for the shaft.
9	- Toe	The CAPWAP predicted Smith-type damping for the toe.
10	Soil Quake - Skin	The CAPWAP predicted shaft quake.
11	- Toe	The CAPWAP predicted toe quake.
12	UNld	Ratio of unloading limit to positive shaft ultimate resistance.
13	CSkn	Ratio of unloading shaft quake to loading quake.
14	CToe	Ratio of unloading toe quake to loading quake.
15	LSkn	Relative shaft resistance magnitude below which unloading quake is used in a reloading situation.
16	LToe	Relative toe resistance magnitude below which unloading quake is used in a reloading situation.
16	SKdp	The radiation damping constant for the shaft resistance.
17	BTdp	The radiation damping constant for the toe resistance.
18	MSkn	Soil mass in the radiation damping model of the shaft resistance.
19	MToe	Soil mass in the radiation damping model of the toe resistance.
20	TGap	The gap between pile toe and firm soil.
21	PLug	The plug mass at the toe of a pile.

Table 3.6: Subsurface and Static Load Information

Col. No.	ENTRY NAME	EXPLANATION
1, 2, 3, 4		see table 3.1
	Subsurface Information	
5	- Site Plan	If available, Y else N.
6	- Boring No.1	Identification of first boring.
7	- Dist.	Distance of Boring No.1 to test pile.
8	- Boring No.2	Identification of second boring.
9	- Dist.	Distance of second boring from test pile.
10	- Soil Profile	If available Y, else N.
11	- SPT	If available Y, else N; see special spreadsheet for SPT data.
12	- CPT	If available Y, else N; see special spreadsheet for CPT data.
13	- Other test	If available Y, else N; see special spreadsheet for other data.
14	- Lab. test	If available Y, else N; see special spreadsheet for lab data.
15	- Grain Analy.	If available Y, else N; see special spreadsheet for grain size data.
16	Static Load Test # 1 - Test Type	See header of spreadsheet for code of type of static test.
17	- Top Transducer	If a load cell was used Y; else N.
18	- Date	Date on which static test No. 1 was started.
19	- Tell Tale	If tell tales were used during test Y; else N.
20	- Strain Gauge	If pile was instrumented with strain gauges Y; else N.
21	- Max. Load	Maximum load applied.
22	- Daviss. Load	Failure load according to Davisson criterion.
23	- Pile Length	Pile length during static load test.
24	- Grade Elev.	Grade elevation during static load test.
25	- Tip Elev.	Pile tip elevation during static load test.
26-35	Static Load Test # 2	As for columns 16 through 25 but for second load test.

Table 3.7: Correlation Analysis Summary

Col. No.	ENTRY NAME	EXPLANATION
1, 2, 3, 4		see table 3.1
5	Time between Static and Dynamic tests	Time between static load test and applicable (nearest in time) dynamic test - called dynamic C-test (for correlation).
6	LTP Static	Davisson Capacity.
7	Static Analysis	Capacity according to soil information and FHWA manual.
8	EOD CAPWAP	CAPWAP capacity from EOD data.
9	BOR1 CAPWAP	CAPWAP capacity from first restrike data.
10	BOR2 CAPWAP	CAPWAP capacity from second restrike data.
11	BOR3 CAPWAP	CAPWAP capacity from third restrike data.
12	BOR St. CAPWE	Standard CAPWEAP capacity from dynamic C-test. Note: Standard CAPWEAP determines capacity from observed blow count, measured pile top data and standard wave equation soil parameters.
13	Dyn. Form ENR	The Engineering News formula result multiplied by safety factor 2.
14	Dyn. Form EMX, DMX	The capacity calculated from a Hiley type formula and based on measured EMX and DMX.
15	Standard GRLWEAP - FMX	Maximum force at gauge location calculated by GRLWEAP with standard input values.
16	- EMX	As for 15 but for maximum transferred energy at gauge location.
17	- BOR Rult	Ultimate capacity calculated by GRLWEAP for observed blow count (output!).
18	- Friction	Skin friction percentage used in analysis.
19	- Qs	Shaft quake input.
20	- Qt	Toe quake input.
21	- Js	Shaft damping factor input.
22	- Jt	Toe damping factor input.

Table 3.7: Correlation Analysis Summary (continued)

Col. No.	ENTRY NAME	EXPLANATION
23	GRLWEAP (EMX, FMX adj.)	
	- FMX	Maximum force at gauge location after adjustment.
24	- EMX	Maximum transferred energy after adjustment.
25	- Rult	GRLWEAP capacity for adjusted FMX, EMX.
26	- eff	The hammer efficiency after adjustment.
27	- Remarks on adj.	Explanatory notes.
28	GRLWEAP Soil Parameters . . . - BOR Blow Count	Beginning of Restrike blow count
29	- BOR FMX	Maximum force calculated.
30	- BOR EMX	Maximum transferred energy calculated.
31	- BOR Rult	Calculated capacity based on blow count and adjusted hammer and driving system parameters.
32	- BOR eff.	Hammer efficiency after adjustment for EMX, FMX
33	- EOD Blow Count	End of driving blow count for set-up factor calculation.
34	- EOD Rult	GRLWEAP capacity for EOD blow count and BOR damping and quake values; efficiency as per EOD measurements if available.
35	- EOD eff	Hammer efficiency used for EOD analysis.
36	- Qs	Shaft quake - result (usually unadjusted).
37	- Qt	Toe quake - result.
38	- Js	Shaft damping factor - result.
39	- Jt	Toe damping factor result.
40	- Set-Up factor	Ratio of BOR to EOD capacity.

Table 3.8: Additional Spreadsheets

For each case (identified with the individual ID# in Columns 1 of the previous spreadsheets) there is one of the following spreadsheets (if corresponding data is available)

Col. No.	ENTRY NAME	EXPLANATION
1	Static Load Test	Contents are at least the pile top load and pile top set data of one load test. Header contains complete description. Pile length area and elastic modulus information for Davisson criterion. Columns below as per field logs or redigitized from plots. Pile top movement is result averaged from individual gauge readings.
2	Driving Records	Header information for cross reference. Grade elevation for recalculation of pile tip elevation from depth information.
3	Soil Data	Header data self-explanatory. If more than one boring are needed additional boring results follow within same spreadsheet. SPT results are contained in this spreadsheet.
4	SPT data	Contents self explanatory.
5	CPT data	Contents self explanatory.
6	Other test	Any additional soil strength information
7	Lab. test	Any laboratory test results.
8	Grain Analy.	Grain analysis data.

Table 3.9: General Description of Data Base Entries

Material Abbrev. S=Steel, C=Concrete, T=Timber

Type Abbreviations:
M=Monotube, PSC= Pre-Stressed Concrete, RC=Reinforced Concrete, SC=Spun Cylinder, G=Guild Mandrel, CEP=Closed-Ended Pipe, T=Timber, PSS=Prestressed/Stinger, R=Step Taper/Raymond, H=H-Pile Without Tip Protection, HT=H-Pile w/ Tip Protection, PSC/H = Pre-Stressed Concrete w/ H Pile Tip, CEP/C=Closed-Ended Pipe w/Conical point, OEP=Open-Ended Pipe, CSWP=Closed-Ended Spiral Welded Pipe, CEP/H=Closed-Ended Pipe w/H Pile Tip

ID #	Location Site	Pile Name	Mat.	Type	Uniform Y/N	Size (in,cm)	EOD Total Pile Length Ft,m	Time betwn Static & DynTest (h.mi)	LTP Static kips, KN
1	Appalachi., FL	PIER 3R	C	PSC	N	24	98.00	24.00	950
2	Appalachi., FL	PIER 14R	C	PSC	N	30	112.00	120.00	953
3	Appalachi., FL	PIER 25R	C	PSC	N	24	110.00	24.00	710
4	Appalachi., FL	PIER 41B	C	PSC	N	24	95.00	72.00	520
5	Appalachi., FL	PIER 101B	C	PSC	N	24	92.00	24.00	800
6	Appalachi., FL	PIER 133B	C	PSC	N	24	134.00	24.00	800
-7	Appalachi., FL	PIER 145B	C	PSC	N	24	136.00	24.00	980
8	Pagan River, VA	TP-1	C	PSC	Y	24	110.00	120.00	508
9	Charles River, MA	TP-5	C	PSC	Y	14	100.00	168.00	520
10	West Bay Brdg., FL	TP-9	C	PSC	N	30	135.00	816.00	925
11	West Bay Brdg., FL	TP-15	C	PSC	N	30	109.00	360.00	835
12	Mobile Tunnel, AL	CT-1	C	PSC	Y	18	67.00	240.00	381
13	Mobile Tunnel, AL	CT-2	C	PSC	Y	18	77.00	264.00	572
14	Mobile Tunnel, AL	CT-3	C	PSC	N	24	67.00	288.00	650
15	Mobile Tunnel, AL	CT-4	C	PSC	N	24	77.00	288.00	850
16	Mobile Tunnel, AL	CT-5	C	PSC	N	36	74.00	336.00	1100
17	Omaha, NE	T-1	S	H	Y	10x42	75.00	264.00	306
18	Omaha, NE	T-2	C	PSC	Y	12	65.00	192.00	380
19	Omaha, NE	T-3	C	PSC	Y	14	65.00	336.00	383
20	Omaha, NE	T-4	S	CEP	Y	12.75x0.5	70.00	168.00	287
--21	Portland, ME	A4	S	HT	Y	14x117	150.25	336.00	900(max)
22	Portland ,ME	A5	S	CEP	Y	18x0.5	120.00	744.00	446
23	Portland ,ME	B17	S	CEP	Y	18x0.5	80.50	624.00	440
24	Portland ,ME	B23	S	CEP	Y	18x0.5	59.75	336.00	353
-25	Alsea Bay, OR	CT-1	C	PSC	N	20	135.00	240.00	1450
26	White City, VT	A1,P15	S	HT	Y	14x73	95.00	120.00	330
27	White City, VT	A2,P10	S	HT	Y	14x73	95.00	168.00	388
28	W.B. Rouge, LA	TP-3	C	PSC	N	24	103.00	144.00	388
29	GRL, MB-AL	TP-1	S	OEP	Y	12.75x1	50.00	-	270
30	GRL, MB-AL	TP-2	S	OEP	Y	12.75x1	140.00	-	760
31	Turnpike, PA	63S	S	H	N	12x53	70.00	96.00	282
32	Choctawhat., FL	TP-26	C	PSC	N	30	125.00	528.00	807
33	Seattle, WA	S-A	S	CEP/H	N	48x0.75	160.00	600.00	1262
34	Orlando, FL	D-22	C	PSC	Y	14	115.00	216.00	842
35	Orlando, FL	D-23	S	CEP	Y	12.75x0.25	90.00	168.00	497
--36	Orlando, FL	R-29	S	CEP	Y	12.75x0.375	175.00	144.00	784
37	Dubuque, IA	P-1A	S	H	Y	14x89	120.00	384.00	932
38	Dubuque, IA	P-1B	S	CEP	Y	14x0.5	100.00	408.00	660
-39	Dubuque, IA	P-2A	S	H	Y	14x89	115.00	-	509
-40	Dubuque, IA	P-2B	S	CEP	Y	14x0.5	80.00	-	375
41	Cleveland, OH	TP-4	S	H	N	14x89	120.00	720.00	556
42	Cleveland, OH	TP-2	S	OEP	N	18x0.5	120.00	528.00	720
43	Cleveland, OH	TP-5	S	H	Y	12x53	120.00	312.00	308
44	Norwood, OH	TP-50	S	CSWP	Y	12x0.203	40.00	168.00	153
45	Hennipin, MN	T-2	S	H	Y	14x73	100.00	96.00	757

Table 3.9: General Description of Data Base Entries (continued)

ID #	Location Site	Pile Name	Mat.	Type	Uniform Y/N	Size (in,cm)	EOD Total Pile Length Ft,m	Time betwn Static & DynTest (h.mi)	LTP Static kips, KN
46	Choctawhat., FL	FSB3	C	PSC	Y	24	83.91	24.00	498
47	Choctawhat., FL	PR.11	C	PSC	N	30	106.02	96.00	1410
48	Choctawhat., FL	PR.17	C	PSC	N	30	102.04	48.00	1491
49	Choctawhat., FL	PR.23	C	PSC	N	30	101.04	24.00	632
50	Choctawhat., FL	PR.29	C	PSC	N	30	106.32	24.00	900
51	Choctawhat., FL	PR.35	C	PSC	N	30	102.09	24.00	1447
--52	Choctawhat., FL	PR.41	C	PSC	N	30	106.19	72.00	1376
--53	Choctawhat., FL	FSB26	C	PSC	N	24	84.05	72.00	938
54	Natchez, MS	P12	S	H	Y	14x73	40.00	120.00	500
55	Cimarron, OK	ST-1	S	CEP	N	26x0.75	63.30	72.00	600
56	Cimarron, OK	CP-1	C	PSC	N	24	64.30	48.00	792
--57	Cimarron, OK	SH-1	S	H	Y	14x117	113.00	72.00	770
--58	Cimarron, OK	CT-1	C	RC	Y	24	63.30	48.00	1620
59	Route 115, MC	ST-1	S	CEP	Y	14x0.375	86.50	144.00	325
60	Route 115, MO	ST-2	S	CEP	Y	14x0.375	65.00	168.00	246
61	Bailey Fork, TN	A1-4	C	PSC	Y	14	45.00	72.00	267
62	White City, FL	TP3	C	PSC	Y	24	50.42	24.00	650
63	White City, FL	TP6	C	PSC	Y	24	43.50	336.00	472
-64	Baytown Br., TX	Pipe	S	OEP	Y	24x0.625	140.00	-	1514
-65	Baytown Br., TX	Concrete	C	PSC	Y	20	101.50	-	987
66	SR 15 Tioga, PA	PIER 2	S	M	N	8"x12" 7-gauge	37.00	96.00	240
67	Annacis, Canada	PIER 1	C	PSC	Y	24	96.79	240.00	395
+68	Dawhoo, SC	PSC 24"	C	PSC	Y	24	90.00	48.00	1060
+69	Dawhoo, SC	PSC 16"	C	PSC	Y	16	80.00	48.00	590
+70	Dawhoo, SC	14HP73	S	H	N	14x73	90.00	48.00	618
71	Socastee, SC	14HP73	S	H	N	14x73	85.00	24.00	313
72	Socastee, SC	PIPE 24"	S	OEP	N	24x0.5	85.00	24.00	600
-73	Socastee, SC	PSC 24"	C	PSC	Y	24	85.00	24.00	1095
74	Doughty St., SC	PSC 12"	C	PSC	Y	12	91.00	48.00	360
75	Battery Cr., SC	PSC 24"L	C	PSC/H	N	24	79.0/81.5	24.00	503
76	Battery Cr., SC	PSC 24"S	C	PSC/H	N	24	64.0/66.5	24.00	1045
--77	Phoenix, AZ	TP-2	S	HT	Y	14x117	51.33	648.00	1460
78	Phoenix, AZ	TP-3	S	HT	Y	14x117	65.50	528.00	1281
79	Phoenix, AZ	TP-4	S	CEP/C	Y	14x0.375	30.75	672.00	740
80	Phoenix, AZ	TP-5	S	CEP/C	Y	14x0.375	42.50	624.00	689
--81	Phoenix, AZ	TP-6	C	PSC	Y	16	32.00	672.00	956
82	Phoenix, AZ	TP-7	C	PSC	Y	16	41.50	624.00	1000
83	Franklin Br., FL	TS-1	C	PSC	Y	24	85.55	648.00	967
84	Franklin Br., FL	TS-4	C	PSC	Y	30	101.75	432.00	820
85	Port of LA, CA	TP	C	PSC	N	24	95.00	168.00	1020
-86	Jones Island, WI	PILE1	S	CEP	Y	12.75x0.375	140.42	168.00	659
87	Jones Island, WI	13-72	S	CEP	Y	12.75x0.312	161.00	288.00	656
88	Jones Island, WI	11-42	S	CEP	Y	12.75x0.312	161.25	576.00	470
89	Jones Island, WI	95B	S	CEP	Y	9.625x0.545	166.17	264.00	580
90	Jones Island, WI	6-5B	S	CEP	Y	9.625x0.545	154.58	216.00	380
-91	Jones Island, WI	393	S	CEP	Y	9.625x0.545	155.42	432.00	600
92	Jones Island, WI	39	S	CEP	Y	9.625x0.545	145.00	48.00	657
93	Jones Island, WI	4	S	CEP	Y	9.625x0.545	165.92	144.00	380
-94	Pittsburgh, PA	2-22	S	H	Y	12X74	70.00	1080.00	580
-95	Pittsburgh, PA	3-12	S	H	Y	12X74	34.00	552.00	305
-96	Pittsburgh, PA	3-13A	S	H	Y	10X57	35.00	984.00	340
-97	Pittsburgh, PA	4-12	S	H	Y	12X74	50.00	1800.00	240
-98	Pittsburgh, PA	4-13	S	H	Y	10X57	36.00	2808.00	310
-99	Pittsburgh, PA	4-14	S	H	Y	10X57	50.00	72.00	367
-100	Pittsburgh, PA	4-15	S	H	Y	12X74	50.00	72.00	480

Table 3.9: General Description of Data Base Entries (continued)

ID #	Location Site	Pile Name	Mat.	Type	Uniform Y/N	Size (in,cm)	EOD Total Pile Length Ft,m	Time betwn Static & DynTest (h.mi)	LTP Static kips, KN
101	Newport, KY	PIER G	C	PSC	Y	14	75.00	72.00	363
102	N/A	SITE 1	S	H	Y	12x53	75.00	4.5	374
103	N/A	SITE 2	S	H	Y	12x53	40.00	5?	521
104	N/A	SITE 3	S	H	Y	12x53	80.00	5?	378
105	Boston, MA	LTP 1	S	H	Y	12x74	90.54	480.00	635
--106	Boston, MA	LTP2	S	H	Y	14x117	89.04	576.00	797(max)
--107	Boston, MA	L4	C	PSC	Y	14	70.00	-	390
--108	San Jose, CA	B5	C	PSC	Y	14	100.00	~48	820(max)
--109	San Jose, CA	B3	C	PSC	Y	14	100.00	~48	672(max)
--110	Toledo, OH	TP	S	CEP	Y	10.75x0.25	78.42	-	252(max)
--111	Hong Kong	NA-13	S	OEP	Y	24x0.55	118.12	384.00	824(max)
--112	Seattle, WA	A-LTP	C	PSC	Y	24	102.00	240.00	1038.00
--113	Seattle, WA	B-LTP	C	PSC	Y	24	87.00	216.00	835.00
--114	Seattle, WA	E-LTP	C	PSC	Y	24	70.00	-	1200(max)
--115	Seattle, WA.	C-LTP	S	OEP	Y	24x1.25	215.50	-	1500(max)
--116	Seattle, WA	D-LTP	S	OEP	Y	24x1.25	160.00	-	2105(max)
117	Kontich, Belgium	0-B	S	H	N	14x142	196.86	-	1378.00
118	Kontich, Belgium	I-C	S	H	N	14x142	65.62	-	474.00
119	Kontich, Belgium	II-A	S	H	N	14x142	55.78	-	296.00
120	Kontich, Belgium	XI-D	S	H	N	14x142	65.62	-	575.00
-121	Tarver, GA	P3-B3	S	CEP	Y	16x0.25	39.70	24.00	261.00
122	China	KL1	C	PSC	N	31.5x4.72	59.06	24.00	148.00
--123	Monticello, MN	No. 5	T	T	N	12.8/8.6	35.00	4.00	144.00
--124	N/A	TP3	S	OEP	N	30/0.75	359.14	1.50	600(max)
--125	Newburgh, NY	TP-P8	S	H	Y	14x117	215.00	-	967.00
126	Arutmin, Indonesia	TP1	S	OEP	Y	36x0.5	98.43	96.00	629.00
127	Jacksonville, FL	33 DD	C	PSC/H	N	18/H10x57	70.00	-	357
128	Jacksonville, FL	33 SS	C	PSC/H	N	18/H10x57	70.00	-	467
129	Fairmount, MN	LTP	T	T	N	15.22/5.52	35.00	2	170
130	Oneonta, NY	LTP	S	CEP	Y	12.5/0.25	87.00	24	218
131	Philadelphia, PA	LTP 19	S	H	Y	10x42	110.00	-	-
132	Cleveland, OH	LTP 74	S	CEP	N	(14x0.219)(12.5	73.70	336	390
133	Cleveland, OH	LTP 72	S	CEP	N	(14x0.203)(12.5	79.00	24	269
134	Cleveland, OH	LTP 52	S	CEP	N	(14x0.203)(12.5	93.00	48	-
135	Cleveland, OH	LTP 62	S	CEP	N	(14x0.203)(12.5	95.00	24	397
136	Cleveland, OH	LTP 63	S	CEP	N	(14x0.219)(12.5	103.00	216	285
137	Kings Bay, GA	TP7	C	PSC	Y	24	93.00	1344	1000
138	Kings Bay, GA	TP11	C	PSC/H	N	24	106.00	552	881
139	Singapore	TJB-UP	C	SC	Y	27	88.59	624	1138
140	Delft, Netherlands	1	C	PSC	Y	9.84	37.37	96	69
141	Delft, Netherlands	2	C	PSC	Y	9.84	48.95	96	127
142	Delft, Netherlands	3	C	PSC	Y	9.84	62.21	96	233
143	Delft, Netherlands	5	C	PSC	Y	9.84	62.11	96	229
144	JFK, NY	P5159	S	CEP	Y	10.75x0.25	58.50	240	120
145	N/A	TP-2	S	CEP	Y	12.75x025	127.00	1992	138
146	San Jose, CA	P1	C	PSC	Y	12	63.30	-	372
147	S.F. Airport, CA	P2	C	PSC	Y	15	48.17	-	287
148	San Jose, CA	P3	C	PSC	Y	12	42.00	-	177
149	Seattle, WA	PIER 9	S	CEP/H	N	48/0.75	142.00	-	1200
150	Seattle, WA	PIER 7	S	CEP/H	N	48/0.75	154.00	-	1348
151	Columbus, OH	CENTER	S	H	Y	12x53	27.00	264	-
152	Columbus, OH	SE	S	H	Y	12x53	26.00	336	-
153	Columbus, OH	NW	S	H	Y	12x53	27.00	240	-
154	West Palm Beach, FL	P4(#1)	C	PSC	Y	18	45.00	48	234
155	West Palm Beach, FL	P18(#2)	C	PSC	Y	18	35.00	24	170

Table 3.9: General Description of Data Base Entries (continued)

ID #	Location Site	Pile Name	Mat.	Type	Uniform Y/N	Size (in,cm)	EOD Total Pile Length Ft,m	Time betwn Static & DynTest (h.mi)	LTP Static kips, KN
156	Whitehall, NY	P41	C	PSC	Y	14	140.00	504	152
157	Westinghouse-FBM, SC	TP3-4	C	PSC	Y	18	31.00	~240	108
158	N/A	PN1499	C	PSC	Y	14	100.00	72	415
159	Canada	D-22S	S	H	Y	12x74	22.50	120	360
160	Canada	E-22S	S	H	Y	12x74	30.00	72	570
161	Canada	P-5X	S	H	Y	12x53	25.00	312	497
162	McDuffie Island, AL	TP-4	S	CEP	Y	10x0.25	57.00	336	230
163	Cleveland, OH	TP-3	S	H	Y	14x89	209.00		-
164	Cleveland, OH	TP-6	S	H	Y	14x89	187.00		-
165	Northbrook, IL	A-15	S	CEP	Y	12.75x0.5	90.33		561
166	Northbrook, IL	A-115	S	CEP	Y	12.75x0.5	90.33		497
167	Scarborough, ME	P7	S	H	Y	14x73	95.00		398
168	Choctawhatchee, FL	TP-6	C	PSC	N	30	125.00		759
169	Green Court, Canada	TP-1	S	CEP	Y	12.75x0.44	68.90		177/220
170	Green Court, Canada	TP-2	S	CEP	Y	12.75x0.44	55.77		160/179
171	Mobile, AL	TP-1	C	PSC	Y	14	57.00		180
172	Mobile , AL	TP-2	C	PSC	Y	14	70.00		572
173	Mobile , AL	TP-3	C	PSC	Y	18	62.00		147
174	Mobile , AL	TP-4	S	H	N	14x89/14x73	112.30		-
175	Colorado Springs, CO	TP-1	S	H	Y	10x57	30.00		194
176	Colorado Springs, CO	TP-2	S	H	Y	10x57	30.00		400
177	Colorado Springs, CO	TP-3	S	H	Y	12x74	30.00		143
178	Colorado Springs, CO	TP-4	S	H	Y	12x74	30.00		272
179	California	51R	C	PSC	Y	14	110.00		
180	California	49R	S	CEP	Y	16x0.5	110.00		
181	California	69R	S	H	Y	14x89	110.00		
182	Fort Lauderdale, FL	317 #28	C	PSC	Y	18	48.00		244
183	Norfolk, VA	P2	C	PSC	Y	12	100.00		380
184	Norfolk, VA	P3	C	PSC	Y	12	100.00		245
185	Duluth, MN	TP1	S	OEP	Y	9.625x0.395	145.33	24.00	425.00
--186	Waterbury, VT	Abt B-P14	S	CEP	Y	12.75x0.375	99.00	168.00	343.00
187	New Orleans, LA	TP3	S	CEP	N	12.75x0.375	70.00	168.00	109.00
188	New Orleans, LA	TP4	T	T	N	16.5/8.5	70.00	192.00	130.00
189	New Orleans, LA	TP6	C	PSC	Y	14	70.00	216.00	119.00
190	New Orleans, LA	TP7	S	CEP	N	12.75x0.375	70.00	240.00	114.00
191	Jakarta, Indonesia	PTB9	C	PSC	Y	15.75	65.62	240.00	644.00
192	McDuffie Island, AL	TP-2	S	G	Y	12x0.075	48.00	264.00	158.00
193	McDuffie Island, AL	TP-3	S	CEP	Y	12.75x0.25	65.00	312.00	347.00
194	McDuffie Island, AL	TP-11	S	M	N	12/8x9 gauge	60.00	288.00	383.00
--195	Luling Brdg., LA	TP2	C	PSC	Y	54x5	84.00	48.00	430.00
196	Luling Brdg., LA	TP3	C	PSC	Y	24	84.00	312.00	414
197	Luling Brdg., LA	TP4	C	PSC	Y	30	84.00	336.00	511
198	Luling Brdg., LA	TP5	C	PSC	N	30	84.00	336.00	555.00
199	Luling Brdg., LA	TP6	C	PSC	Y	36x5	84.00	336.00	541.00
200	Luling Brdg., LA	TP7	C	PSC	N	36x5	84.00	360.00	541.00
--201	Luling Brdg., LA	TP1	C	PSC	Y	54x5	84.00	-	-
202	Cleveland, OH	TP-3	S	H	Y	14x89			

Legend:
+ There is additional static and dynamic data
- Some data do not meet to the requirements for correlation study
-- Correlation study was not performed because of insufficient data

APPENDIX A

INTRODUCTION INTO THE MECHANICS OF TRAVELING WAVES IN A SLENDER, ELASTIC ROD

A.1 THE WAVE EQUATION

Consider a linearly elastic rod having an elastic modulus, E, and a mass density, ρ. When the rod is struck alone, the following differential equation governs the ensuing motion of the rod particles:

$$\rho \frac{\partial^2 u}{\partial t^2} = E \frac{\partial^2 u}{\partial x^2} \qquad \text{(A.1)}$$

Where u is the total displacement at time t and location x, and the left and right hand partial derivatives are the acceleration and change of strain in the rod, respectively. This equation is referred to as the linear one-dimensional wave equation which has a general solution:

$$u = g(x + ct) + f(x - ct) \qquad \text{(A.2)}$$

if we substitute $c^2 = E/\rho$ in equation A.1. The general solution implies that a displacement pattern in the rod may consist of two components, g-wave and f-wave as shown in figure A.1. Thus, the g and f "waves" have merely shifted positively and negatively, respectively in time at a wave speed c without changing shape.

If we apply these findings to piles during impact, then we may get the following situation (assuming no soil resistance) of figure A.2.

Within the initial downward input wave, there are compressive forces, causing proportional downward particle velocities. We can calculate the strain by differentiation with respect to x:

$$\epsilon = \frac{\partial u}{\partial x} \qquad \text{(A.3)}$$

Similarly, the velocity is:

$$\dot{u} = \frac{\partial u}{\partial t} \qquad \text{(A.4)}$$

Preceding page blank

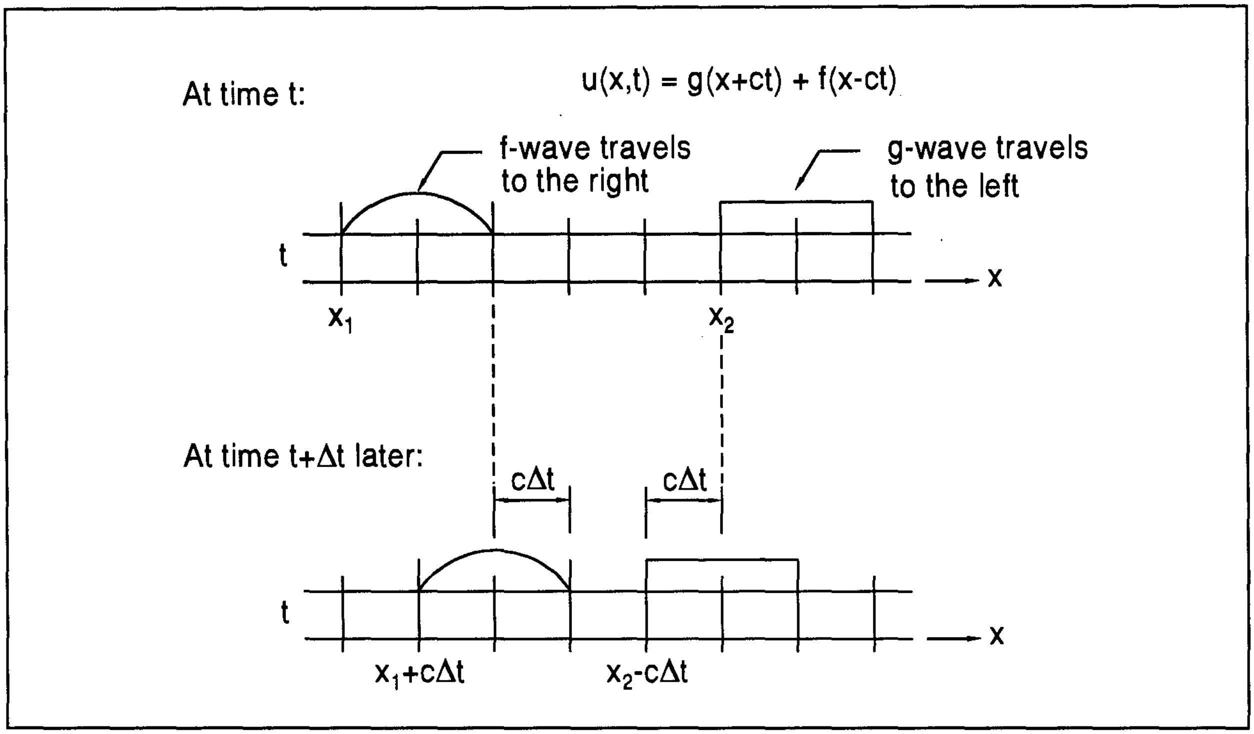

Figure A.1: Wave Travel in a Rod

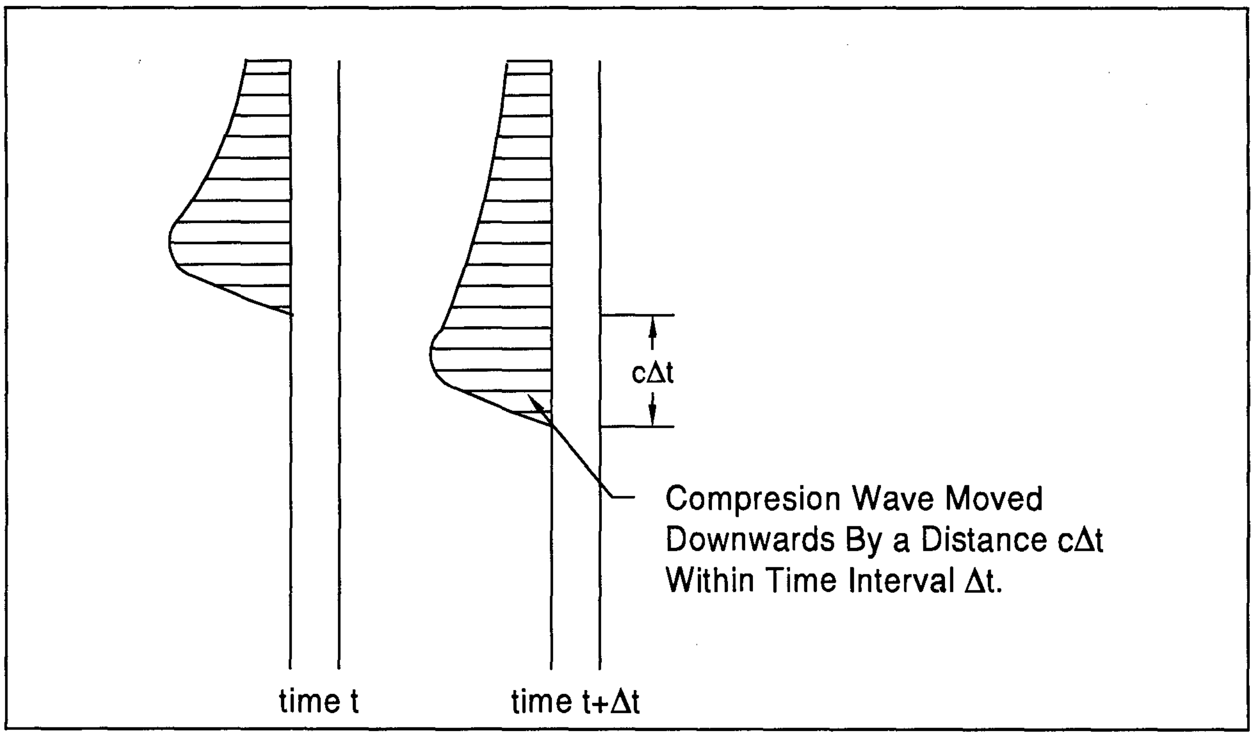

Figure A.2: Example of a Downward Traveling Wave and therefore:

$$\epsilon = g' + f' \tag{A.5}$$

and:

$$\dot{u} = c\,g' - c\,f' \tag{A.6}$$

where the primed quantities are derivatives with respect to the function arguments. We therefore obtain:

$$\epsilon = \frac{\dot{u}}{c} \text{ for g (or downward waves)} \tag{A.7}$$

and:

$$\epsilon = -\frac{\dot{u}}{c} \text{ for f (or upward waves)} \tag{A.8}$$

as long as compressive forces and downward velocities are positive. These two equations are also written in terms of force, after multiplication by elastic modulus (E) and cross sectional area (A), as:

$$F^{\downarrow} = Z\,\dot{u}^{\downarrow} \tag{A.9}$$

and:

$$F^{\uparrow} = -Z\,\dot{u}^{\uparrow} \tag{A.10}$$

where $F^{\downarrow}$ and $F^{\uparrow}$ are the downward and upward waves in terms of force, $\dot{u}^{\downarrow}$ and $\dot{u}^{\uparrow}$ are the respective waves in terms of velocity and:

$$Z = E\,A/c \tag{A.11}$$

is the pile impedance. After a time L/c (L is the pile length), the impact wave or the downward (positive) wave introduced by the pile driving hammer arrives at the pile bottom.

Thus, at the pile end, suddenly an imbalance exists since the wave has neither mass to accelerate nor material to compress and a reflection occurs. In fact, because the pile end is free, the force at that point must be zero due to force equilibrium conditions (figure A.3):

$$R = F^{\downarrow} + F^{\uparrow} \tag{A.12}$$

Thus, if R = 0:

$$F^{\uparrow} = -F^{\downarrow} \tag{A.13}$$

an upward tension wave is generated (figure A.4). The upward traveling tension and downward traveling compression forces of the two waves cancel at the pile bottom. However, the upward

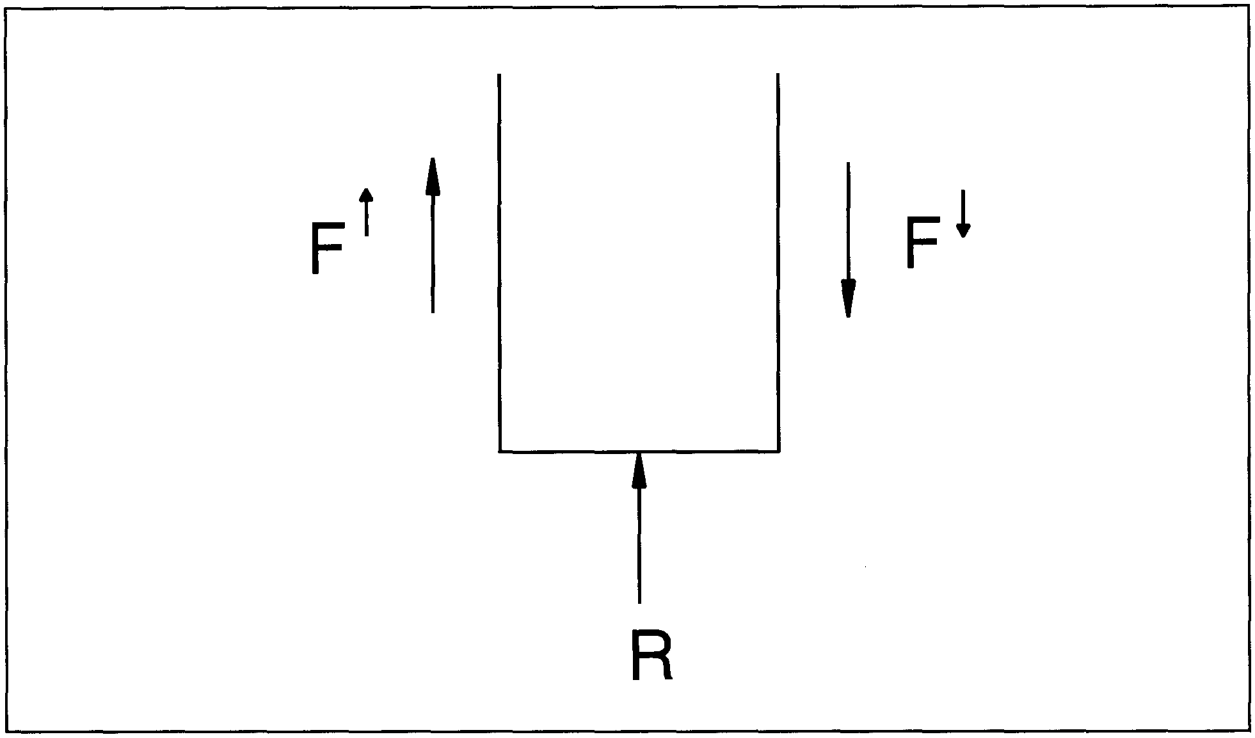

Figure A.3: Wave Balance at Pile With Bottom Resistance

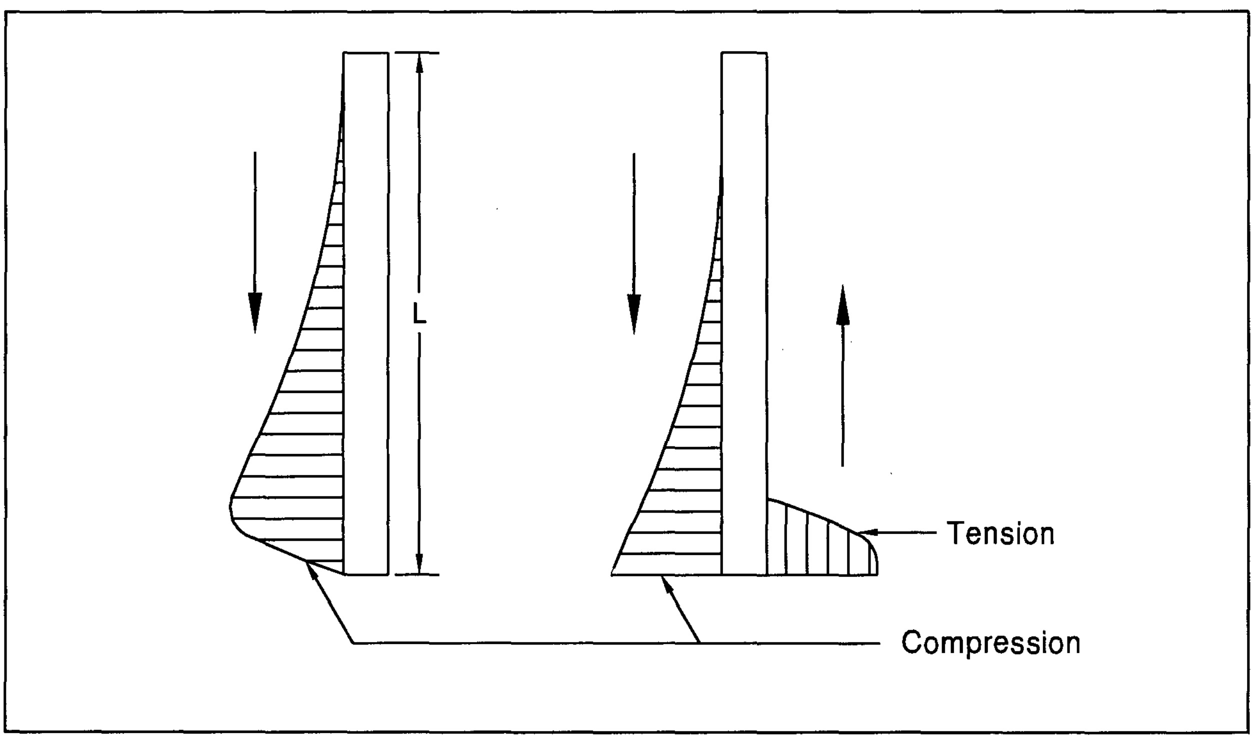

Figure A.4: Reflection At a Free Pile Bottom traveling tensile waves also pull the pile particles downward and, therefore, the pile velocity doubles at the bottom.

For tension waves, particle velocities and wave propagation have the opposite direction while compressive wave particle velocities have the same direction as the wave propagation.

The total force, F, and velocity, $\dot{u}$, measured at any location in a pile is the result of superposition of the downward and upward traveling waves. Thus:

$$F = F^{\downarrow} + F^{\uparrow} \qquad \text{(A.14)}$$

$$\dot{u} = \dot{u}^{\downarrow} + \dot{u}^{\uparrow} \qquad \text{(A.15)}$$

If the velocities are converted to forces using equations (A.9) and (A.10), the forces in the upward and downward waves can be obtained from the solution of these two simultaneous equations:

$$F^{\downarrow} = \frac{(F + Z\dot{u})}{2} \qquad \text{(A.16)}$$

and:

$$F^{\uparrow} = \frac{(F - Z\dot{u})}{2} \qquad \text{(A.17)}$$

In other words, if we know the force, F, and velocity, $\dot{u}$, at a point of the pile, then the downward and upward traveling waves can be determined from the average or half the difference between force, F, and proportional particle velocity, $Z\dot{u}$, respectively.

A.2 RESISTANCE WAVES

If a resistance force starts to act at time t=x/c and at some intermediate point, x, along the pile (it may be activated by an impact starting to travel downward at time t=0 at the pile top), then two waves are created, each having a magnitude of R/2. To satisfy equilibrium and continuity, the upward wave is in compression and the downward wave in tension (figure A.5).

The particle velocities are:

$$\dot{u}_r = -\frac{R}{2Z} \qquad \text{(A.18)}$$

and both waves are directed upward (negative) to maintain continuity.

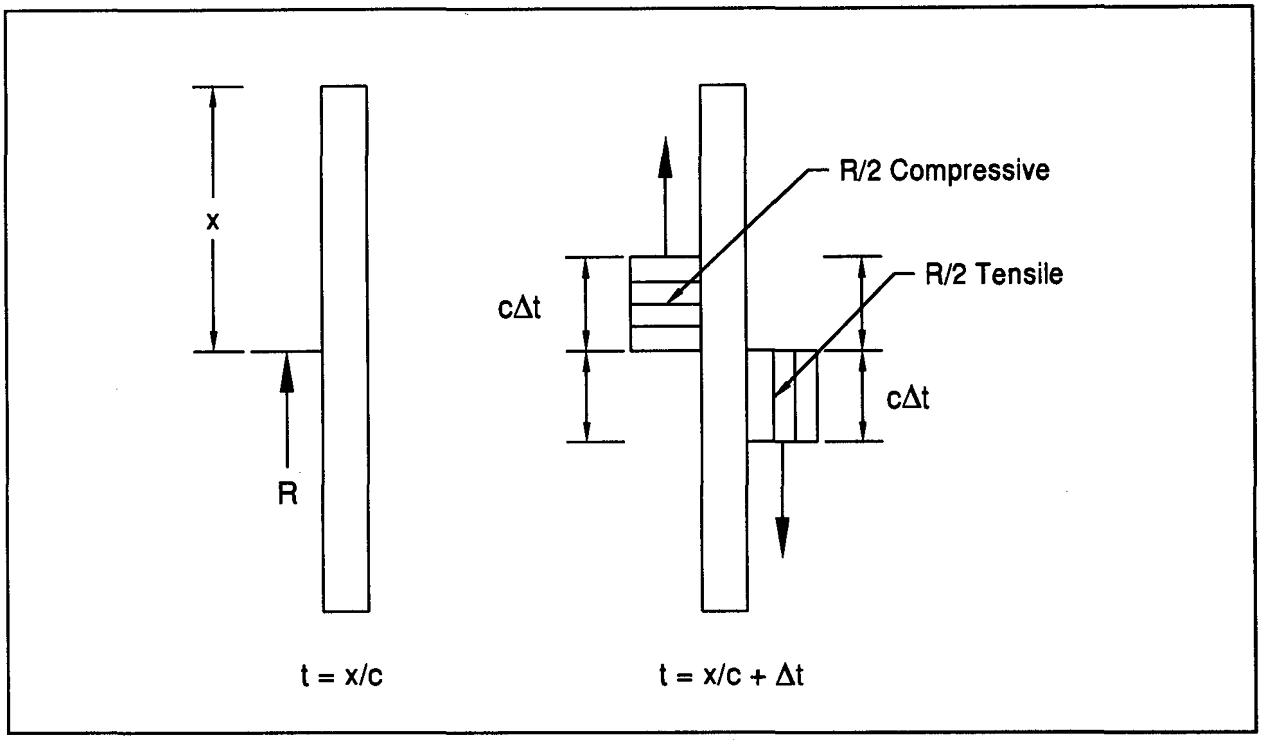

Figure A.5 Generation of Resistance Waves

The upward compression resistance wave reaches the top at time t=2x/c. The tensile resistance wave reaches first the pile bottom at t=L/c where it is reflected in compression. It then travels upward to the top where it arrives at time t=2L/c. This process is easily illustrated in an x-t plot such as figure A.6.

If we assume a free pile top, then forces in the resistance wave again have to cancel and the upward resistance waves are reflected downward in tension with a doubling of the upward directed velocities. Therefore, the top velocity effect will have a total magnitude of R/Z before time 2L/c.

We could also have assumed a fixed top (velocities have to cancel), resulting in a doubling of the upward resistance wave (R/2) for again a total difference of R. Any pile top condition in between completely free and completely fixed will have the same total force - velocity difference R due to superposition. Also, it is not a requirement that measurements be made at the pile top. Consideration of the upward resistance wave (magnitude R/2 in compression) with velocity equal to -R/(2Z) (negative for upward particle motion) gives a total difference between the force and proportional velocity of R/Z (=R/2Z-(-R/2Z)) as previously shown in figure A.6.

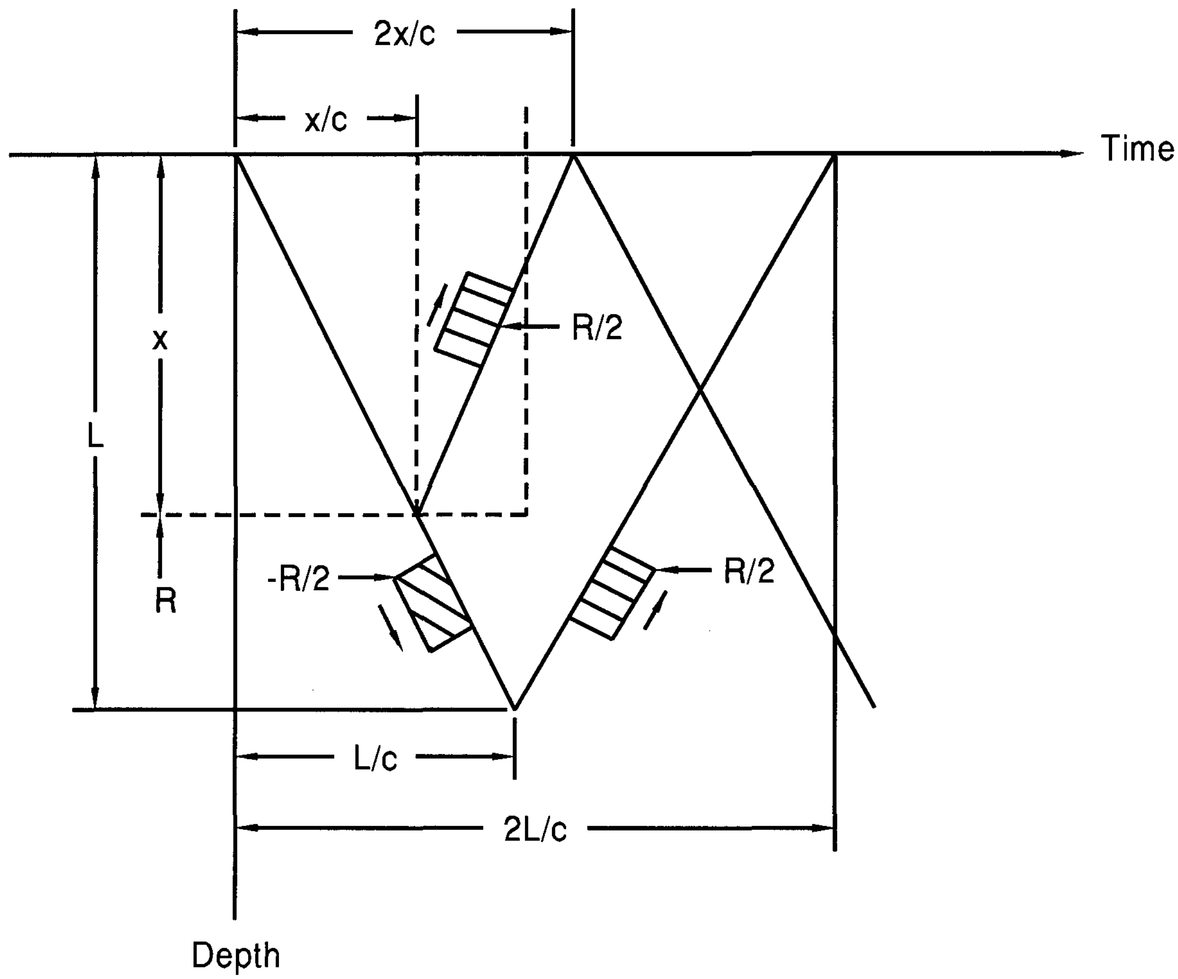

Figure A.6: Resistance Wave Reflections

APPENDIX B

INVESTIGATION OF DYNAMIC SOIL RESISTANCE ON PILES USING GRLWEAP

F. Rausche
Goble Rausche Likins and Associates, Inc., Cleveland, Ohio, USA

G.G. Goble
Department of Civil Engineering, University of Colorado, Boulder, Colo., USA

G. Likins
Pile Dynamics, Inc., Cleveland, Ohio, USA

ABSTRACT: GRLWEAP is a pure analysis program for the prediction of pile stresses and blow counts of a pile driven by an impact hammer. GRLWEAP was shown to produce good simulations of the hammer and pile behavior. For accurate predictions, a good knowledge of both the static and dynamic soil resistance behavior must also exist. However, several researchers have recommended that the damping model, originally proposed by Smith, be changed to an exponential or another more complex law.

The paper investigates various damping models and compares results. It compares GRLWEAP calculated force - velocity histories and evaluates the sensitivity of the bearing graph results relative to the various damping models.

The results from this study lead to additional options of the GRLWEAP program. Recommendations for the applications of the expanded soil model options are developed, documented and presented in the paper.

1 INTRODUCTION

Analysis of impact pile driving by the so-called wave equation method has become well accepted in many countries. In general, the approach yields satisfactory stress predictions and, combined with observed blow counts from restrikes, reasonably accurate bearing capacity predictions. Even though good progress towards improved predictions has been made since the original concept was proposed by (Smith 1960), two main error sources remain: The first one is an unknown hammer performance, and the second is unknown dynamic soil behavior. The first error source can only be eliminated by measurements, the dynamic modeling of the soil may be improved either by well correlated damping and quake parameters or by a more realistic soil model. This paper investigates relationships between different formulations of one part of the dynamic soil representation in the wave equation approach, the damping model.

The commonly used wave equation program GRLWEAP is based on the earlier introduced WEAP program (Goble, Rausche 1976) and offers several options for soil damping calculations. This paper investigates the differences between four of these options and develops relationships between them. A review of related approaches described in the literature will precede the formulations contained in GRLWEAP.

2 BASIC TERMS AND RELATIONSHIPS

In order to avoid confusing terminology the following definitions are proposed.

1. Static soil resistance, R_s, is a function of the relative displacement of the pile to the soil and is therefore assumed to be present both during static and dynamic loading. While R_s is a function of displacement and therefore varies with time, the related R_u, i.e., the ultimate static soil resistance is a constant ($-R_u < R_s < R_u$).

2. The damping resistance, R_d, is that portion of the soil resistance which is not present during static load applications. It varies in time and is commonly thought to be related to pile velocity.

3. The total resistance, R_t, is also often called the dynamic resistance. It is the sum of static and damping resistance. Of course, under static loads, damping resistance is zero and total resistance is then equal to the static resistance.

4. The slip layer is a zone in the pile-soil interface where one commonly expects the relative motion between pile wall and soil mass to occur.

GRLWEAP has been widely accepted and used in many countries around the world. Its manual recommends that the damping resistance is calculated according to Smith's original approach and includes a few proposed damping parameters which often yield reasonably accurate results. Most of these values are identical to those originally proposed by Smith. However, since there are no obvious links between Smith's model and standard geotechnical soil test parameters, several investigators of the dynamic behavior of piling have expressed concern that the current approach is unreliable for either previously untested soil conditions or certain extreme conditions (e.g., very high or very low pile velocities) for which no experience base exists. Limited dynamic laboratory tests (Gibson, Coyle 1968; Heerema 1979; Litkouhi, Poskitt 1980) also indicated that the damping forces do not vary linearly with pile velocity as is normally assumed by the standard wave equation approach. Furthermore, there exists a discomfort about ignoring the forces and motions of the soil beyond the slip layer.

Acceptance of new soil models has been slow, probably because none of the researchers has been able to demonstrate an improved correlation between dynamic predictions and static test results compared to existing methods. In fact, a complete set of generally acceptable dynamic soil resistance parameters is still missing for the non-linear damping model. Also, it is not certain that a more realistic damping model would yield much improved predictions of

Preceding page blank

pile bearing capacity with penetration per blow. After all, effects from capacity changes due to set-up or relaxation, residual stresses, differences between the dynamic and static failure modes, incomplete capacity activation (when the permanent set achieved by a hammer blow is small) are soil model deficiencies which often have a much greater influence on the analysis results than the choice of the soil damping model. However, the non-linear damping model could play an important role when soil behavior is characterized in an impact driving test performed at one particular hammer impact velocity and when these results are to be extended to other situations. For example, in an SPT test the hammer impact velocity is typically 3 m/s, while pile driving may be done at ram speeds of 5 m/s. Because of the non-linearity of the damping resistance, such differences may be important for a proper test interpretation.

3 DISCUSSION OF DAMPING APPROACHES

3.1 Smith damping

Smith represented the forces exerted in the pile-soil interface by an elasto-plastic spring to represent static resistance and a quasi linear dashpot to model the damping resistance (Figure 1). He also assumed that the soil mass beyond the slip layer was infinitely rigid. Thus, energy actually transmitted to the deforming and moving soil was tacitly included in the losses represented by spring and dashpot. Smith expressed the total resistance force exerted by the soil on the moving pile as follows:

$$R_t = R_s(1 + J_s v) \qquad (1.a)$$

with J_s [s/m] being Smith's damping factor and v the pile velocity. Actually, Equation 1.a cannot be directly used for calculations since the damping force would assume a sign given by the product of the temporary static resistance and the velocity. A meaningful result would only be obtained if the damping force had the sign of the velocity. Therefore, one calculates the Smith damping resistance using the absolute value of R_s and the total resistance then becomes

$$R_t = R_s + |R_s| J_s v \qquad (1.b)$$

Equation (1.b) shows both components of the total resistance very clearly and therefore is the preferred form.

3.2 Gibson and Coyle

Gibson and Coyle (1968) published results of triaxial tests at the Texas A&M University which compared the total dynamic resistance with the static values at various velocities. The authors concluded that

$$R_t = R_s + R_s J_T v^N. \qquad (2)$$

Clearly, this power law was closely modeled after the original Smith approach. The experiments indicated exponents of N = 0.18 for clays and N = 0.20 for sands.

3.3 Case damping

Goble and Rausche (1976) included the non-dimensional Case damping approach in the WEAP program. This

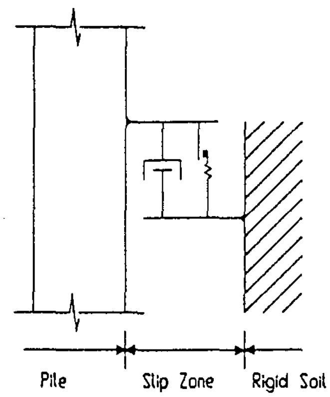

Fig. 1 Smith's soil model

approach had earlier been used for Case Method and CAPWAP capacity calculations (Rausche, Moses, Goble 1972). The soil resistance calculation is simplified to

$$R_t = R_s + J_c(Z)v \qquad (3.a)$$

where Z [kN/m/s] is the pile impedance (Z = EA/c where E is the pile's elastic modulus, A the cross sectional area, and c the stress wave speed). This simple concept can also be expressed in a Smith-type formula:

$$R_t = R_s + R_u J_{s2} v. \qquad (3.b)$$

In Equation (3.b), R_u is the ultimate static resistance which, of course, is constant and J_{s2} is a "Smith-2" damping factor. Since the product of R_u and J_{S2} [s/m] is a constant, the equivalent Case damping factor becomes

$$J_c = J_{s2}(R_u)/Z. \qquad (3.c)$$

Thus, the actual velocity multiplier is a constant ($J_s R_u$) and the damping force is linearly viscous.

3.4 Heerema's tests

Heerema (1979) used a flat metal plate in contact with a soil sample and also concluded that a power law should be used to calculate the total soil interface force. Thus, with the current definition,

$$R_t = R_s(a + J_H v^{0.2}) \qquad (4)$$

where "a" [1] and J_H [$(s/m)^{0.2}$] depend on the shear strength of the soil.

3.5 Litkouhi and Poskitt

In 1980 these authors performed model pile tests (model pile size 10 mm diameter by 260 mm length) and determined for skin and shaft separately the ratio R_t/R_s for various pile velocities and soil types (Litkouhi, Poskitt 1980). The author's then used the Gibson-Coyle approach and calculated both for skin and toe the parameter J_T and exponent N to obtain a best fit with observed data.

4 COMPARISON OF SMITH AND CASE (SMITH-2) DAMPING

Smith's approach gives lower damping resistance forces than the equivalent Case approach just before full static resistance activation and also later during unloading (or pile rebounding). For a quantitative evaluation of this difference, three comparison runs were performed (Table 1). They included a large offshore steel pipe (75 m long, 1830 mm diameter and 50 mm wall thickness), and both a small (275 mm square, 15 m long) and a large (900 mm square, 15 m long) concrete pile. As per the GRLWEAP recommendations, the quakes were all set to 2.5 mm except the toe quake for the large concrete pile which was the recommended 900/120 = 7.5 mm. Since the large quake caused a relatively slow increase of R_s, somewhat different results were obtained for the large concrete pile with the two damping approaches. For the other two cases, the results were nearly identical, however, only because the

Table 1. Input details of Case study

Case	Pile Type	Area m2	Length m	Hammer	Quakes Skin/Toe mm
1	72"Pipe	0.2750	75	MHU 1700	2.5/2.5
2	275mmPC	0.0756	15	5-ton drop	2.5/2.5
3	30"PSC	0.8100	15	D 62-22	2.5/7.5

"Smith-2" damping parameters were reduced by 10% compared to the standard "Smith-1" values. Table 2 lists results and indicates differences with respect to the standard Smith-1 result. These differences are generally small.

The original Smith damping approach yields small damping forces at the end of a hammer blow when the static resistance has decreased to small values. Figure 2, for example, shows calculated pile top velocities from analyses according to both Equations 1.b and 3.b. Figure 2 also includes damping forces as a function of time. These forces are the sum of all skin and toe damping values. The usually observed dampened behavior of the pile top velocity is obviously better represented by the Smith-2 analysis. For this reason, CAPWAP analyses which must match actual measurements yield reasonable results only with either the Case or Smith-2 damping approach. The toe damping resistance of a large displacement pile is the only exception and is sometimes best modeled with slowly increasing damping factors until the full static resistance has been activated. Therefore, ideally, a combination of both approaches would be chosen: Smith-1 until full static resistance activation is reached and Smith-2 thereafter. It is not complicated to use this combined resistance multiplier in damping calculations since the maximum activated resistance force, R_a, which has exactly these properties may be used as a multiplier instead of R_s or R_u.

5 DISCUSSION OF THE POWER LAW APPROACH

The experiments, leading to the exponential relationship between velocity and damping force, generally involved the measurement of a maximum damping force which occurred at that one instant when the sample was suddenly loaded.

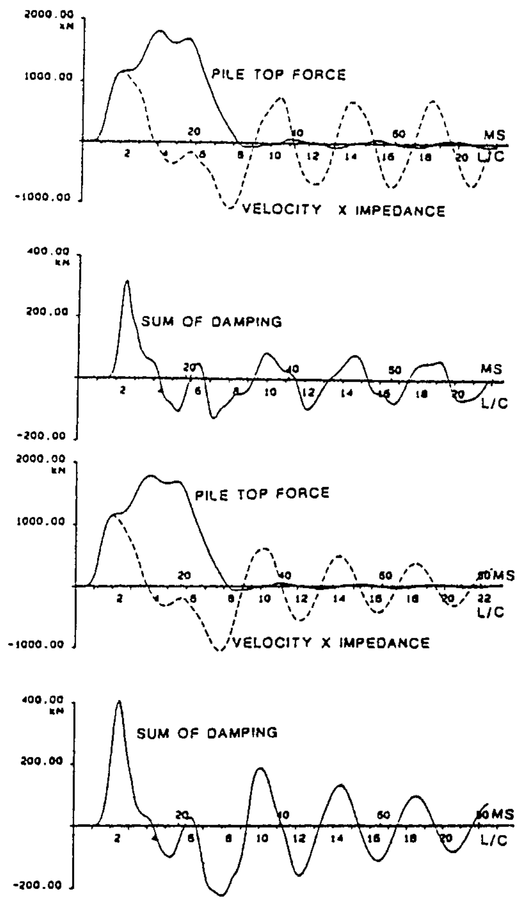

Fig. 2 Velocity force and damping forces over time for Smith-1 (top) and Smith-2 damping approach.

i.e., when the velocity was highest. However, under a hammer blow the velocity of a particular point along the pile increases to a maximum during a time period of several milliseconds, then relatively slowly decreases to smaller values and finally becomes negative during rebound. However, both before and after a pile segment reaches maximum velocity, the functional relationship between velocity and damping force was not determined by the experiments. Thus, it may be argued that the maximum damping force and associated maximum velocity define Gibson's damping factor, J_T. Under such circumstances, equivalent Smith damping factors can be calculated for maximum velocities which differ from a reference maximum velocity. Assuming that the reference maximum velocity is 3 m/s, the multipliers for equivalent Smith damping factors can be found in Figure 3. For example, if the maximum pile velocity is 1 m/s, the Smith factor should be approximately 2.4 times greater than normally assumed. Figure 3 may be helpful when determining standard Smith damping factors (for "normal" pile driving situations) from tests with very low (refusal situations) or high velocities (hammers with large drop heights). It also shows that the standard Smith damping factors could yield highly inaccurate results at very low maximum velocities.

Table 2. Comparison of GRLWEAP damping approaches with standard Smith damping results

Case/ Model	Damping Skin/Toe s/m	Capacity at 150 B/m kN	Diff. %	Capacity at 300B/m kN	Diff. %	Max. Tension Stress MPa	Diff. %	Max. Compres. Stress MPa	Diff. %
1/Smith 1	.6/.165	36400		43500		71.0		268	
1/Smith 2	.54/.15	36700	0.8	43600	0.2	76.0	7.0	270	0.7
1/Gibson (N=.18)	1.25/1.25	29250	-19.6	33500	-23.0	109.0	53.5	269	0.4
1/Gibson/GRL (N=.20)	1.25/1.25	39700	9.1	42600	-2.1	113.0	59.2	263	-1.9
1/Gibson/GRL (N=.18)	1.25/1.25	40000	9.9	42900	-1.4	115.0	62.0	263	-1.9
2/Smith 1	.165/.5	1390		1610		7.2		25.9	
2/Smith 2	.15/.45	1410	1.4	1620	0.6	7.0	-2.8	26.4	1.9
2/Gibson	.65/.65	980	-29.5	1170	-27.3	4.5	-37.5	26.0	0.4
2/Gibson/GRL	.65/.65	1370	-1.4	1560	-3.1	5.9	-18.1	25.3	-2.3
3/Smith 1	.165/.5	2600		3460		6.2		10.5	
3/Smith 2	.15/.45	2430	-6.5	3260	-5.8	6.2	0.0	10.5	0.0
3/Gibson	.65/.65	1660	-36.2	2400	-30.6	6.6	6.5	11.1	5.7
3/Gibson/GRL	.65/.65	2300	-11.5	3150	-9.0	6.4	3.2	10.6	1.0

Gibson and Coyle's equation cannot be used directly to calculate damping forces for all times during a hammer blow. Modifications must be made to Equation 2 to (a) assure velocity opposing damping forces and (b) avoid mathematically undefined values. A usable equation would read:

$$R_t = R_s + |R_s| J_T |v|^N \{v/|v|\}. \qquad (5.a)$$

The factor in {} is merely the sign of velocity v. Equation (5.a) is the "Smith-3" or Gibson option in GRLWEAP. As will be shown, it does not yield satisfactory results (Figure 4.a). Obviously, the Gibson approach needs further modifications before the power law approach can become useful. First the R_s multiplier in (5.a) was replaced by R_u as proposed earlier in this paper. Then the velocity, v, in the power term was replaced by v_x which is the maximum velocity having occurred prior to or at the time during a hammer blow at which R_t is calculated. Equation (5.a) then becomes

$$R_t = R_s + R_u J_W v_x^N \{v/v_x\} \qquad (5.b)$$

The temporary maximum velocity, v_x, is increasing before and constant after the absolute maximum velocity has been reached. It is never negative or decreasing which is an important feature as will be shown. Furthermore, since v_x is constant throughout most of the analyzed time (it is constant after the peak velocity is reached), a nearly linearly viscous approach results. Obviously, at the instant when maximum velocity is reached $R_d = J_T R_u v_x^N$ (since $v = v_x$) as exactly recommended by Gibson and Coyle. For ease of reference Equation (5.b) will be referred to as the Gibson/GRL method; it is the Smith-4 method in GRLWEAP. Both methods have been used to reanalyze the examples

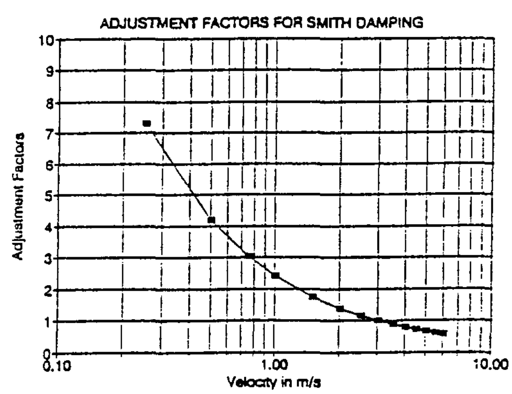

Fig. 3 Multipliers for conversion of Gibson to Smith-1 damping factors.

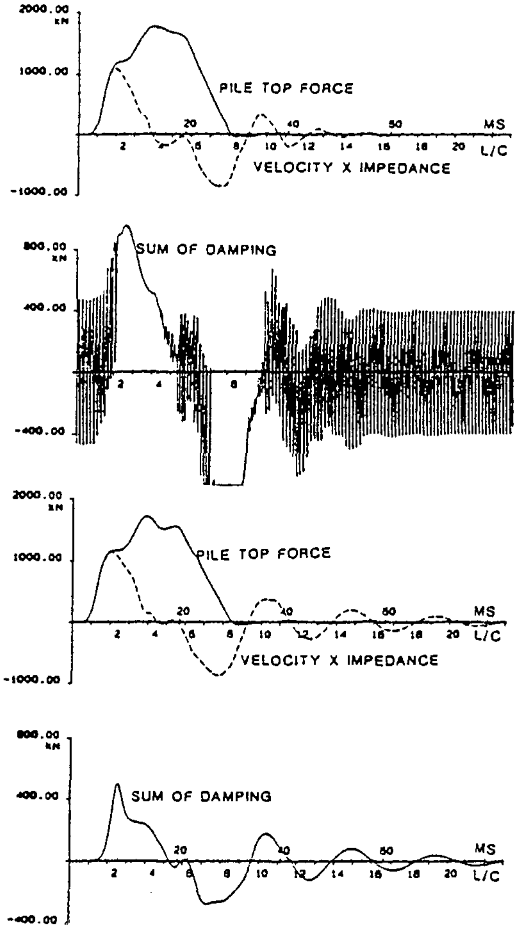

Fig. 4 Velocities, forces at pile top and damping forces as a function of time for Gibson and Gibson-GRL damping approaches.

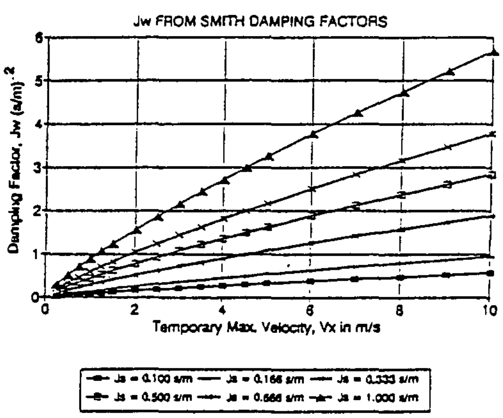

Fig. 5 Conversion of Smith to GRL damping factors.

discussed previously. Results were again entered in Table 2. The Gibson, J_T, and Gibson/GRL (WEAP), J_W, damping factors were used identically for skin and toe with 0.65 and 1.25 $(s/m)^N$ and the exponent N with 0.18 as for clay. These values correspond to recommendations contained in the literature. Two comparison analyses were also run for the same situation and N = 0.20 and 0.18 using the new approach. It can be concluded that, for practical purposes, there are no significant differences between these two exponents and N = 0.20 is sufficiently accurate.

Table 2 indicates that Gibson's method yields very low capacities compared to the standard Smith approach which is attributed to very high damping at low velocities both before and after maximum velocity (Figure 4.a). On the other hand, the new Gibson/GRL approach yields very reasonable results. Furthermore, while Gibson's damping force versus time relationship includes high frequency variations whenever the velocity approaches zero, Equation (5.b) produces a smooth and realistically dampened relationship. This is demonstrated for the small concrete pile in Figure 4.

The new method would not be very useful without a set of recommended damping factors. Figure 5 provides a conversion from Smith-1 to Gibson/GRL damping factors with N = 0.2 and including a 10% correction for the R_s to R_x conversion. The Figure gives corrections for various commonly encountered Smith-1 damping factors. For example, for clay one normally uses 0.67 s/m as a skin damping factor. For this Smith value Figure 5 suggests 1.44 $[(s/m)^{0.2}]$ for J_{GRL} at v_x = 3 m/s. For a high velocity v_x = 5 m/s, J_W would be 2.17 $[(s/m)^{0.2}]$. These conversions would approximately yield the same results from Smith-1 and Gibson/GRL. However, the purpose of using the new method would be to obtain valid results over the whole range of possible v_x values. It would, therefore, be reasonable to assume that Smith-1 provides relatively reliable results for an average velocity maximum of say v_x = 3 m/s, find the corresponding J_W damping factor for this velocity and the soil type, and use that factor for all other, high or low velocity situations.

6 SUMMARY

A new damping method has been developed and included in GRLWEAP. It has the advantage of

1. yielding results in good agreement with the Smith approach which has been well correlated for a standard situation such as the ones analyzed,

2. producing a well dampened pile top behavior over long analysis times which best matches measured pile velocities histories and

3. generating calculated damping forces which are physically possible. This new formula combines the past experience of wave equation and CAPWAP correlations with laboratory measured values. It appears that the approach can be directly used, even without additional experimental work. To accomplish this, the current standard Smith damping factors may be easily converted to the Smith-4 or WEAP J_W factors for any appropriately chosen reference velocity, e.g., V_X = 3 m/s (see also Figure 5).

4. The study also indicated that under normal circumstances Smith-1 damping factors may be replaced by Smith-2 values with a 10% decrease.

REFERENCES

Gibson, G. C. and Coyle, H. M. 1968. Soil damping constants related to common soil properties in sands and clays. Research Report No. 125-1, Texas Transportation Institute, Texas A&M University.

Goble, G. G. and Rausche, F. 1976. Wave equation analyses of pile driving-program manuals. Department of Transportation, Report No. FHWA IP-76-14.3.

Heerema, E. P. 1979. Relationships between wall friction, displacement velocity, and horizontal stress in clay and in sand, for pile driveability analysis. Ground Engineering, Vol. 12, No. 1.

Litkouhi, S. and Poskitt, T. J. 1980. Damping constants for pile driveability calculations. Geotechnique 30, No. 1: 77-86.

Rausche, F., Moses, F. and Goble, G. G. 1972. Soil resistance predictions from pile dynamics. Journal of the Soil Mechanics and Foundations Division, ASCE, Vol. 98, No. SM9, Proc. Paper 9220: 917-937.

Smith, E. A. L. 1960. Pile driving analysis by the wave equation. Transactions of ASCE, Paper No. 3306, Vol. 127, Part 1.

APPENDIX C

WAVE EQUATION ANALYSIS

C.1 INTRODUCTION

During recent years, pile driving analysis "by the wave equation" has become a frequently used tool in design and construction control. Engineers have either worked with "canned programs" such as WEAP or TTI or they have retained the services of a consulting firm to analyze their particular pile-soil systems. The proprietary GRLWEAP program is most widely used throughout the world.

All users should familiarize themselves with the background of this analysis to avoid misinterpretation. The program manuals (GRL and Associates, 1995 and Hirsch et al., 1976) are, therefore, a highly recommended source of information. This appendix briefly summarizes mathematical and physical details pertaining to GRLWEAP.

C.1.1 The Wave Equation Pile Model

Figure C.1 shows a pile and its model. For a wave equation analysis to be truly applicable, the pile should be a long and slender (length of at least 10 times the width) rod of elastic material. The pile may consist of different materials.

Figure C.1 shows a lumped mass pile model in its most general form which consists of a mass, spring and sometimes a dashpot. The pile is segmented and average properties: A (cross sectional area), E (Young's Modulus) and ρ (mass density) are assigned to each segment of length ΔL (usually 0.305 ft or 1 m).

The spring is fully described by a stiffness value, k_p:

$$k_p = \frac{EA}{\Delta L} \tag{C.1}$$

The segment's mass is defined as:

$$m_p = A(\Delta L)\rho \tag{C.2}$$

and the dashpot constant may be expressed as a small percentage (say 1 percent), p_p, of the pile's impedance, Z. Thus, with:

$$Z = EA/c = \sqrt{(k_p m_p)} \tag{C.3}$$

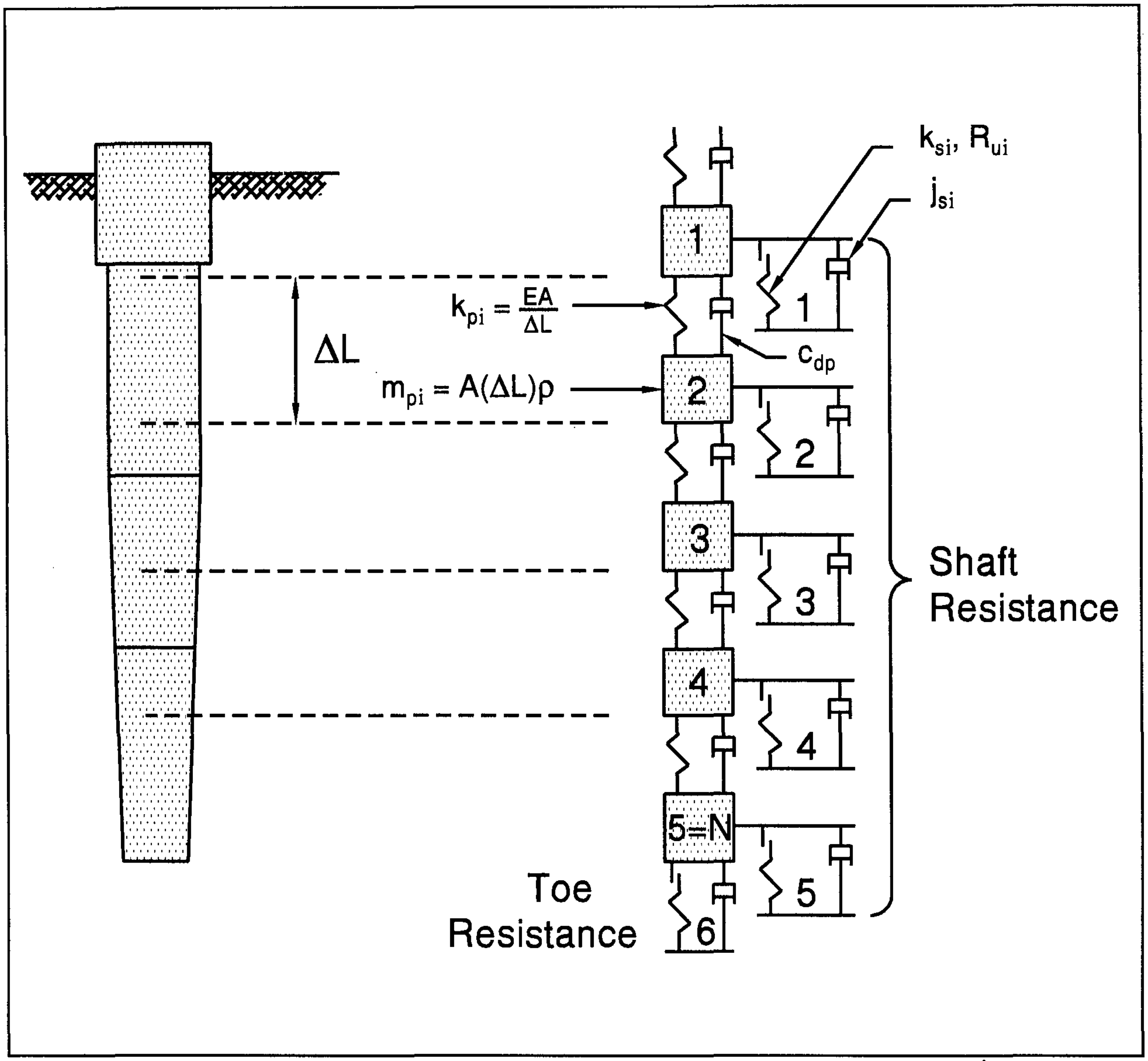

Figure C.1: Segmentation of a Non-Uniform Pile

the dashpot constant is:

$$c_{dp} = p_p Z \tag{C.4}$$

These quantities completely describe the pile's dynamic behavior unless slacks are present. Slacks allow for deformations between pile segments with reduced or zero forces. For example, a tension slack allows for a zero tension force separation between two segments. This separation may be unlimited as is the case with "can" splices. Compressive slacks may occur in mechanical splices. These devices may have a slight separation before hammer impact. Thus, the pile section above the mechanical splice must be under compression before normal wave transmission can take place. Since such devices absorb some wave energy, it is advisable to use bilinear or nonlinear properties for springs with slacks. For further details on this relatively infrequent situation, the GRLWEAP manuals should be consulted.

C.1.2 The Wave Equation Hammer Model

GRLWEAP distinguishes the following hammer types: open end diesel (OED), closed end diesel (CED) and external combustion hammers (ECH). The ECH may be divided into single acting air-steam, double acting air-steam, single and double acting hydraulic, rope suspended, free fall and other hammer types. The ram is modeled by one or more segments of typically 1 m length.

For hammers with relatively long rams, several ram segments of approximately 0.305 ft (1 m) length should be assigned. The ram segment stiffness and masses are computed from averages of ram areas, moduli and mass densities as for the pile model. The computation of the ram spring stiffnesses may be complicated by a nonuniform or lead filled ram. However, it is unnecessary to use great accuracy in these computations. If a ram stiffness has been computed and a hammer cushion material is present then the two stiffnesses are combined into a single one using Kirchhoff's Law.

Newer ECH types include both single and double acting hydraulic hammers (HH). Rams of single acting HH often fall absolutely freely after being lifted by a hydraulic cylinder which then quickly retracts. Double acting HH have been built with internal ram velocity monitors. As for all double acting ECH, it is not necessary to model these double acting features since these hammers are treated like a single acting ones with an "equivalent stroke."

Diesel hammers include an <u>impact block</u> between ram and cushion. The corresponding mass, m_a, and stiffness, k_a, are easily computed from average cross sectional area, mass density and Young's Modulus. For the diesel hammer, the bottom ram spring is combined with the impact block spring using Kirchhoff's law. Thus, with k_r as the stiffness of the bottom ram segment, the combined spring stiffness is:

$$k_{ra} = \frac{k_a k_r}{k_a + k_r} \tag{C.5}$$

Masses and springs are the major components of a hammer model. Sometimes, the elastic behavior of the hammer springs cannot be described by an ideal elastic behavior. In those cases, coefficients of restitution and round-out deformations may be needed. Such extensions to the basic hammer model will be described in the section on driving system modeling.

C.1.3 The Thermodynamic Model of Diesel Hammers

Depending on the particular wave equation program used, thermodynamic modeling may be very simple or more complex. For example, the TTI program uses only a preprogrammed force versus time function which the GRLWEAP program calculates pressure according to the Gas Law.

There are two types of diesel fuel injection; liquid and atomized injection. For liquid injection, impact of the ram atomizes the fuel; for atomized injection, high pressure injectors are used. GRLWEAP models these two mechanisms differently, but distinguishes the following three phases for both types of injection:

(a) compression.

(b) ignition.

(c) expansion.

The GRLWEAP thermodynamic model (figure C.2) requires the input of the Gas Law's compression and expansion exponents, the compressive stroke, the cross sectional area of the ram, the combustion chamber volume at impact and the maximum combustion pressure. For impact atomization, the combustion delay time (positive or negative to model pre-ignition) and the duration of ignition are needed. For atomized injection the two corresponding inputs are volume where ignition starts and volume when combustion ends. Further details on diesel hammer models can be found in GRL and Associates, Inc. 1995.

C.1.4 The Wave Equation Model of Driving Systems

The wave equation represents the hammer cushion, helmet, and pile cushion as a spring-mass-spring system hammer. Sometimes, a dashpot is also included. The model only requires the hammer cushion stiffness, k_c, the helmet mass, m_h, and the pile cushion stiffness, k_{cu}. The following <u>extensions</u> are made.

C.1.4.1 Bilinear Springs

For driving system components, all wave equation programs require the input of a coefficient of restitution for each spring. The coefficient of restitution may be denoted c_c for the hammer cushion spring, and c_{cu} for the pile cushion spring. The coefficient of restitution increases the stiffness during the expansion of a spring (figure C.3). In that manner, energy dissipation of the

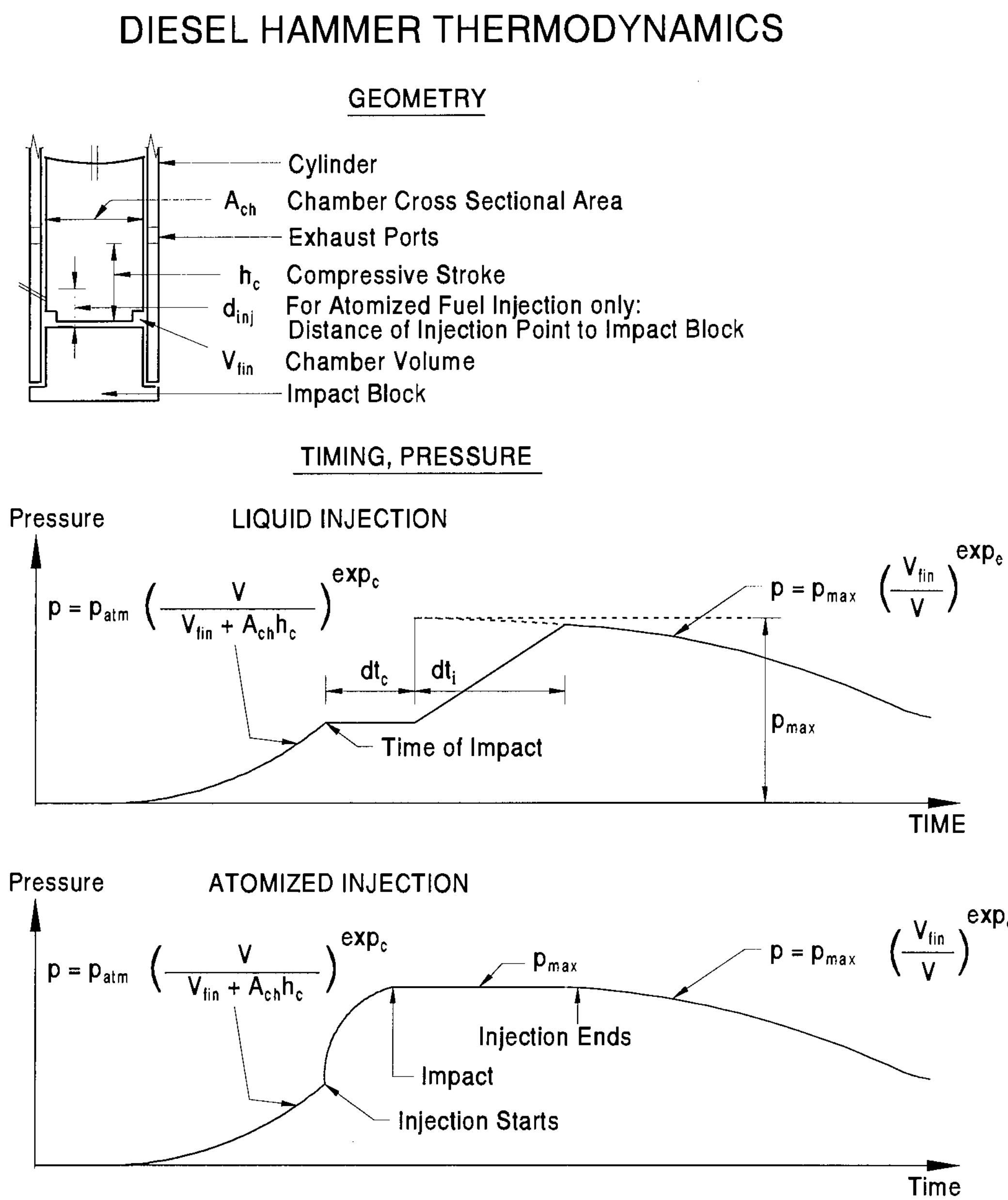

	p_{atm}	Atmospheric Pressure
	p_{max}	Maximum Combustion Pressure
Note:	$p_{max} A_{ch}$	Explosive Force
	dt_c	Combustion Delay
	dt_i	Ignition Duration
exp_c	Compression	Gas Law Exponents
exp_e	Expansion	Gas Law Exponents

Figure C.2: Diesel Hammer Thermodynamics

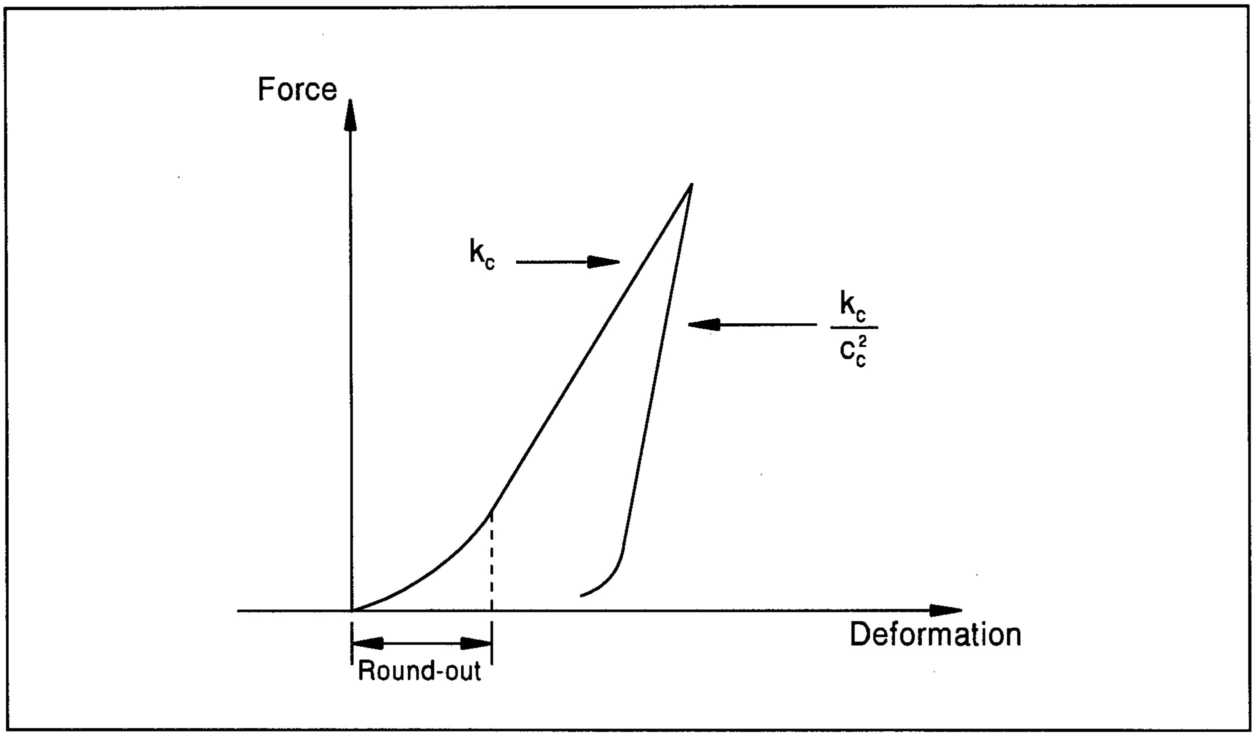

Figure C.3: Force Deformation of Non-linear Springs

spring can be represented. For example, the hammer cushion spring expansion stiffness is:

$$k_{ce} = \frac{k_c}{c_c^2} \tag{C.6}$$

C.1.4.2 Nonlinear Springs

GRLWEAP uses partially nonlinear springs for the curvilinear force deformation relationship at the onset of impact. Figure C.3 shows the force nonlinearity modeled by a linearly variable stiffness within the range of a specified "round-out deformation." This concept is particularly useful for the modeling of soft cushions.

C.1.4.3 Hammer Cushions/Dashpots

Improved agreement between computed and measured forces and motions can be achieved if the wave equation includes a dashpot in parallel with the hammer cushion spring. The dashpot constant is computed using a small percentage, p_h, of the impedance of the ram-cushion system. Thus:

$$c_{dc} = p_h\sqrt{m_r k_c} \tag{C.7}$$

This dashpot parameter cannot be derived from basic material properties. Usually GRLWEAP assigns a c_{dc}- value automatically.

C.1.5 The Soil Model

The wave equation soil model relates the soil resistance forces to the pile motion. For example, the static soil resistance at segment i is denoted by R_{si} and is related to the segment displacement u_i. The dynamic resistance, R_{di}, is directly related to the segment velocity, $\dot{u}_i$. It is assumed that the soil does not move.

For the static resistance, a soil compression value, q_i, is introduced and called quake. Usually, the engineer assigns one quake value for all pile shaft segments and one for the toe. The quake is that deformation at which the elasto-plastic soil resistance value reaches R_{ui} (see figure C.4). Thus:

$$R_{si} = u_i(R_{ui}/q_i) \tag{C.8}$$

The bracketed term is the soil stiffness. The static resistance can never become greater than the ultimate resistance, or:

$$R_{si} \leq R_{ui} \tag{C.9}$$

When the piles rebounds, R_{si} decreases according to its stiffness, R_{ui}/q_i. Denoting a negative resistance bound by R_{ei}, the static resistance must obey:

$$R_{si} \geq -R_{ei} \tag{C.10}$$

For end bearing:

$$R_{ei} = 0 \tag{C.11}$$

and for shaft resistance:

$$R_{ei} = R_{ui} \tag{C.12}$$

A shaft resistance percentage, r_s, is introduced. The total shaft resistance, R_{su}, therefore, becomes:

$$R_{su} = r_s R_{ut} /100 \tag{C.13}$$

where R_{ut} is the total ultimate pile capacity being analyzed, and R_{su} is distributed to the individual pile segments according to static formula considerations by the analyzing engineer.

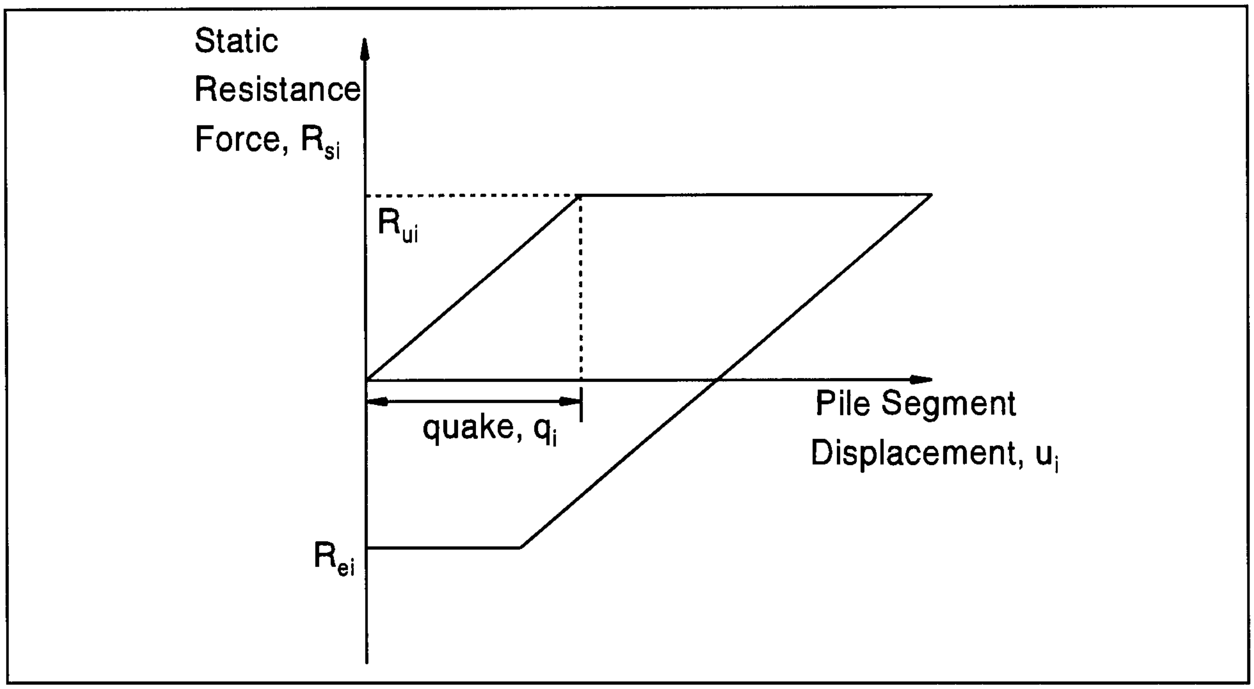

Figure C.4: Static Soil Resistance versus Pile Displacement

The end bearing, R_{tu}, is:

$$R_{tu} = (100 - r_s)R_{ut}/100 \tag{C.14}$$

Soil damping (figure C.5) is modeled in several ways. However, the approach introduced by Smith is the one most commonly used. It calculates the dynamic soil resistance as:

$$R_{di} = j_{si} R_{si} \dot{u}_i \tag{C.15}$$

The Smith damping factor, j_{si}, has been partially non-dimensionalized by the static resistance at the same segment and therefore has dimension second/meter (s/m). For most cases, one shaft damping factor is chosen for all shaft segments.

It is important to investigate Smith's concept. Obviously, as long as the static resistance, R_{si}, is zero, damping is zero even for non-zero velocities. As the static resistance increases so does the effective damping factor J_{si} R_{si}. Once R_{si} reaches the ultimate value, R_{ui}, it will not further change until rebound starts. Thus, the effective damping factor now remains constant and viscous damping occurs. Later, during rebound, damping decreases quickly since R_{si} decreases. Thus, Smith's approach often has been blamed for a relatively undampened behavior of the calculated pile quantities. As discussed in appendix B, GRLWEAP therefore offers also the "Viscous Smith" damping approach:

$$R_{di} = j_{si} R_{ui} \dot{u}_i \tag{C.16}$$

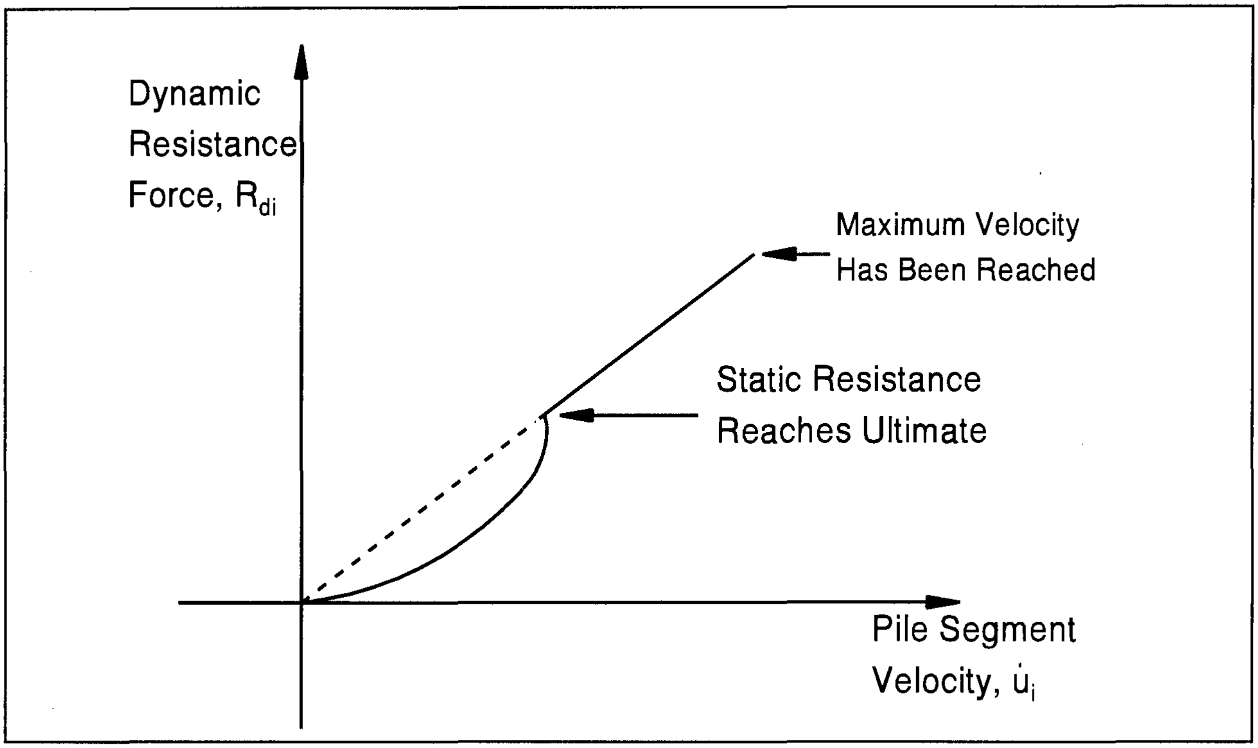

Figure C.5: Dynamic Soil Resistance versus Pile Velocity

C.1.6 Force Balance at Hammer or Pile Segment

Consider the segment shown in figure C.6. The segment is subjected to forces, F_{ti} and F_{bi}, from neighboring springs and dashpots. These forces can be computed if the displacements and velocities of the top and bottom neighbor segments (i-l and i+l, respectively) are known:

$$F_{ti} = k_{pi}(u_{i-1} - u_i) + c_{dp}(\dot{u}_{i-1} - \dot{u}_i) \tag{C.17}$$

The stiffness, k_i, and the dashpot coefficient, c_{di}, respectively, represent springs or dashpots of either hammer, pile, or driving system. They act on the top of the segment mass, m_i. Similarly one finds:

$$F_{bi} = k_{pi+1}(u_i - u_{i+1}) + c_{dp+1}(\dot{u}_i - \dot{u}_{i+1}) \tag{C.18}$$

The total soil resistance, R_i, if present, acts on segment i:

$$R_i = R_{si} + R_{di} \tag{C.19}$$

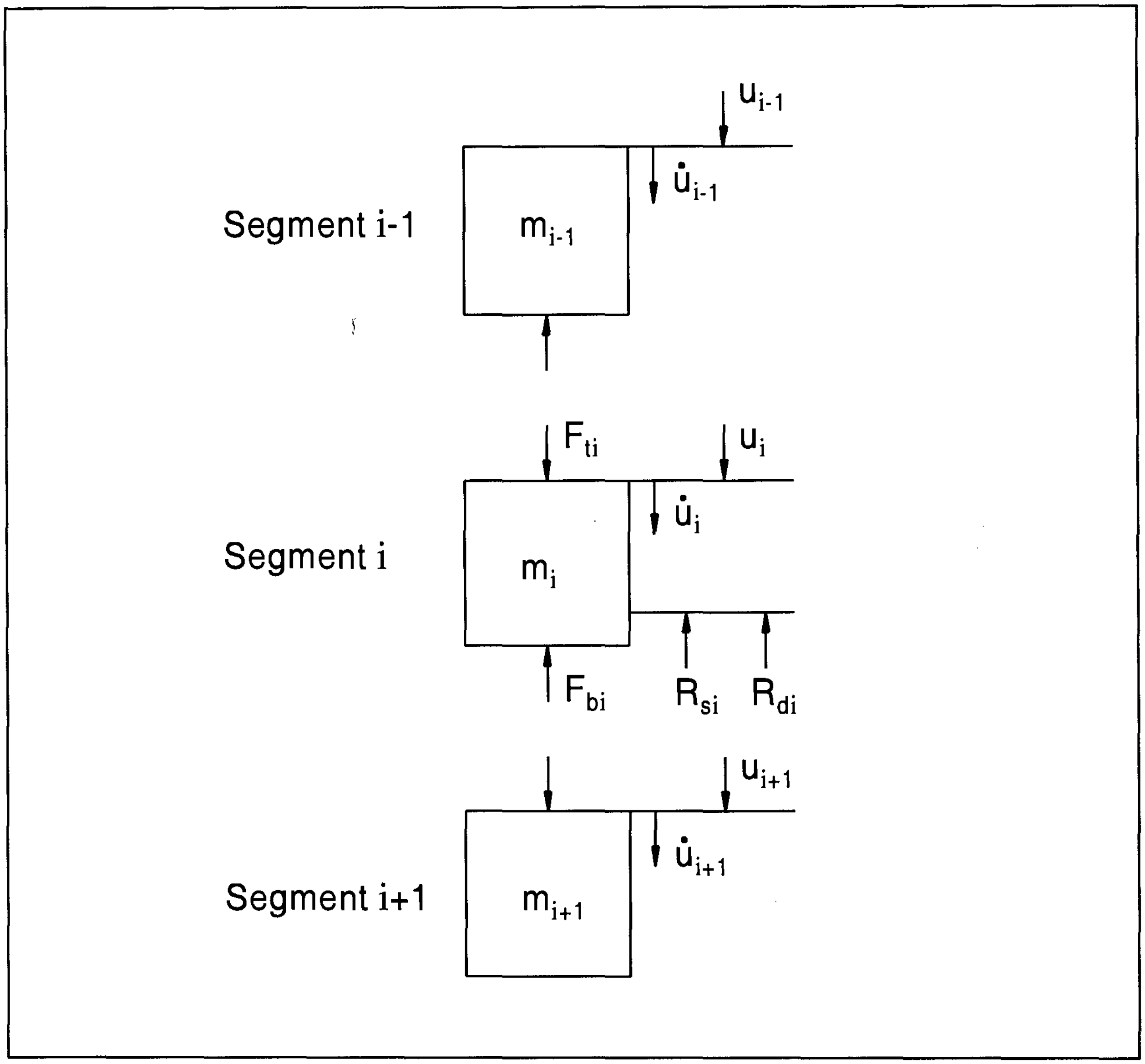

Figure C.6: Forces Acting on Segment i

From Newton's Second Law, the acceleration, $\ddot{u}_i$, of segment i can be computed:

$$\ddot{u}_i = g + \frac{F_{ti} - F_{bi} - R_i}{m_i} \tag{C.20}$$

where g is the gravitational acceleration (32.17 ft/s^2 or 9.81 m/s^2). For the pile segments, g is usually set to zero, which implies that the soil resistance forces necessary to support the pile weight are not included in the dynamic analysis. Therefore, the bearing capacity, dynamically determined by wave equation analysis does not include the pile weight (an exception is the residual stress analysis).

C.1.7 Integration

For integration, a time increment, Δt, must be determined small enough for a stable computational process and large enough for negligible accumulated round-off errors and economical time of computation. Experience shows that sufficiently accurate results may be obtained if:

$$\Delta t = (1/\phi)\sqrt{\mathrm{Min}(m_i/k_i)} \tag{C.21}$$

The square-rooted expression is the minimum mass to stiffness ratio of any neighboring mass-spring combination, and actually represents the shortest wave travel time in any one segment of the total system. This is called the critical time. The factor, ϕ, is a "safety factor" against numerical instability; it must be greater than one (1).

After the acceleration, $\ddot{u}$, of a segment is determined, integration begins. Both velocity, $\dot{u}$, and displacement, u, are computed from the integration of acceleration. In the beginning of the non-residual analysis, the ram has an initial velocity; helmet and pile masses are at rest. Denoting the known velocity and displacement values by $\dot{u}_{oi}$ and u_{oi}, respectively (the subscript "o" stands for "original"), and the values after a time increment has passed by $\dot{u}_{ni}$ and u_{ni}, ("n" stands for "new") new values can be computed as:

$$\dot{u}_{ni} = \dot{u}_{oi} + \ddot{u}_i \Delta t \tag{C.22}$$

and:

$$u_{ni} = u_{oi} + \dot{u}_{oi} \Delta t \tag{C.23}$$

This is a simple Euler integration; the displacement is computed by assuming that the velocity stays constant during the time increment. An improved, so-called Newark, method of calculation is:

$$\dot{u}_{ni} = \dot{u}_{oi} + (\ddot{u}_{oi} + \ddot{u}_{ni}) \frac{\Delta t}{2} \tag{C.24}$$

and:

$$u_{ni} = u_{oi} + \dot{u}_{oi} \Delta t + (2\ddot{u}_{oi} + \ddot{u}_{ni}) \frac{\Delta t^2}{6} \tag{C.25}$$

which assumes that the acceleration is linearly variable during an interval Δt. Both approaches are used: the Euler integration for a prediction of velocity and displacement (before forces F_{ti} and F_{bi} are calculated) and the more complicated formula as a refined calculation after the acceleration has been determined.

C.1.8 Computational Procedure

In the simplest case of an external combustion hammer and no consideration of residual stresses, the following procedure is followed. The initial conditions imposed on the model are zero displacements for all but the ram segments which may be placed slightly above (negative displacements) the anvil or hammer cushion spring. The ram segments are the only segments not at rest. They are given an initial velocity which is computed from rated hammer stroke, h, and efficiency, e_h:

$$v_{ri} = \sqrt{2ghe_h} \tag{C.26}$$

After one or more time increments, integration of the ram velocity yields a displacement of the ram which brings the ram into contact with the hammer cushion spring. The ram displacement is greater than that of the helmet and therefore the hammer cushion spring compresses which in turn causes a hammer cushion compression force. This force causes the helmet to accelerate and the ram to decelerate. Integration of acceleration or deceleration leads to new velocity values for helmet and ram. New velocity values are also integrated and yield new displacement (and thus different force) values.

A complication exists where at the time the force balance is evaluated, the displacements and thus the forces are not known for the new time increment. It must be first assumed that velocities have not changed and displacements are approximately calculated. This first assumption leads to errors which are lower when time increments are very small. Because of the practical limit of both computational effort and accumulated round-off error, a prediction-correction type analysis has proven advantageous.

After forces, accelerations and velocities are computed, the new velocities are compared with the previous ones. If they do not meet a convergence criterion, a new cycle of computation may be started within the same time increment using the new forces and displacements for an improved set of velocity values.

Once the pile displacements decrease (pile rebound) due to the action of resistance forces, a maximum pile toe displacement has been determined. According to Smith, the blow count is calculated by subtracting the toe quake from this maximum toe penetration. This approach assumes that the pile rebounds as much as the toe quake. Considerable errors may be introduced by this definition of blow count when shaft and toe quakes differ substantially. In particular, where there is only a small end bearing, the toe quake may have little effect on both pile tip penetration and rebound. Rather both shaft and toe quakes generally govern the magnitude of the final pile set. For this reason, a weighted average of the quake values is calculated in GRLWEAP:

$$q_{av} = \frac{1}{N} \sum_{i=1}^{N} q_i R_{ui} \tag{C.27}$$

This value is subtracted from the maximum toe displacement and inverted to yield the blow count.

For diesel hammers, the computational procedure differs in the beginning of the analysis. First, the ram velocity at the time of port closure is calculated under the assumption of no friction losses. Then, the compression cycle calculation begins, again under the assumption of no losses in the hammer. This cycle already involves the calculation of soil resistance forces since the diesel hammer precompression forces are transmitted to the pile where they produce significant soil compressions. Approximately 2 ms prior to impact or ignition, the ram velocity, v_r, is reduced by the hammer efficiency, with an exponent of approximately 1/2, yielding an impact velocity:

$$v_{ri} = v_r (e_h)^{exp} \tag{C.28}$$

The analysis then proceeds until the ram has rebounded to the exhaust ports. The stroke is then simply calculated assuming no friction losses.

C.1.9 Residual Stress Analysis Procedure

This analysis type corrects the shortcomings of the standard wave equation procedure as follows. The false assumption of zero soil and pile stresses in the beginning of the analysis is corrected by always performing several analyses in sequence and using the final stress pattern of one analysis for the initial conditions of the next one. Thus, a continuous driving process is actually simulated with as many hammer blows as needed to reach convergence of the residual soil and pile forces at the end of consecutive blows. This approach also allows for a correction of the very simplistic blow count calculation of the basic wave equation approach. The reason is that after residual stress convergence the pile compression is constant from blow to blow and the permanent pile set is evident from the permanent penetration of any point along the pile, not just the pile toe. Thus, the blow count can now be calculated from the inverse of the set occurring between the last two, converging "hammer blows" of an analysis. This approach accurately includes the effect of different quake magnitudes or large pile deformations.

APPENDIX D

DYNAMIC PILE TESTING AND ANALYSIS: CASE METHOD AND CAPWAP

D.1 INTRODUCTION TO CASE METHOD

The "Case Method" refers to the methods developed at Case Institute of Technology beginning in the 1960's. The objective of that research effort was a real-time calculation of pile bearing capacity for every hammer blow from pile top force and acceleration measurements. Today, the term "Case Method" refers to both measurement techniques and interpretations of soil effects, pile stresses, pile integrity and hammer performance by use of a Pile Driving Analyzer. The data is often then subjected to further rigorous numerical analysis using the CAPWAP program.

D.1.1 Case Method Capacity Derivation

The following derivations are based on one dimensional wave propagation. For a pile with impedance, Z, the force at time t and the measuring location M, $F_M(t)$, and the velocity $\dot{u}_M(t)$ may be used to determine both upward and downward traveling waves at time t [$F_M^{\uparrow}(t)$ and $F_M^{\downarrow}(t)$]. If measured forces and velocities at time j are denoted by F_{Mj} and $\dot{u}_{Mj}$, respectively, then the two waves at the point of measurement are:

$$F_{Mj}^{\uparrow} = (F_{Mj} - Z\dot{u}_{Mj})/2 \qquad \text{(D.1)}$$

$$F_{Mj}^{\downarrow} = (F_{Mj} + Z\dot{u}_{Mj})/2 \qquad \text{(D.2)}$$

If a resistance force at location x below the pile top begins at time $t = t_1 + x/c$ (caused by an impact at time $t = t_1$ at the pile top), then two waves are created, each having a magnitude of $R_x/2$ (figure D.1). To satisfy equilibrium and continuity, the upward wave is in compression and the downward wave in tension. The upward compressive wave reaches the top at time $t_x = t_1 + 2x/c$. The downward tensile wave reflects at the pile bottom at time $t_L = t_1 + L/c$ as a compression wave, and then travels upward, arriving at the top at time $t_2 = t_1 + 2L/c$. A resistance force at the pile bottom R_b beginning at time $t_L = t_1 + L/c$ causes a compressive upward traveling wave which also arrives at the pile top at time $t_2 = t_1 + 2L/c$.

If all resistance forces are constant throughout the time $t_1 + x/c < t < t_1 + 2(L-x)/c$, then at time $t_2 = t_1 + 2L/c$, the measured force and velocity data contain the effects of:

Preceding page blank

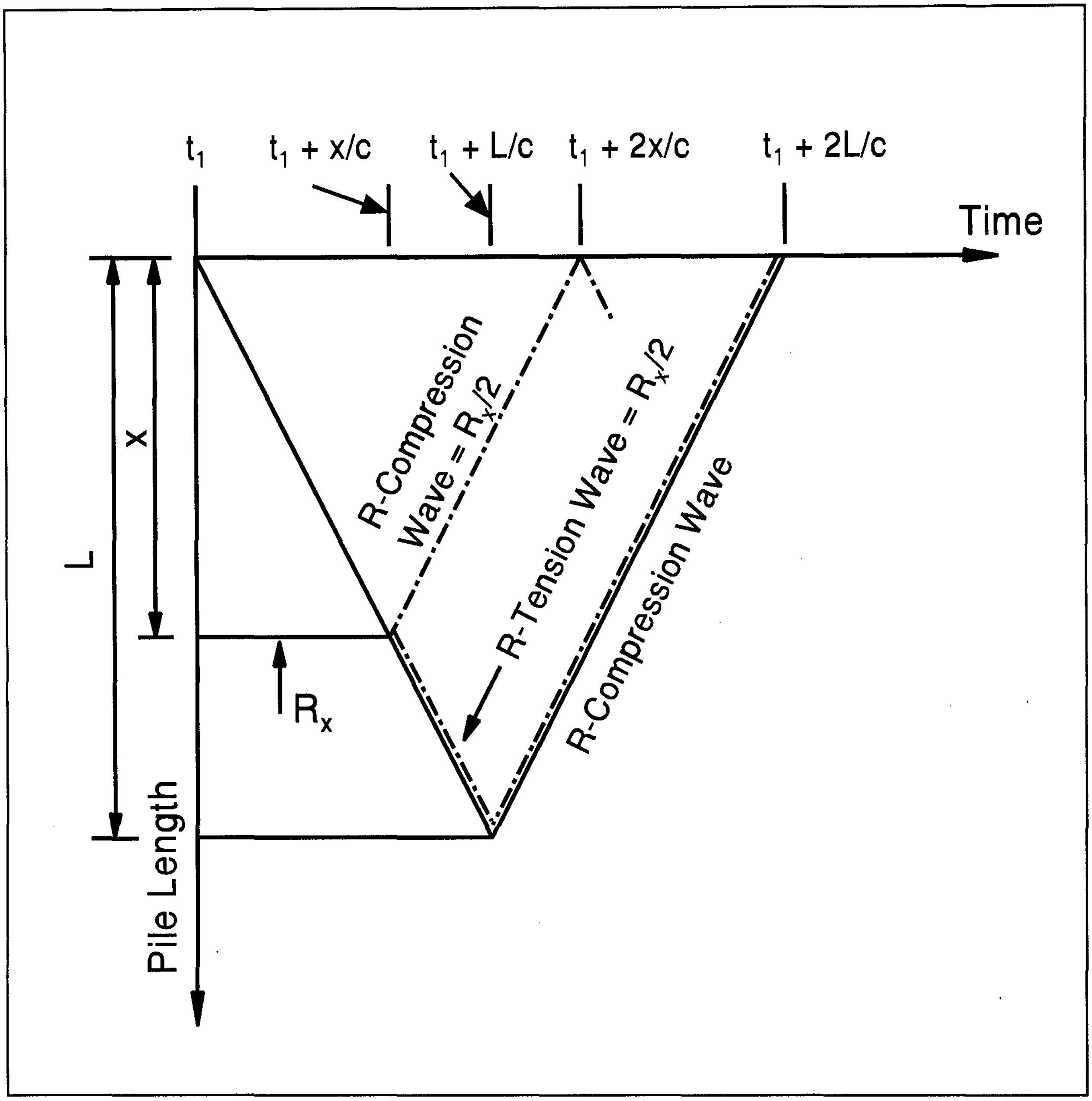

Figure D.1: Waves Caused by a Resistance R_x, at Location x Below the Pile Top Generated by an Impact Wave Which Started to Move Down the Pile at Time t_1.

(a) The upward traveling tension wave due to reflection at the pile bottom of the initial downward moving compression input at a time 2L/c earlier, $[-F^{\downarrow}_{M1}]$.

(b) The summation of all upward traveling compression resistance waves $[R_x/2]$.

(c) The initially downward traveling tension resistance waves now traveling upward in compression after reflection at the bottom [$R_x/2$] and the upward wave from the bottom resistance [R_b].

(d) All downward traveling waves, [$F^{\downarrow}_{M2}$].

Wave (b) and wave (c) have a combined magnitude R (equal to the sum of all R_x plus R_b) representing the entire soil resistance since they contains both half waves of shaft friction and the full end bearing. Thus, the combination of all upward traveling waves contains the full resistance (b and c) and the bottom reflected (tension) impact wave of time t_1 (a):

$$F^{\uparrow}(t_2) = R - F^{\downarrow}(t_1) \tag{D.3}$$

or:

$$(F_{M2} - Z\dot{u}_{M2})/2 = R - (F_{M1} + Z\dot{u}_{M1})/2 \tag{D.4}$$

Rearranging, we can now solve for the total soil resistance:

$$R = (F_{M1} + Z\dot{u}_{M1} + F_{M2} - Z\dot{u}_{M2})/2 \tag{D.5}$$

where the indices 1 and 2 refer to times t_1 and $t_2 = t_1 + 2L/c$.

D.1.2 Static Capacity

In equation (D.3), R is the total resistance encountered during the time period 2L/c. This total resistance is the sum of the static resistance and the dynamic resistance. To estimate the static resistance, R_s, the following considerations are necessary:

(a) Elimination of soil damping.

(b) Proper choice of time t_1 such that R_s is already at full magnitude when F_M and $\dot{u}_M$ samples are taken.

(c) Correction for an R_s that decreases during 2L/c because of early pile rebound (negative velocity, $\dot{u}_m$, before 2L/c).

(d) Changes of time dependent soil strength (setup or relaxation). Since the dynamic methods give the <u>resistance at the time of testing</u>, end of driving tests indicate the remolded soil strength which may not be equal to the service capacity after a waiting period due to reconsolidation, dissipation of excess pore pressure, etc. (It is always recommended to restrike the pile after a wait period for the calculation of the long-term service load.)

(e) The pile must experience permanent set during the blow. If no permanent penetration (or only a very small one) is achieved, then only a portion of the resistance has been mobilized. This is roughly analogous to a static proof test not run to failure, resulting in near zero net set after removal of the load (we then know only that the pile has at least the tested capacity).

Consideration (d) involves soil mechanics which affect the application of the Case Method but not its computation. Consideration (e) is self-explanatory. The first three considerations will now be investigated in more detail.

Damping is associated with velocity. The pile bottom velocity can be calculated from the top measurements as follows:

$$\dot{u}_b(t) = F^{\downarrow}(t\text{-}L/c)/Z - F^{\uparrow}(t+L/c)/Z = (F_{M1} + Z\dot{u}_{M1} - R)/Z \qquad \text{(D.6)}$$

By defining the damping force R_d as $J_c\, Z\, \dot{u}_b$ (J_c is the dimensionless Case damping constant), we can then solve for the damping. Since the total resistance is the sum of the static and damping forces, the static resistance can be estimated from:

$$R_s = R - R_d = R - J_c(F_{M1} + Z\dot{u}_{M1} - R) \qquad \text{(D.7)}$$

or expanding into terms of only F_M, v_M, and J_c:

$$R_s = (l\text{-}J_c)[F_{M1} + Z\dot{u}_{M1}]/2 + (l+J_c)\ [F_{M2} - Z\dot{u}_{M2}]/2 \qquad \text{(D.8)}$$

The damping constant has been empirically related to the soil grain size near the pile toe, or can be computed directly from this R_S equation if the failure load from either a static load test or calculated by CAPWAP is known, since J_c is then the only unknown.

The static soil resistance is a function of pile displacement. The resistance elastically increases until the pile reaches a certain displacement (called the "quake") and then remains constant (plastic) until rebound starts. Typical quakes are 0.1 in (2.5 mm), although values up to 1.0 in (25mm) have been observed for the pile toe.

For each time t_1 beginning at the first velocity peak, a resistance R_s may be determined from equation (D.8). In many cases, the displacement at the first peak velocity at any point along the pile exceeds the soil quake, assuring that the full resistance is mobilized. However, when a large toe quake condition exists, considerable soil compression is required to activate the full capacity. In this case the full or "maximum R_s" (called R_{max}) will occur later and can be found by delaying t_1 after the peak. Large toe quakes are often observed for displacement piles with large diameters or in saturated soils. The R_{max} method may also be necessary if the displacement is small at the initial velocity peak due to a low energy input or a short rise time.

If the pile toe velocity at some time is zero, the toe damping is also zero. Thus, any resistance at that specific time is static and, therefore, independent of the damping constant. This solution can be seen graphically in figure D.2 as the first point where the curves R(t) and $R_s(t)$ are equal after time t_1. For piles with zero or very little shaft friction, the R_{auto} Method is a perfect solution. For piles with moderate friction, an additional method is available (RA2) to estimate capacity independent of damping constant selection.

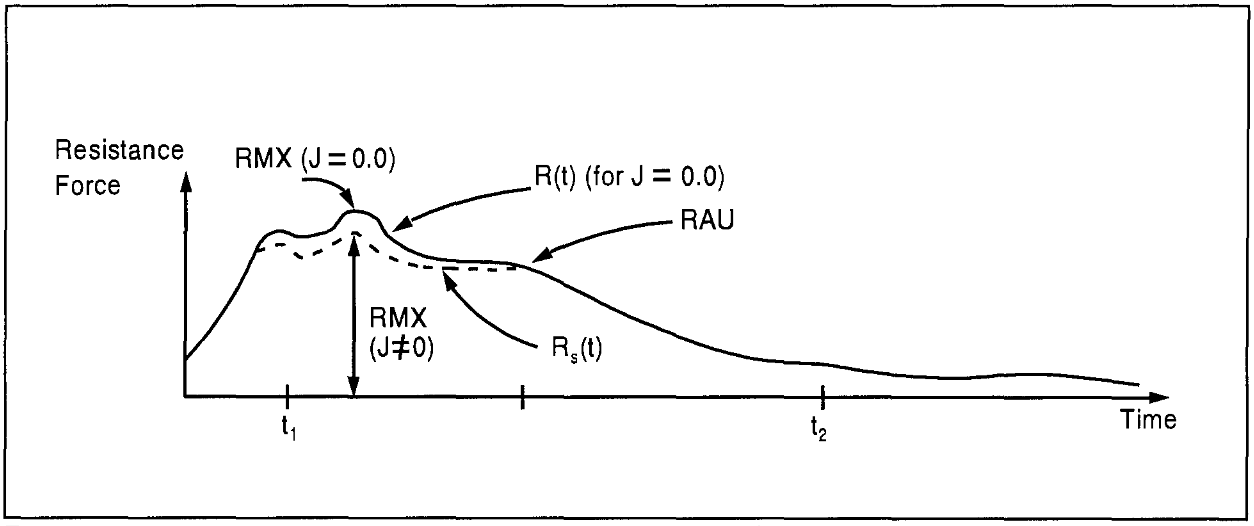

Figure D.2: Typical Resistance vs. Time Plot For a Pile Showing the Total Resistance R(t), the Static Resistance $R_s(t)$, and Other Selected Resistance Values.

For piles with little shaft friction, the pile bottom force, velocity and displacement may be computed directly from the pile top measurements. The pile bottom force F_b (due to soil resistance) is:

$$F_b(t) = F_M^{\downarrow}(t-L/c) + F_M^{\uparrow}(t+L/c) \tag{D.9}$$

Similarly, the bottom velocity is:

$$\dot{u}_b = [F_M^{\downarrow}(t-L/c) - F_M^{\uparrow}(t+L/c)]/Z \tag{D.10}$$

and the bottom displacement becomes:

$$u_b = \int \dot{u}_b dt \tag{D.11}$$

A static toe resistance force-displacement graph may be obtained from F_b by subtracting the damping resistance $J_c Z\dot{u}_b$ and plotting this force against the displacement at the corresponding time. (This procedure is referred to as PEBWAP, Pile End Bearing Wave Analysis Program.)

Consideration (c) is necessary because the Case Method computes the simultaneously acting soil resistance. For long piles with significant shaft resistance, the Case Method may underpredict capacity; specifically, when the pile top moves upward before time 2L/c causing some shaft friction to unload while the toe is still loading. The basic Case Method can then be "corrected" by adding the unloaded resistance. The dynamic component is then subtracted.

D.1.3 Pile Driving Stresses

Pile damage is usually the result of either poor hammer alignment (causing high local contact stresses) or high driving stresses. For friction piles, the maximum compression stress generally occurs at the pile top, whereas for end bearing piles, the pile bottom stress may be critical.

For concrete piles, tension stresses are also important. If soil resistance is small compared to the impact force, the impact compression stress wave will reflect from the pile bottom at time L/c as an upward tension stress wave. From the upward wave at time 2L/c, one can calculate the upward tension stress wave transmitted along the entire pile shaft, but the net tension stress at any location also superimposes the continuing downward stress waves. The maximum net tension stress, F_{tn}, is calculated when the downward compression stress wave is a minimum by:

$$F_{tn} = F^{\uparrow}(t_2) + F^{\downarrow}(t_3) \tag{D.12}$$

where t_3 is the time of minimum downward stress wave before time 2L/c.

D.1.4 Pile Integrity Evaluation

For a uniform pile, an upward traveling tension wave should be observed only after reflection from the pile bottom or at time 2L/c after impact. An upward tension wave can only be observed prior to 2L/c if there is a reduction in impedance (area or modulus), or damage. Consider the equilibrium conditions for the downward waves $F_2^{\downarrow}$ and $F_1^{\downarrow}$ and the upward reflection wave $F_1^{\uparrow}$ at a cross section change with impedances Z_1 and Z_2 as shown in figure D.3. Since there is initially no upward traveling wave from the lower pile section (section 2):

$$F_1^{\downarrow} + F_1^{\uparrow} = F_2^{\downarrow} \tag{D.13}$$

and from velocity continuity considerations:

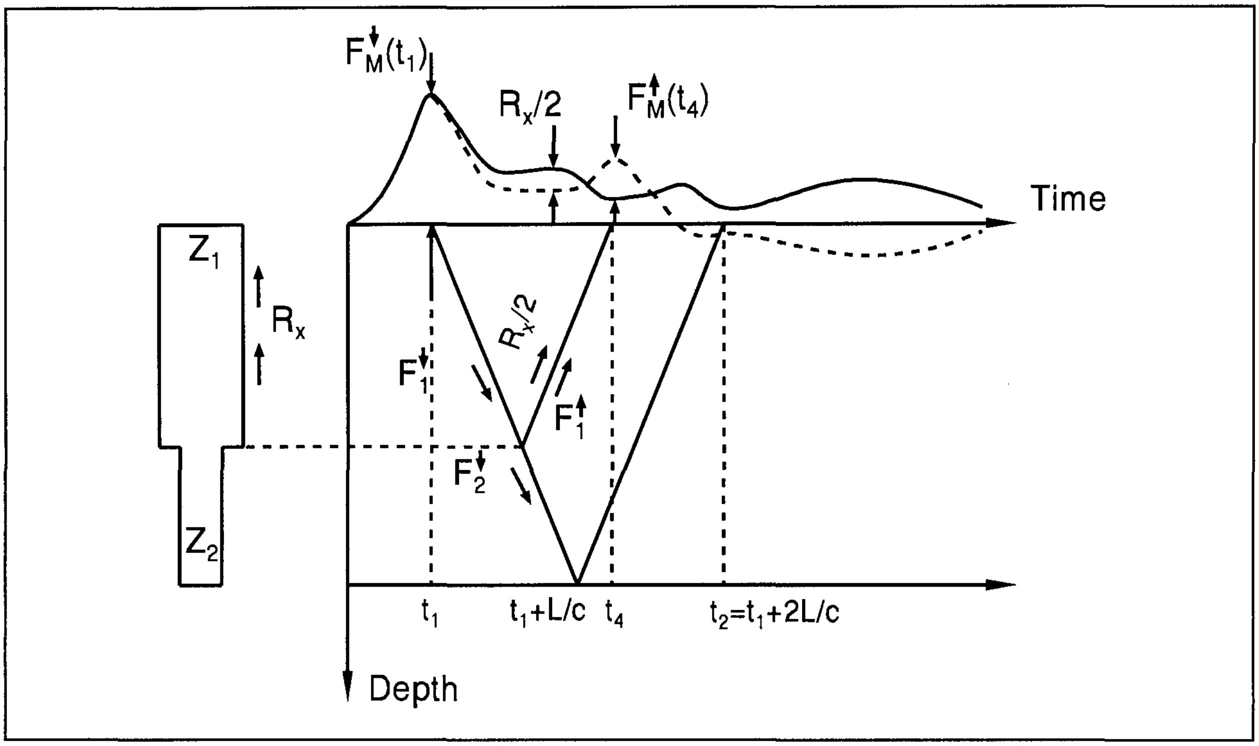

Figure D.3: Typical Plots of Pile Top Force and Velocity of a Damaged Pile

$$(F_1^{\downarrow} - F_1^{\uparrow})/Z_1 = F_2^{\downarrow}/Z_2 \tag{D.14}$$

Solving these equations results in the relative cross sectional change $\beta = Z_2/Z_1$:

$$\beta = (F_1^{\downarrow} + F_1^{\uparrow})/(F_1^{\downarrow} - F_1^{\uparrow}) \tag{D.15}$$

The wave force, $F_1^{\downarrow}$, can be found from the superposition of the initial downward wave with the downward resistance tension waves, $R_x/2$. (R_x is the sum of all resistance above the location x of cross sectional change):

$$F_1^{\downarrow} = F_M^{\downarrow}(t_1) - R_x/2 \tag{D.16}$$

The upward wave at time $t_4 = t_1 + 2x/c$ is the sum of effects of the resistance above location x and the cross section change (negative if $Z_2 < Z_1$):

$$F_M^{\uparrow}(t_4) = R_x/2 + F_1^{\uparrow} \tag{D.17}$$

We can then solve for β (often called Beta Method):

$$\beta = (F_M^{\downarrow}(t_1) - R_x + F_M^{\uparrow}(t_4))/(F_M^{\downarrow}(t_1) - F_M^{\uparrow}(t_4)) \tag{D.18}$$

The time t_4 should be chosen when the upward wave at the pile top, $F_M^{\uparrow}$, has a temporary minimum. For a uniform pile, $F_M^{\uparrow}(t_4)$ should monotonically increase to a value of $R_x/2$ and β will be equal to 1.0. If a uniform pile indicates a β less than 1.0 prior to 2L/c, the pile is damaged at location $x = ct_4/2$ and the impedance reduction can be estimated directly from the β value. The following classification scale has been proposed:

$\beta =$	1.0	uniform pile
	0.8-1.0	pile with slight damage
	0.6-0.8	damaged pile
	below 0.6	broken pile

D.1.5 Hammer Performance Evaluation

The energy transmitted past the measuring location can be calculated from the work done:

$$W = \int F_M du \tag{D.19}$$

or:

$$E(t) = \int F_M \dot{u}_M \, dt \tag{D.20}$$

The maximum value of this expression E_{max} or ENTHRU or can be compared with the hammer manufacturer's maximum rating as a guide to efficiency of operation.

D.1.6 Background of CAPWAP

CAPWAP (CAse Pile Wave Analyses Program) combines measured force and velocity data with wave equation analysis to obtain the soil resistance effects acting on the pile. Because force and velocity measurements are input as the pile top excitation, it is unnecessary to model the hammer and the driving system as in the wave equation analysis.

The pile is numerically modeled by a series of pile segments. In most cases, the pile properties are well known. CAPWAP uses continuous and uniform segments for pile modeling, rather than masses and springs as in the traditional wave equation analysis. Research work for this method of analysis was originally done by Fischer in Sweden. The pile is divided into a number (say N_p) of segments. Each segment is of uniform cross section, but the segments may be different from each other. Denoting a segment number by i, it has a defined length dL_i such that its wave travel time dt_i (= dL_i/ci) equals the analysis time increment, dt.

Next, a soil model (similar to Smith's wave equation model) is assumed including the total resistance and its distribution, the damping constants, and the quakes. CAPWAP can use either measured force, measured velocity or measured wave down as the input to the first segment, and performs the computations for the dynamic event, in time increment steps similar to those used for wave equation analysis. The record length analyzed extends at least 20 ms after 2L/c time (L is the total pile length below measuring gauges, c is the stress wave speed).

If the pile top force is prescribed, then an acceleration and therefore velocity can be computed, which may be compared with the measured velocity. Alternatively, for a prescribed velocity the forces can be compared and for a wave down imposed as a top boundary condition, wave up is the compared quantity.

Comparison of the computed with the measured pile top response is then evaluated as follows:

(a) From the time period between impact and time 2L/c after impact, differences require changes in the resistance distribution.

(b) From the time period immediately following the first return of the stress wave from the pile toe, damping effects are separated from the static soil resistance.

(c) From the later record portion, loading and unloading quakes are estimated.

Improvements in the soil parameters may be done in a rather formal manner, and an automated routine usually produces satisfactory results for standard situations. However, for nonuniform piles or complex soil situations the necessary steps are often done interactively by an engineer who uses CAPWAP experience, knowledge of wave mechanics, geotechnical information and program automated features for input decisions. In any event, an experienced engineer should always review the results and make further result adjustments if necessary.

D.1.7 The Soil Model

D.1.7.1 Basic Relationships and Static Resistance

According to the basic Smith approach, the displacement and velocity of a pile segment relative to the soil is the basis for computing the soil resistance forces. The Smith soil model consists of an elasto-plastic spring and a linear dashpot. As shown in figure D.4, at pile segment i, the soil resistance force is modeled by three parameters:

ultimate resistance, R_{uk}
quake, q_k
viscous damping factor, J_{sk}

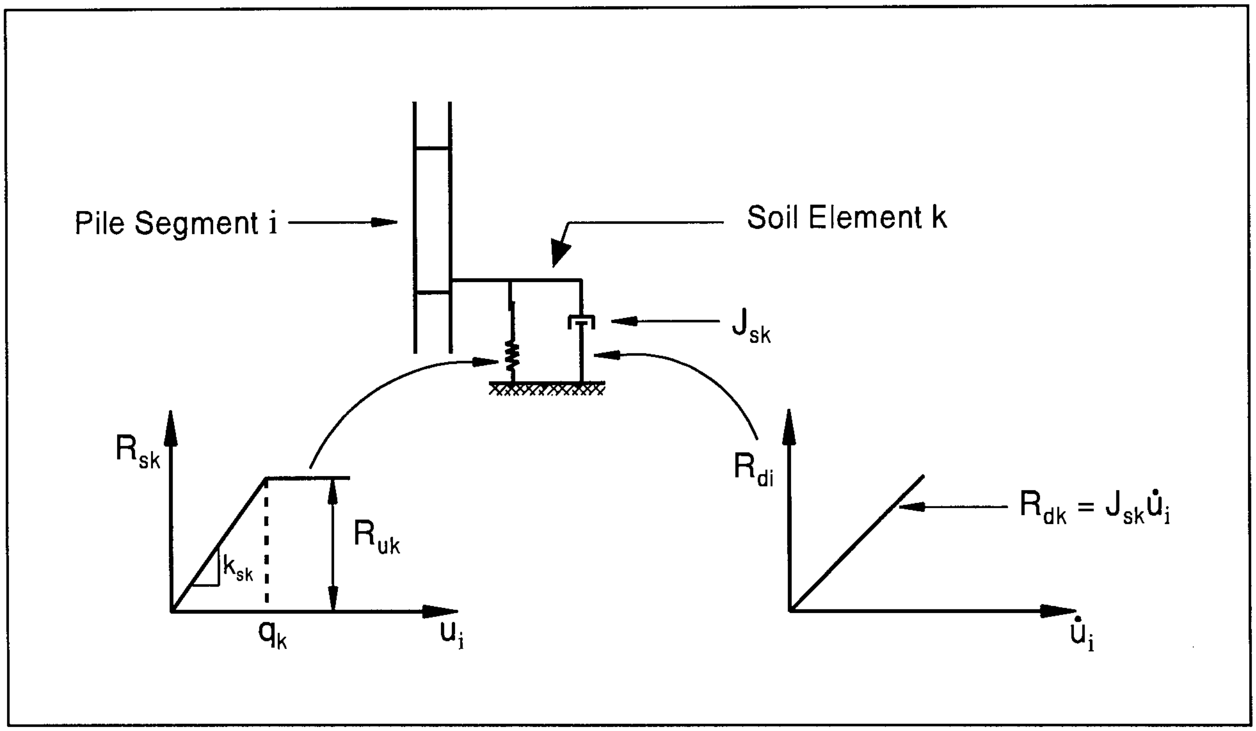

Figure D.4: The Smith Soil Resistance Model
(Viscous Damping Model Instead of a Strict Smith Damping is Shown)

The total static bearing capacity, R_{ut}, is the sum of all R_{uk}. The total (static plus dynamic) resistance force at soil element k, R_k, is computed from:

$$R_k = R_{sk} + R_{dk} \tag{D.21}$$

where R_{sk} and R_{dk} are time varying static and dynamic soil resistance forces at soil element k.

Soil resistance forces may act at each pile segment. However, since the pile segments are usually short for the CAPWAP method, it may be sufficient to have one soil resistance element at the bottom element for end bearing and one shaft resistance element at every second pile segment. Also, soil elements need only be assigned to the portion of pile with embedment in the soil. Thus, the number of pile segments, NP, may be different from the number of shaft resistance elements, NS. Consider a "soil element k" at pile segment i. Knowing pile segment velocity, $\dot{u}_i$, and displacement, u_i, and a viscous damping factor, J_{sk}, the k-th resistance force becomes:

$$R_k = R_{sk} + J_{sk}\,\dot{u}_i \tag{D.22}$$

with the static resistance represented by:

$$R_{sk} = k_{sk}\,u_i \tag{D.22a}$$

where:

$$-U_n R_{uk} < R_{sk} < R_{uk} \tag{D.22b}$$

and:

$$0 < U_n < 1 \tag{D.22c}$$

Note that negative ultimate resistance limit, U_n, is always zero for **end bearing**. Smith's static resistance wave equation model for **shaft** resistance assumes that during rebound an uplift (or negative) capacity can be reached which is the same magnitude as the ultimate compressive shaft resistance. Extensive experience in CAPWAP signal matching has shown this hypothesis to be not true. (Note that this "negative" resistance has nothing to do with the geotechnical term "negative shaft friction" which occurs when the soil through consolidation moves downwards relative to the pile.)

The U_n value may take values between 0 and 1, inclusively, for the shaft and a variable UNld is used in CAPWAP. UNld = 1 corresponds to the original Smith approach while UNld = 0 means that no negative shaft resistance is considered in the analysis. Thus, the ultimate uplift shaft resistance, occurring during the blow analyzed, is the product of UNld and the positive ultimate resistance at any segment. UNld is assumed to be constant along the shaft. In easy driving, UNld has no effect (no rebound). In hard driving, UNld may be chosen as low as 0. The effect of UNld is most easily observed in the later portion of the record. Lower values tend to raise the later portion of the computed curve.

The quantity, k_{sk}, in equation (D.22a) is the soil stiffness of the k-th shaft resistance force. For positive (downward) velocities:

$$k_{sk} = R_{uk} / q_k \tag{D.23}$$

with q_k being the actual shaft loading quake. Shaft Quakes, q_k, (QSkn is used in CAPWAP) cannot be zero (ideal plastic case) for reasons of numerical stability. They also cannot exceed the maximum pile segment displacement or incomplete resistance activation would result. Large shaft quakes tend to make resistance stay on longer and therefore the computed force curve remains higher longer into the data record for higher quake values. Large shaft quakes also delay activation of resistance and therefore more resistance is calculated for the upper segments when shaft quakes are made larger. Experience and laboratory tests have generally shown the shaft quakes to be relatively small and the traditional wave equation value of 0.1 in (2.54 mm) is often the best value.

Toe quakes, q_t, (QToe in CAPWAP) has been determined by CAPWAP to be a very variable parameter depending on both pile size and soil conditions. The toe quake must be less than the pile bottom displacement for full activation of the assigned toe resistance.

Based on CAPWAP signal matching experience, another extension of the basic Smith soil resistance law was necessary for the pile toe. For piles on a very hard end bearing layer, a so-called resistance gap, g_t, (TGap in CAPWAP) between the pile toe and soil sometimes exists. It causes a strain hardening type resistance *i.e.*, as the pile moves through the gap distance, the static toe resistance remains zero. It starts to increase linearly only once the displacement exceeds the gap. The sum of the maximum gap plus toe quake must be less than the maximum pile toe displacement occurring during a blow. The static soil resistance subject to the gap, g_t, is therefore:

$$R_{st} = k_{st} \, (u_{NP} - g_t) \tag{D.24}$$

for:

$$g_t < u_{NP} \tag{D.25}$$

where u_{NP} is the displacement of the pile's bottom segment. R_{st} is zero for displacements less than the gap and equal to R_{ut} for displacements greater than the sum of gap and toe quake. During unloading, the toe resistance follows the unloading quake.

A gap often is simultaneously present with a large quake, allowing for high tension even in the presence of high resistance. Generally, the gap only affects the record portion around the time 2L/c after impact. In conventional wave equation analyses, the toe quake should be equal to the sum of the gap and toe quake.

For negative (upward, rebound) pile velocities, a modified quake is calculated for both shaft and toe:

$$q_{ku} = q_k \, c_k \tag{D.26a}$$

$$q_{tu} = q_t \, c_t \tag{D.26b}$$

and the corresponding unloading stiffness is then:

$$k_{sku} = R_{uk}/q_{ku} \tag{D.27a}$$

$$k_{stu} = R_{ut}/q_{tu} \tag{D.27b}$$

Thus, <u>Shaft and Toe Unloading Quake Multiplier</u>, c_k and c_t, (CSkin and CToe in CAPWAP), respectively, is used to assign unloading quakes lower than the loading quakes. The multiplier default is 1.0 which makes loading and unloading quakes equal, as for the standard Smith wave equation model. The same quake value is applied to all shaft elements. The actual unloading quake cannot be zero for numerical reasons. Like the loading quake, a low unloading quake causes a quick shedding of load and therefore lowers the computed force record at the end of the record. For long friction piles, unloading may already occur before 2L/c and CSkn may then affect the resistance distribution.

Unloading quakes should not exceed 1 except under conditions of radiation damping or at the toe when a gap exists.

The basic model for static resistance was also expanded by a "reloading" option. This option specified the resistance level above which the loading quake is used in a second or later loading cycle. Such an option is unnecessary in Smith's algorithm where loading and unloading stiffnesses are equal.

Figures D.5 and D.6 illustrate the complete static resistance versus soil deformation behavior for shaft and toe, respectively.

D.1.7.2 Plug

A plug or soil mass at the pile toe has been used throughout the CAPWAP development for the "trimming" of matches. In CAPWAP, soil mass is thought to act like an external, passive resistance rather than an actual change in pile model. Thus, the soil mass resistance force, R_M, at time j, acting against the pile bottom is:

$$R_{Mj} = W_s (\dot{u}_{bj} - \dot{u}_{bj-1}) / (g \Delta t) \tag{D.28}$$

where W_s is the weight of the plug, $\dot{u}_b$ is the pile bottom velocity, g is gravitational acceleration, and Δt is the computational time increment.

D.1.7.3 Damping

Viscous forces (which are a function of velocity) also resists pile penetration. The traditional Smith wave equation definition is:

$$R_{dk} = J_{sk} \dot{u}_i \tag{D.29}$$

which makes the dynamic resistance dependent upon both pile segment velocity and soil element resistance by a dimensional Smith damping factor, J_{sk}, for soil element k. However, it is more convenient in CAPWAP matching to use linear viscous coefficients rather than the Smith values since they produce predictable damping forces independent of static resistance forces. A recomputation of Smith damping factors from viscous factors, J_{vk}, is approximately possible using:

$$J_{sk} = J_{vk}/R_{uk} \tag{D.30}$$

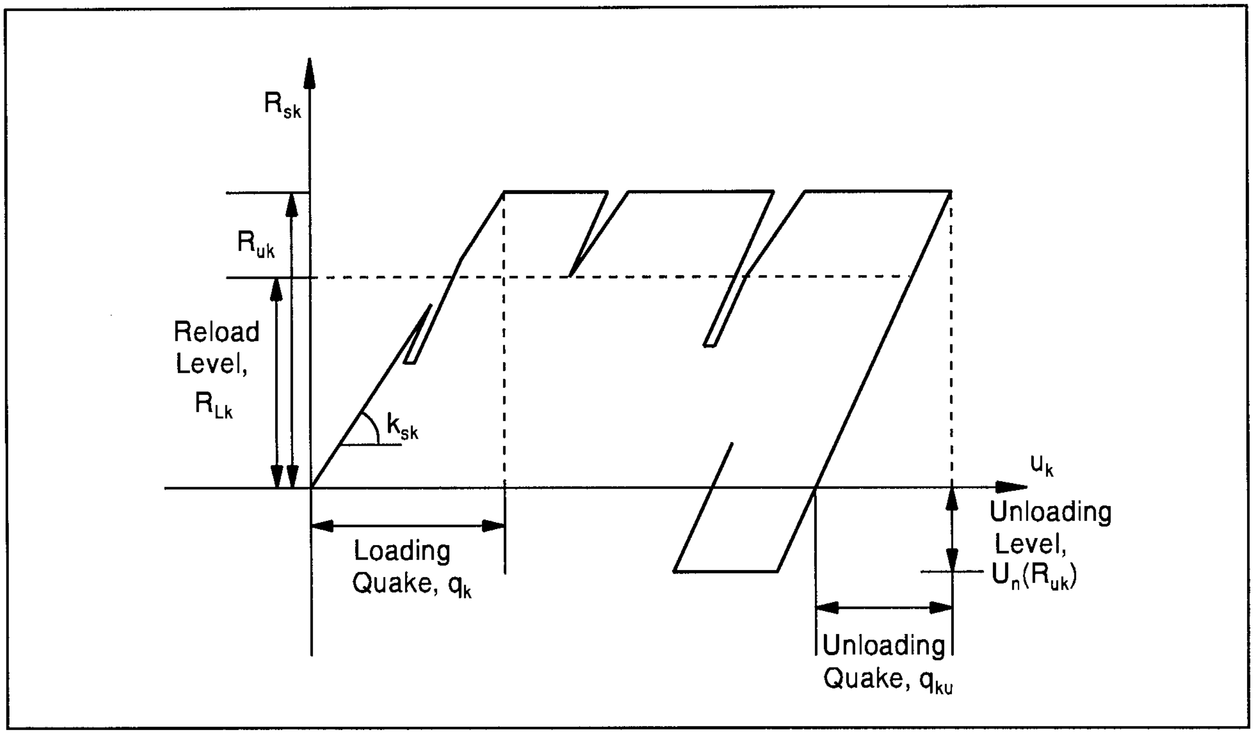

Figure D.5: Static Shaft Resistance

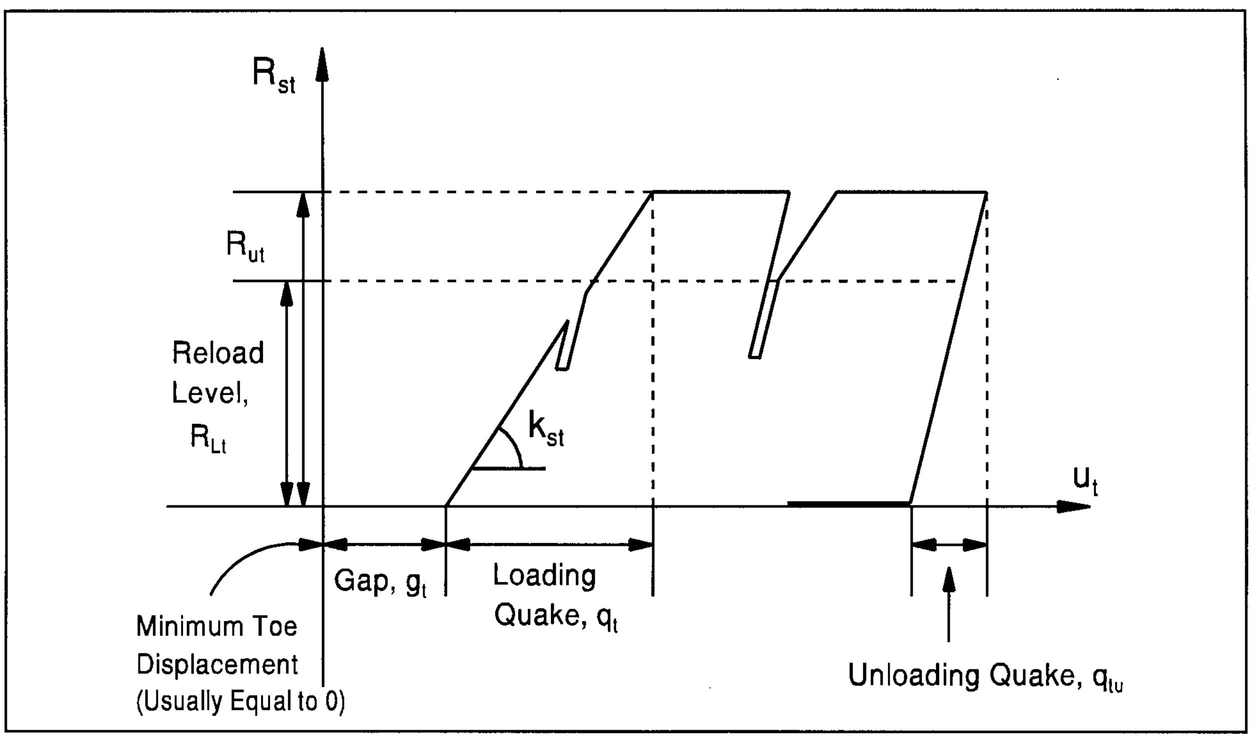

Figure D.6: Static Toe Resistance

To avoid referring to individual viscous shaft damping parameters, the Case shaft damping factor J_c is defined as the nondimensionalized (Case Method type) sum of the viscous damping factors:

$$J_c = \mathrm{Sum}(J_{vk})/Z \qquad \text{(D.31)}$$

where Z is the pile impedance. The Case shaft damping factor, J_c, (JSkn in CAPWAP) can be specified as a non-dimensional quantity. It can be as low as zero (although this is very uncommon) and maxima of 3 have been observed. However, there is no reason why JSkn could not be higher for long piles with low impedance, but at no segment should there be a Case damping factor greater than 1.0. Thus, an absolute upper limit for Case shaft damping is NS, the number of soil elements.

The Smith soil damping approach lends itself better for damping recommendations than the Case damping approach because it is related to the static soil resistance. For that reason, the Smith shaft damping value (SSkn) is calculated and displayed by CAPWAP. Each time a viscous JSkn is entered, the Smith SSkn value is recalculated. SSkn can also be entered and the corresponding JSkn calculated, however, any subsequent change of soil resistance will then change SSkn since the new JSkn remains unchanged. Recommendations for Smith shaft damping values are a minimum of 0.025 s/ft (0.075 s/m) and a maximum of 0.33 ft/s (1 s/m). However, smaller and larger values have been observed on occasion.

Similarly, for the pile toe, one obtains the Case toe damping factor, J_t:

$$J_t = J_{vNS+1}/Z \qquad \text{(D.32)}$$

where "NS+1" refers to the toe element, NP being the total number of pile segments. Toe damping can also be specified, either with the Case (JToe) or with the Smith (SToe) approach. The maximum Case toe damping value should not exceed 1. Recommended Smith toe damping values are similar to Smith shaft damping values.

It has been observed that the linear viscous shaft damping model is better suited for CAPWAP signal matching than the original Smith approach of equation (D.29). While it is also usually better for the pile toe, occasionally the original Smith model is better, particularly when the activated resistance at 2L/c is low. An option for toe damping type (OPtd) can be selected as either linear viscous (OPtd = 0), Smith (1), or a combination (2) of viscous before and Smith after the ultimate toe resistance has been first fully activated. OPtd options 1 and 2 are usually observed when toe quake is relatively high and/or a toe gap is present.

D.1.7.4 Radiation Damping

When the pile exerts a force on the soil it causes movement of the soil around the pile. Soil movements can be particularly important when the pile motions are small such that a true shear failure does not occur. An example is a pile on hard rock. As the pile exerts compression forces against the rock, a wave is generated in the rock and the soil resistance appears to be a function of velocity rather than displacement. This example explains why we talk about "Radiation Damping" (the energy is radiated away rather than consumed by soil shearing) and why we use a mass and a dashpot to replace the assumed rigid soil support of the Smith model.

As the pile penetrates, the soil surrounding the shaft moves. One example is a drilled shaft with a very rough surface installed in a cohesionless soil. Another case observed is where observed friction during the first 2L/c is high but the apparent total resistance is low after 2L/c. This situation would normally result in low static but high damping resistance causing Smith shaft damping values in excess of 0.4 ft/s (1.3 m/s). There is a growing awareness (Likins et al., 1992) that a radiation damping model to represent soil motion must be used in such cases to obtain reasonable correlation with static load tests by limiting the maximum Smith damping factor for the shaft to 0.4 ft/s (1.3 m/s).

CAPWAP's soil model includes a radiation damper underneath a soil mass. Figure D.7 shows this device under the Smith mass-dashpot-spring resistance model for both shaft and toe. Of course, it appears that the pile may not be capable of supporting any static load if the soil support dashpot has a damping factor less than infinity. This philosophical dilemma may be resolved by assuming that J_{ss}, or J_{st}, the damping factors of the soil support, are less than infinity <u>only during the dynamic event</u>.

The soil mass M_s (M_t) and dashpot J_{ss} (J_{st}) appear to establish a good model for energy dissipating waves in soil or rock which do not fail elasto-plastically, *i.e.*, which do not shear. The governing equations are only changing in that the pile motion variables, u and $\dot{u}$ are replaced by the relative quantities, u_r and $\dot{u}_r$. The motion of the soil support mass (velocity, $\dot{u}_{ss}$, and displacement, u_{ss}) is calculated simply from:

$$\dot{u}_{ss,j} = \dot{u}_{ss,j-1} + (R_k + \dot{u}_{ss,j-1}\, J_{ss}) \,/\, (J_{ss} + M_s \,/\Delta t) \qquad \text{(D.33)}$$

and:

$$u_{ss,j} = u_{ss,j-1} + (\dot{u}_{ss,j-1})\ \Delta t \qquad \text{(D.34)}$$

Then:

$$u_{r,j} = u_{k,j} - u_{ss,j} \qquad \text{(D.35)}$$

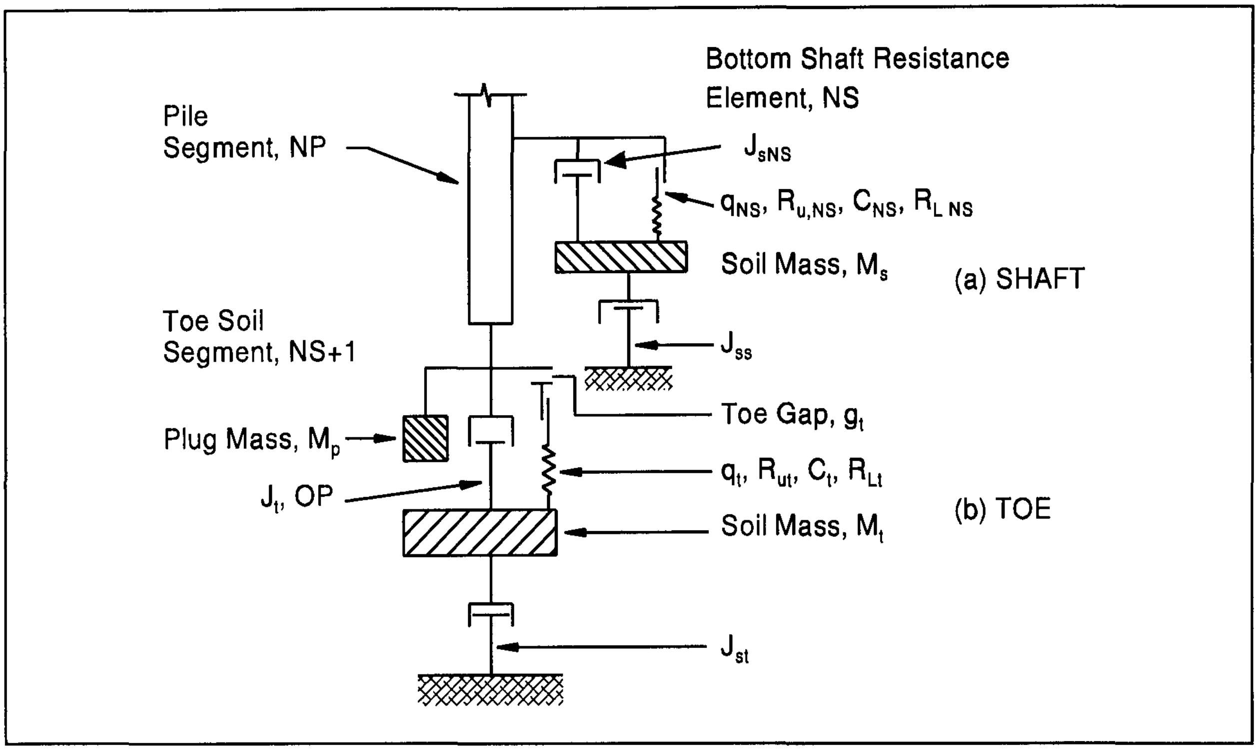

Figure D.7: The Extended CAPWAP Soil Resistance Model (a) Shaft (b) Toe

and:

$$\dot{u}_{r,j} = \dot{u}_{k,j} - \dot{u}_{ss,j} \tag{D.36}$$

The toe soil support mass (MToe) delays the effect of the toe soil (radiation) dashpot (BTdp). A recommended starting value could be calculated from the soil mass underneath the toe plate, extending to a depth of 3 pile diameters. The toe soil support dashpot value (BTdp) is conveniently applied to piles which do not penetrate into the soil or rock. If toe radiation damping has to be modeled, BTdp may be as low as 20 percent of the pile impedance.

The shaft soil dashpot (SKdp) is useful to model soil motion along the shaft. Very high values are acceptable but they reduce the effectiveness of the approach.

D.1.7.5 Algorithm for Wave Propagation

For pile properties E_i, ρi (elastic modulus, mass density), the wave speed of a pile segment is:

$$c_i = (E_i/\rho_i)^{1/2} \tag{D.37}$$

where c_i, E_i and ρ_i, are average properties over a pile segment's length.

Using the impedance, Z_i, (equals E_iA_i/c_i where A_i is the area of pile segment i) the downward travelling wave $F_i^{\downarrow}$ at pile segment i can be calculated from:

$$F_i^{\downarrow} = [F_i(t) + Z_i \, \dot{u}_i(t)]/2 \tag{D.38a}$$

Similarly, for the upwards traveling wave:

$$F_i^{\uparrow} = [F_i(t) - Z_i \, \dot{u}_i(t)]/2 \tag{D.38b}$$

At any time j, both upwards and downwards traveling waves, $F^{\uparrow}_{i,j}$ and $F^{\downarrow}_{i,j}$, respectively, are present in segment i. For two neighboring segments of equal properties:

$$F^{\uparrow}_{i,j+1} = F^{\uparrow}_{i+1,j} \tag{D.39a}$$

and:

$$F^{\downarrow}_{i,j+1} = F^{\downarrow}_{i-1,j} \tag{D.39b}$$

If the cross sectional properties change between segments i and i+1, then the pile impedance, Z_i, has to be considered for reflections:

$$Z_i = E_i \, A_i/c_i \tag{D.40}$$

where A_i is the cross sectional area of segment i. Defining:

$$Z_{r,i} = Z_i/(Z_i + Z_{i+1}) \tag{D.41a}$$

and:

$$Z_{s,i-1} = Z_i/(Z_i + Z_{i-1}) \tag{D.41b}$$

the new wave values for the next time increment are also affected by the total resistance, R_i, (static plus damping) at element i and may be determined from:

$$F^{\uparrow}_{i,j+1} = Z_{r,i}[2F^{\uparrow}_{i+1,j} - F^{\downarrow}_{i,j} + R_i] + Z_{s,i+1} \, F^{\downarrow}_{i,j} \tag{D.42a}$$

$$F^{\downarrow}_{i,j+1} = Z_{s,i}[2F^{\downarrow}_{i-1,j} - F^{\uparrow}_{i,j} - R_i] + Z_{r,i-1}F^{\uparrow}_{i,j} \tag{D.42b}$$

Internal pile material damping may be added (although generally unnecessary for reasons of numerical stability) by computing the change of a wave and reducing the new wave by a specified fraction, P_p. Thus:

$$F^{\uparrow *}_{i,j} = F^{\uparrow}_{i,j} - P_p \, (F^{\uparrow}_{i,j} - F^{\uparrow}_{i,j-1}) \tag{D.43a}$$

$$F^{\downarrow *}_{i,j} = F^{\downarrow}_{i,j} - P_p\,(F^{\downarrow}_{i,j} - F^{\downarrow}_{i,j-1}) \tag{D.43b}$$

The * indicates the dampened wave value. The pile damping value, P_p, (Plld in CAPWAP) smoothens the computed curve. However, caution should be exercised. For example, the pile damping in steel is probably rather low and Plld should not be much greater than 0.01 for steel piles. Typically, for concrete piles, P_p equals 0.02. Timber may require slightly larger values. For very long piles, it may be necessary to reduce the material damping. Note that this numerical damping of the stress wave produces a slight delay in the return of the stress wave.

At the pile top, either force, $F_{M,j}$, or velocity, $\dot{u}_{M,j}$, or wave down $F^{\downarrow}_{M,j}$ are prescribed (M for "measured") at time j. Then the complementary computed (c for "computed") quantity is either:

$$F_{c,j} = Z_1\dot{u}_{M,j} + 2F^{\uparrow}_{1,j-1} \tag{D.44}$$

or:

$$\dot{u}_{c,j} = [F_{M,j} - 2F^{\uparrow}_{1,j-1}]/Z_1 \tag{D.45}$$

or calculated wave-up which is a direct result of the continuous analysis (the calculated wave-up is the upward traveling wave in the first segment).

Selection of the "Analysis Type" (ANat) is done by the user. Wave-up matching has the advantage that phase shifts, due to an inaccurate wave speed assumption, are easily detected and avoided and is the preferred analysis type. Note that for comparison of measured quantities after wave matching has been finished, the "calculated" top force is the measured wave-down plus the calculated wave-up. CAPWAP results should always include a comparison of calculated and measured pile top force or velocity.

At the pile toe, force equilibrium requires that:

$$F^{\uparrow}_{NP,j} = -F^{\downarrow}_{NP,j-1} + R_{NS} + R_{NS+1} \tag{D.46}$$

with R_{NS+1} denoting the toe resistance (static plus dynamic).

The actual force at segment i (from which the stress can be computed) is the sum of upward and downward force waves:

$$F_{i,j} = F^{\uparrow}_{i,j} + F^{\downarrow}_{i,j-1} \tag{D.47}$$

and similarly the velocity can be derived from the difference of the force waves (divided by impedance):

$$\dot{u}_{i,j} = [F^{\downarrow}_{i,j-1} - F^{\uparrow}_{i,j}]/Z_i \tag{D.48}$$

and displacements become:

$$u_{i,j} = u_{i,j-1} + (1/2)(\dot{u}_{i,j,-1} + \dot{u}_{i,j})dt \tag{D.49}$$

Since the PDA digitizing an analog velocity, no digital double integration is required (acceleration may only be obtained from velocity by differentiation), and such a simple integration to displacement is sufficiently accurate. This completes the computational description. Note that the computation is direct and that no predictor-corrector approach is needed as in better lumped mass wave equation analysis programs such as WEAP.

The continuous segment analysis has the advantage of shorter computation times than the lumped mass analysis. It also more accurately follows the wave propagation; the wave generated at the pile top arrives unchanged at the pile bottom, while the lumped mass analysis tends to smoothen the wave (particularly early programs using simple Euler integration). On the other hand, it is difficult to use a continuous model for any pile material non-linearities or slacks or complicated hammer models, making the continuous approach more applicable to CAPWAP than to wave equation analysis.

D.1.7.6 Pile Slack

The pile model may include slacks for splice or crack modeling. Basically, a crack causes complete reflection if it is open or completely transmits waves if it is closed. It transmits full tension forces after the relative displacement, u_r, of the two segments neighboring the splice has been completely opened ($u_r < S_t$). Similarly, for a compression splice, the relative compression of two neighboring segments has to be greater than the compression slack ($u_r > S_c$) for a full transmission of compression forces. (Tensile displacements are considered negative.)

Unfortunately, this simple slack model does not represent reality sufficiently well to help match actual crack or splice behavior. The model was, therefore, modified to consider that some force would always be transmitted across a crack or splice (*e.g.*, due to reinforcing, cracks over only part of the section, or other non-perfect separation). Two models are built into the program. The first is a rounded-out slack model, as in GRLWEAP. As the two cross sections near the specified slack distance, the forces transmitted increase until reaching the force of the continuous section as in figure D.8. The model may be expressed as:

$$F^{\uparrow}_{i,j} = (-F^{\downarrow}_{i,j-1} + R_i/2)\, r + (F^{\uparrow *}_{i,j})\, (1-r) \tag{D.50}$$

with r being a so-called slack efficiency: when r is 0 then there is no slack effect, when r is 1 then there is a full slack effect with partial reflection from a fully opened slack for intermediate values. The $F^{\uparrow *}_{i,j}$ term is the upward wave calculated for an unspliced section. For the downward wave, one obtains correspondingly:

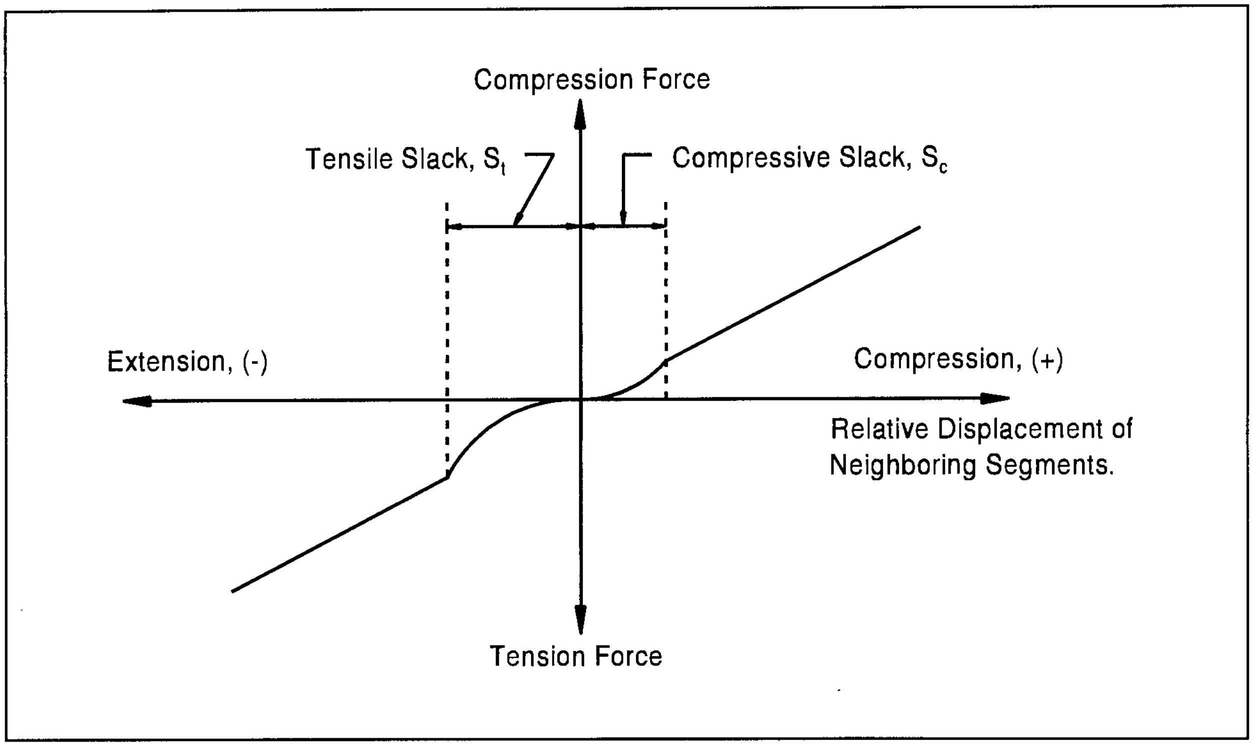

Figure D.8: Slack Model

$$F^{\downarrow}_{i+1,j} = (-F^{\uparrow}_{i+1,j-1} - R_i/2)\ r + (F^{\downarrow *}_{i+1,j})\ (1-r) \qquad \text{(D.51)}$$

In the second model, when compressive or tensile slacks (S_c or S_t) are prescribed greater than a value "10", they are then interpreted as maximum slack forces, F_s, (compressive is positive or tensile is negative) and the following equations govern:

$$F^{\uparrow}_{i,j} = F^{\downarrow}_{i,j-1} + R_i/2 + F_s \qquad \text{(D.52a)}$$

and:

$$F^{\downarrow}_{i+1,j} = -F^{\uparrow}_{i+1,j-1} - R_i/2 + F_s \qquad \text{(D.52b)}$$

In other words, as a slack opens, a minimum force F_s, is always transmitted. There would be no maximum slack distance.

D.1.7.7 Residual Stress Analysis (RSA)

For background information, we recommend reading of the description of RSA in the GRLWEAP manual. In short, residual stresses occur because at the end of a blow the soil tries to resist the pile's full rebound. Longer flexible friction piles are more susceptible to residual soil than are short, stiff piles or piles with little friction. It was found in earlier studies, that consideration of residual stresses in the analysis tends to produce lower calculated blow counts than those from conventional analyses. The reason is that energy stored in the pile at the end of a blow will be available to do useful work in later blows.

CAPWAP calculated resistance distributions may be inaccurate if residual stresses are not considered. The reason is that, at the end of a blow some of the upper soil resistance forces are directed downwards (negative), while portions of the lower friction and the end bearing are still directed upwards to maintain equilibrium. When the next blow produces a stress wave, activation of the upper resistance forces requires deformations which first bring the negative friction forces to zero before positive resistance is generated. At and near the pile toe, resistance which has been partially preloaded by the previous blow takes less deformation to activate fully. Since the conventional CAPWAP analysis assumes resistances and displacements are initially zero, it underpredicts the lower shaft and end bearing resistances and overpredicts them in the upper strata. By performing residual stress analyses in CAPWAP, the correct distribution can be obtained.

The RSA includes the following steps:

- In a first analysis, **all** variables are initialized to zero. Several additional analyses are then performed with all variables **except the pile segment displacements and the soil resistance forces** initialized to zero.

- After each analysis, CAPWAP performs a static analysis (velocities and therefore damping resistance forces are zero) which produces soil resistance forces in static equilibrium and corresponding residual pile segment displacements.

- The following dynamic analyses are all performed with non-zero initial soil forces and pile segment displacements. In preparation of each analysis, CAPWAP calculates the initial upwards and downwards traveling stress waves in the pile from residual (static) resistance forces.

- CAPWAP performs as many analyses as indicated by the REss option value. After each analysis, the residual pile compression (difference between pile top and pile toe displacement) is calculated.

- In RSA, CAPWAP calculates the blow count (BLctFin) from the final pile top set occurring during the last analysis.

- CAPWAP displays the pile top sets of the last two analyses and the corresponding compression values. If the percentage change of pile compression between the two last analyses is high, then convergence has not been achieved and it may be necessary to perform additional consecutive analyses.

It has been found that indeed the calculated resistance distributions of conventional analyses may overestimate the upper resistance forces. In contrast to GRLWEAP, however, CAPWAP's RSA usually does not produce higher capacities **measured** compared to non-RSA.

For $U_n = 0$, no residual forces can exist. Thus, a non-zero U_n value should be entered before attempting RSA.

Non-convergence is possible in situations where the pile assumes different displacement configurations in certain series of blows. For example, blow (or analysis) 1, 3, 5, ... may have the same pile compression, however, blow 2, 4, 6, ... may assume a different displacement pattern.

D.1.7.8 Summary of Unknowns

With three basic unknowns for each soil resistance force (resistance, quake, and damping), there is a total of 3(NS+1) unknowns. In most instances, all shaft quakes and all Smith shaft damping factors are equal. Equal Smith shaft damping factors are equivalent to viscous damping factors which are proportional to the static resistance values. Thus, there are NS+1 unknown R_{uk} values and two unknowns each for damping and quakes (total unknowns: NS+5).

The extensions of the CAPWAP soil model add another two unknowns for the unloading quakes (shaft and toe), one for the unloading level, two for reloading levels, and three for the toe damping option, gap, and plug. Four parameters are available for radiation damping and the residual stress analysis option is one more unknown. Thus, the total number of unknowns is NS + 18.

The distribution of ultimate shaft resistance forces can be directly determined from the record portion between the time of impact and the time of the first wave return. The remaining 17 quantities have to be determined from the later record portion. Table D.1 lists all unknowns and options, their dimensions and recommended or possible ranges.

Table D.1: CAPWAP Unknowns					
Quantity	Program Symbol	Dimension	Recommended Minimum	Recommended Maximum	Recommended Starting Value
Shaft Quake	QSkn	in/cm	0.01/0.025	max u[2]	0.1/0.25
Toe Quake	QToe	in/cm	0.01/0.025	max u_{toe} - TGap	0.1/0.25
Shaft Unld Quake[1]	CSkn	--	0.01	1.0	1.0
Toe Unld Quake[1]	CToe	--	0.01	1.0	1.0
Unloading Level[1]	UNld	--	0	1.0	1.0
Shaft Reloading Level[1]	LSkn		-1.0	1.0	-1.0
Toe Reloading Level[1]	LToe	--	0.0	1.0	0
Shaft Damping					
Case	JSkn	--	N/A	NS	0.1
Smith	SSkn	s/ft or s/m	0.025/0.08	0.31/1.0[3]	N/A
Toe Damping					
Case	JToe	--	N/A	1.0	0.1
Smith	SToe	s/ft or s/m	0.025/0.08	0.31/1.0[3]	N/A
Smith Damping Option	OPtd	--	0	2.0	0
Pile Damping	Plld	--	0	0.03	0
Shaft Soil Dashpot	SKdp	--	0.02	N/A	0
Shaft Soil Mass	MSkn	Fu	0	N/A	0
Toe Soil Dashpot	BTdp	--	0.02	N/A	0
Toe Soil Mass	MToe	Fu	0	N/A	0
Plug Mass	PLug	Fu	0	3 toe weight	0
Toe Gap	TGap	in/cm	0	max u_{toe} - Q_{toe}	0
Residual Stress Option	REss	--	0	5	0

Notations:
(1) Multiplier
(2) Maximum displacement
(3) Higher values are possible though uncommon
Fu - Force unit; NS - Total number of soil elements

D.1.8 Match Quality Evaluation

The match quality (MQ) is evaluated by summing the absolute relative differences between the computed and measured pile top variable:

$$MQ = \Sigma \, [|f_{jc} - f_{jM}| / F_M] \tag{D.53}$$

with f_{jc} and f_{jM} being the computed and measured pile top variables, respectively, at time j and F_M is the maximum measured pile top force. The analysis time period is subdivided into four intervals as in figure D.9.

1. The first period extends from the onset of impact over a period 2L/c. This period generally indicates the shaft frictional distribution. The summation in equation (D.53) is normalized with respect to time to avoid an excessive influence on MQ as pile length increases.

2. The second period starts 2L/c after the peak and lasts for a period equal to the rise time (t_r) plus 3 ms, and is usually important for proper determination of toe resistance parameters and total resistance (static plus damping).

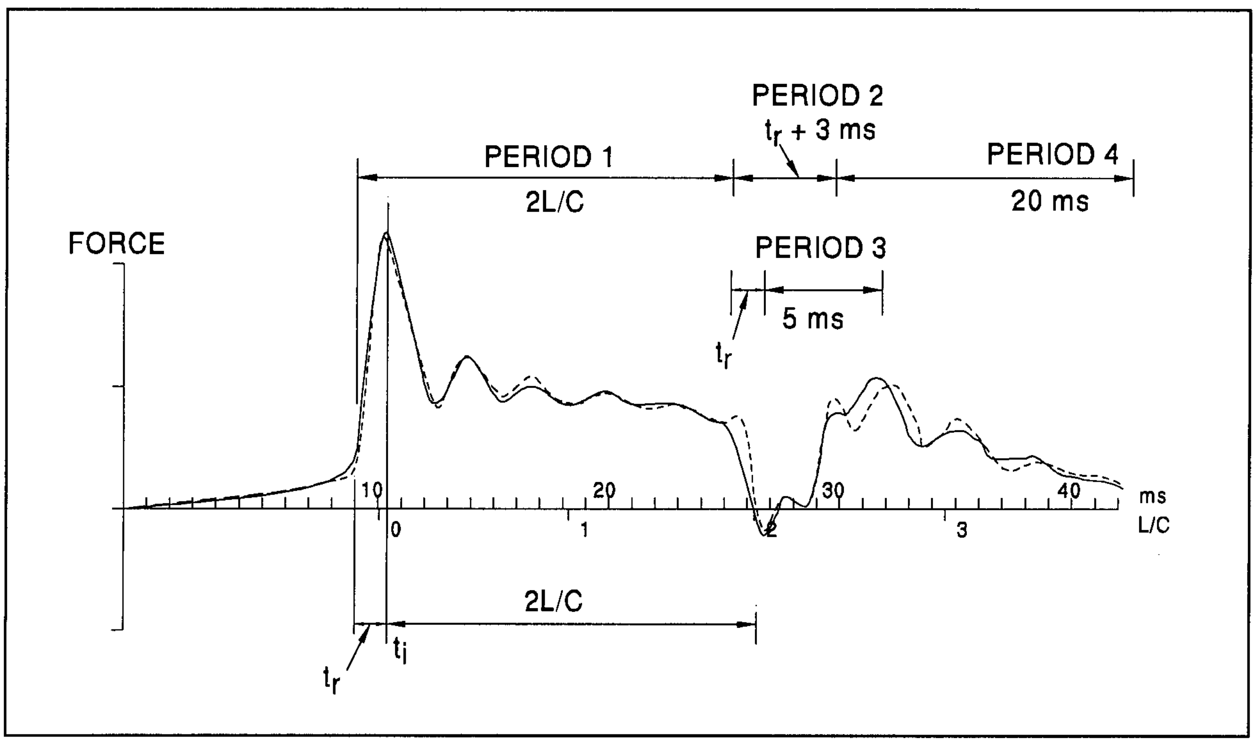

Figure D.9: Error Evaluation - CAPWAP

3. The third time period starts 2L/c after the peak impact velocity and extends over the next 5 ms. During this interval, the proper R_{ut} is most clearly apparent.

4. Finally, an interval of up to 20 ms is investigated, starting at the end of the second interval. During this late record portion, the unloading behavior of the soil affects the pile top variables.

The overall match quality reflects the match quality in all four periods. Because of the overlap of intervals 2 and 3, the time just after 2L/c has double weight compared to other times. The magnitude of R_{ut} therefore affects MQ more than the other soil resistance parameters.

D.1.9 Blow Count Matching

Besides matching the measured and computed pile top variables as a function of time, the agreement of computed with field observed blow count is often a useful guide in the evaluation process. The blow count is computed in three different ways:

$$BCT_q = 1.0 / (u_{tm} - q_{av}) \tag{D.54}$$

$$BCT_f = 1.0 / u_{tf} \tag{D.55}$$

$$BCT_r = 1.0 / (u_{now} - u_{bef}) \tag{D.56}$$

In equation (D.54), u_{tm} is the maximum computed toe displacement and q_{av} is an average quake, weighted with respect to resistance values:

$$q_{av} = \Sigma\ (q_i\ R_{ui}) / R_u \tag{D.57}$$

with q_i and R_{ui} being the segment quake and ultimate resistance values, respectively, and R_u is the total ultimate capacity. This blow count definition is identical to that in GRLWEAP.

Equation (D.55) is based on the final calculated toe displacement, u_{tf}. This value depends on the end time of the analysis and is generally a less reliable indication. Equation (D.56) is the blow count calculation in the residual stress analysis from the difference between the pile top displacement of the last, u_{now}, and previous dynamic analysis, u_{bef}, and is probably more accurate than the other definitions. Blow count calculation is always unreliable when radiation damping is employed.

APPENDIX E

GROUND SURFACE MEASUREMENTS DURING SPT AND PILE DRIVING

E.1 INTRODUCTION

The objective of improved soil parameter determination for dynamic analyses of pile driving can only be met if more information than the normal SPT or Cone data is available. It is natural to gather additional information by simple means during the normal testing or driving procedures. For example, during SPT it should be a simple matter to detect the soil's shear wave speed in a manner similar but inverse to the Seismic Cone (where the shear wave is induced at the ground surface and the arrival time measured at the cone tip). During pile driving, if it were possible to detect the effect of the start of the pile toe motion, then again a well defined vertical wave speed should be known.

Ground surface measurements were attempted using standard geophones (Mark Products, Type L28) and recording the motion on a seven channel cassette instrumentation recorder. Surface sensors were placed to collect vertical velocities. They were reproduced by the tape recorder and digitized by a Model GCPC, Pile Driving Analyzer. A specialized program was then employed to plot the records at various time scales. This program also plotted a "resultant" (VR) velocity which is meaningless for these unrelated records. The plots also include two vertical lines each with a number, indicating time in milliseconds, near its bottom for the calculation of wave travel times.

Ground surface measurements were collected once during pile driving at the ID# 43 site in Cleveland and another time at the special test site during the SPT with a newly developed automatic SPT hammer. Both efforts are described in the following.

E.2 PILE DRIVING SITE

The pile was an HP12x53 (HP310x79) with 160 ft (48.8 m) length; it was driven by a Vulcan 506 hammer into a 48 ft (14.6 m) silty sand overlying a silty clay layer. During driving, geophones were placed at distances of 13, 24.5 and 48.5 ft (4.0, 7.5 and 14.9 m) from the axis of the pile but only two geophones were recorded at the same time. For the most meaningful shear wave velocities, records from the 13 and 48.5 ft (4.0 and 14.9 m) geophones were used (a total distance of 35.5 ft or 10.8 m between geophones).

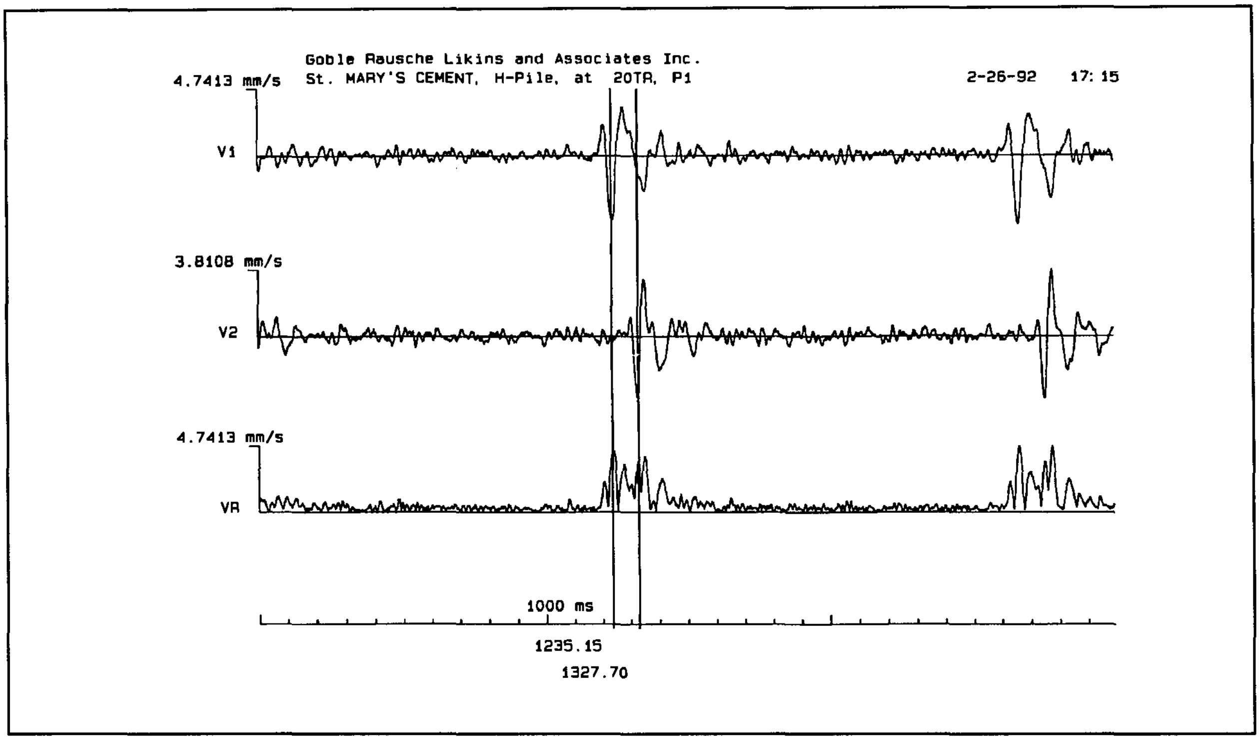

Figure E.1: H-Pile at 78 ft (23.8 m) Depth; Vs = 35.5/(1328 - 1235) = 382 ft/s (116 m/s)

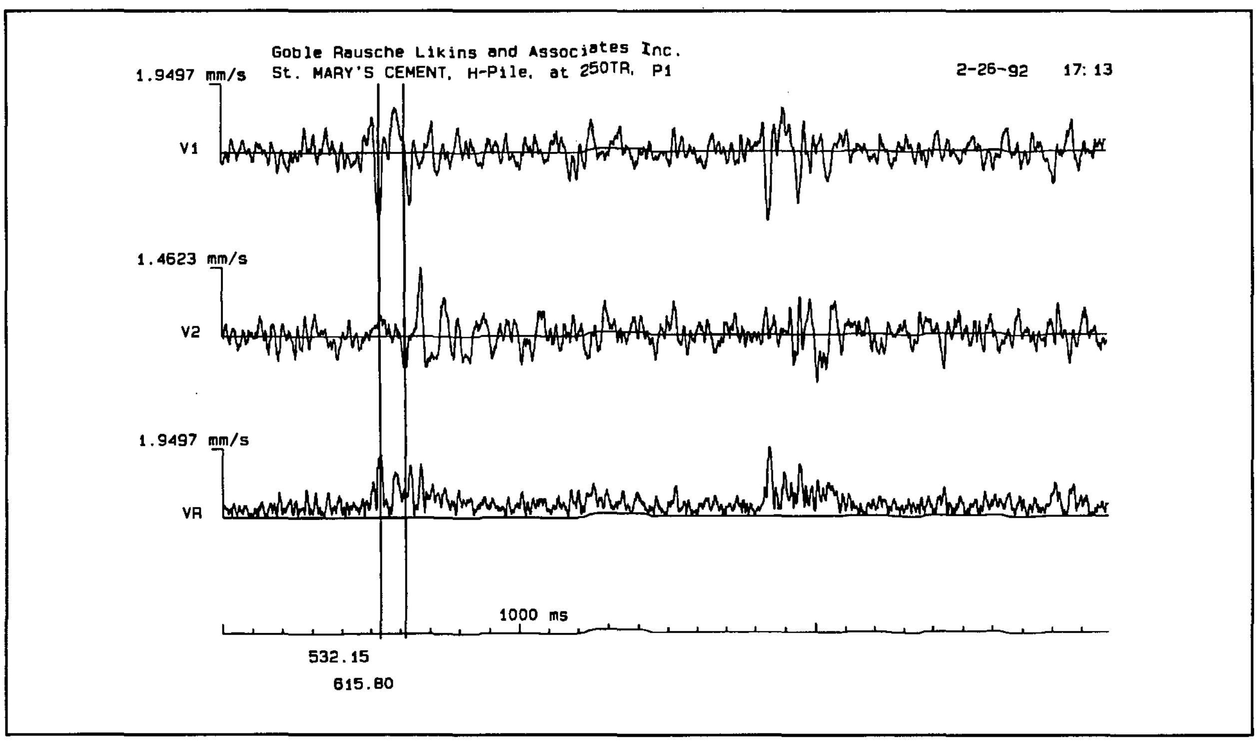

Figure E.2: H-Pile at 106 ft (32.3 m) Depth; Vs = 35.5/(615.8 - 532.2) = 42.5 ft/s (130 m/s)

Figures E.1 and E.2 show V1 (13 ft or 4.0 m) and V2 (48.5 ft or 14.9 m) records from respective pile tip depths of 78 and 106 ft (23.8 and 32.3 m) depth. Investigation of these records allows for the calculation of shear wave velocities. This pile's resistance was primarily shaft friction. For that reason, it is not surprising that no distinct pile toe signal is apparent (should reach the surface approximately 200 ms after impact). If a pile toe longitudinal wave would reach the top then it would probably be masked by the shear wave effects.

E.3 SPT SITE

Ground surface measurements from two different SPT sampler depths were taken. One was taken when the sampler had reached 25 ft (7.6 m) depth, the other one when it was at 50 ft (15.2 m) depth. Figures E.3 and E.5 show respective 6-s records. They include a signal taken on the top of the rod (V3) (for timing purposes), one at a distance of 2.0 ft or 0.6 m (V1) and another one at 6.8 ft or 2.1 m (V2) from the rod.

The ground surface velocity traces were difficult to interpret since three distinctly different events occurred. Based on the timing information from the rod top (V3), it was concluded that the event preceding rod impact was a ram release which caused the SPT rig to rebound, thereby exerting an impact on the ground surface. The free fall of the ram through a 30-in (762- mm) distance takes 390 ms based on theoretical calculation. It can be seen in the time expanded records of figures E.4 and E.6 that the time between supposed ram release and rod impact is 502 and 455 (see the time indicators at the bottom of the cursors in figures E.4 and E.6, respectively, and take their differences) or greater than 390 ms. (It probably takes some time between ram release and a reaction on the ground surface or due to the friction within the ram system.)

A similar ground surface motion occurs between the time of rod impact and ram release. It is theorized that this motion results from a rig rebound due to ram re-engagement.

During and shortly after the ram impact, a relatively small ground surface motion can be observed. This motion could partially be the result of some shear wave caused by a horizontal impact of the rod against the ground and, of course, of a compressive wave from the sampler. In figure E.7, cursors were placed at corresponding wave shapes in V1 and V2. They indicate a surface shear wave travel time of 9 ms from the 2 ft (0.6 m) to the 6.8 ft (2.1 m) sensor. The surface shear wave velocity therefore appears to be 4.8/.009 or 530 ft/s (162 m/s). However, surface shear wave speeds are relatively unimportant for the study of soil properties for deep foundations. Investigation of the records from sampler created waves at the surface would, therefore, appear to be much more important. A longitudinal wave arrival from the sampler should arrive at the ground surface approximately 60 ms after rod impact for the 50 ft (15.2 m) depth. Figure E.7 unfortunately does not clearly reveal such an event.

E.4 CONCLUSIONS

Although these ground surface measurement records are interesting and instructive, they did not provide the basis for meaningful qualitative interpretations. Most meaningful would be either a compressive or a shear wave speed calculation which, if taken for every SPT sample, would yield shear wave velocities for each soil layer sampled. Unfortunately, however, because of interference with shear waves of several sources, the arrival time of the compressive wave from the toe was not clearly apparent in either pile driving or SPT records. However, since the concept is convincingly simple and straight forward, additional efforts should be made with the SPT with better control during testing.

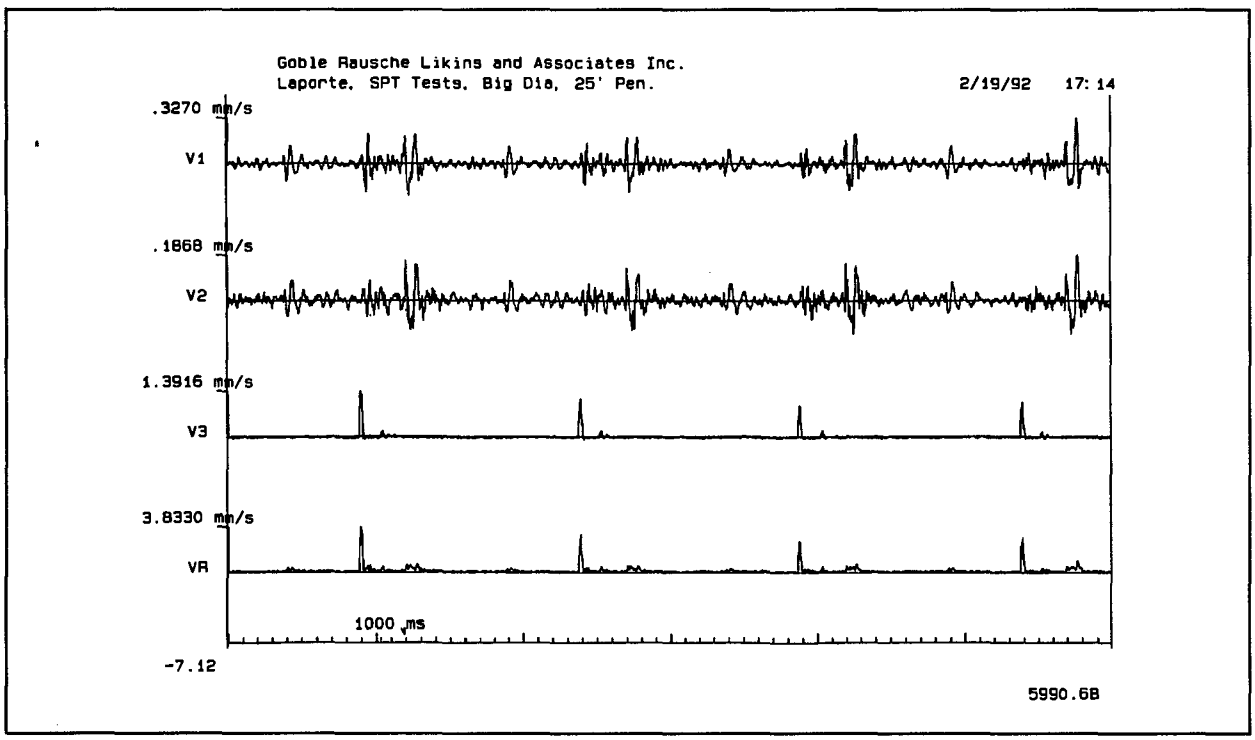

Figure E.3: SPT Results

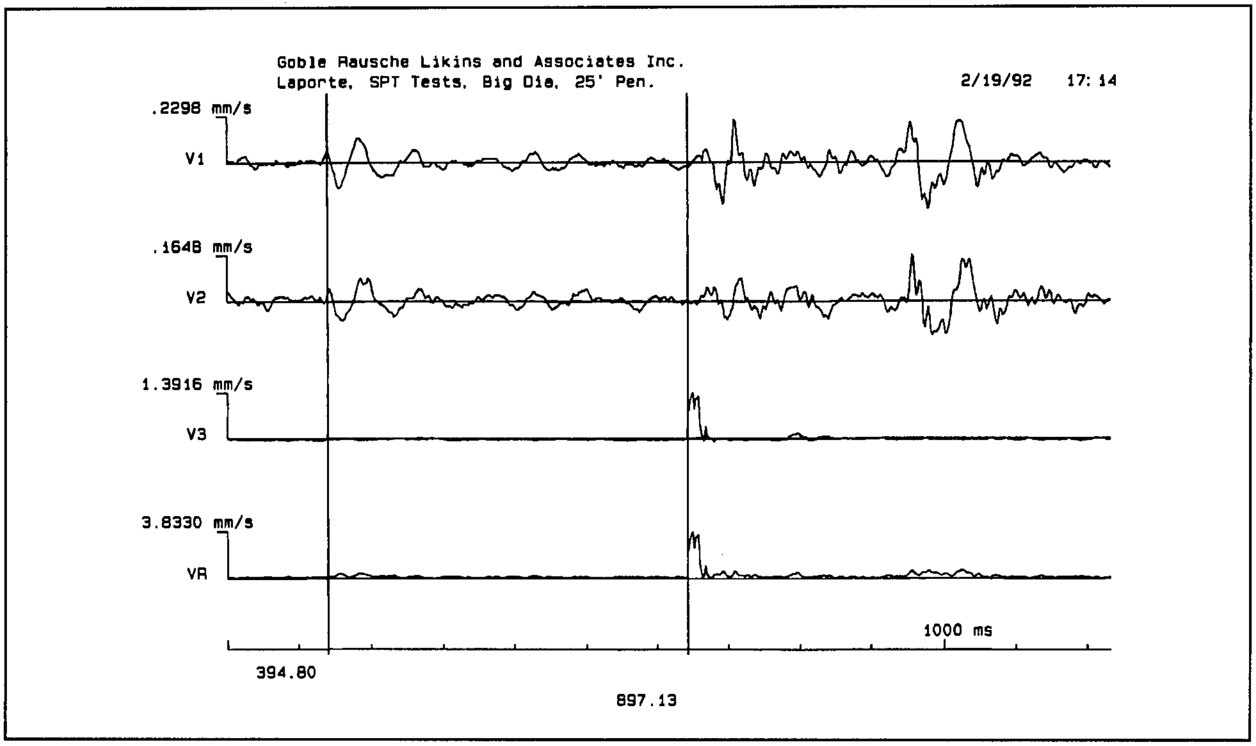

Figure E.4: SPT Results, 25 ft

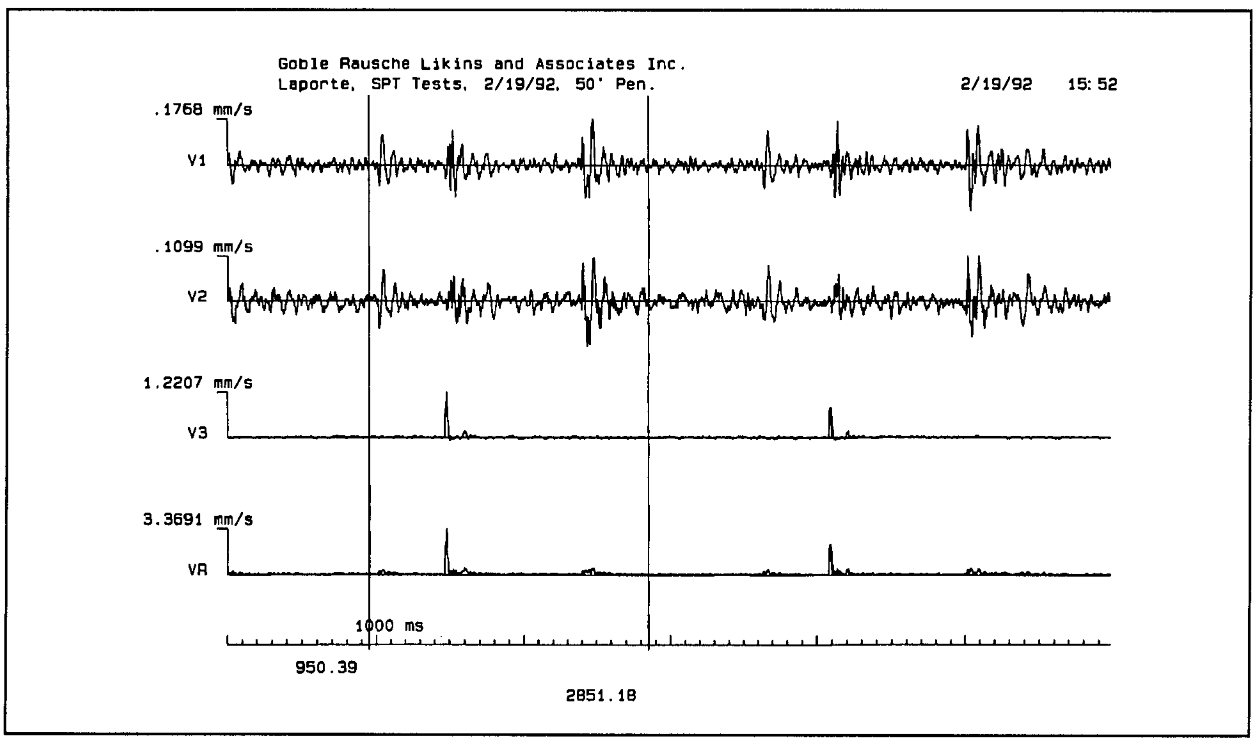

Figure E.5: SPT Results, 50 ft, 6 s

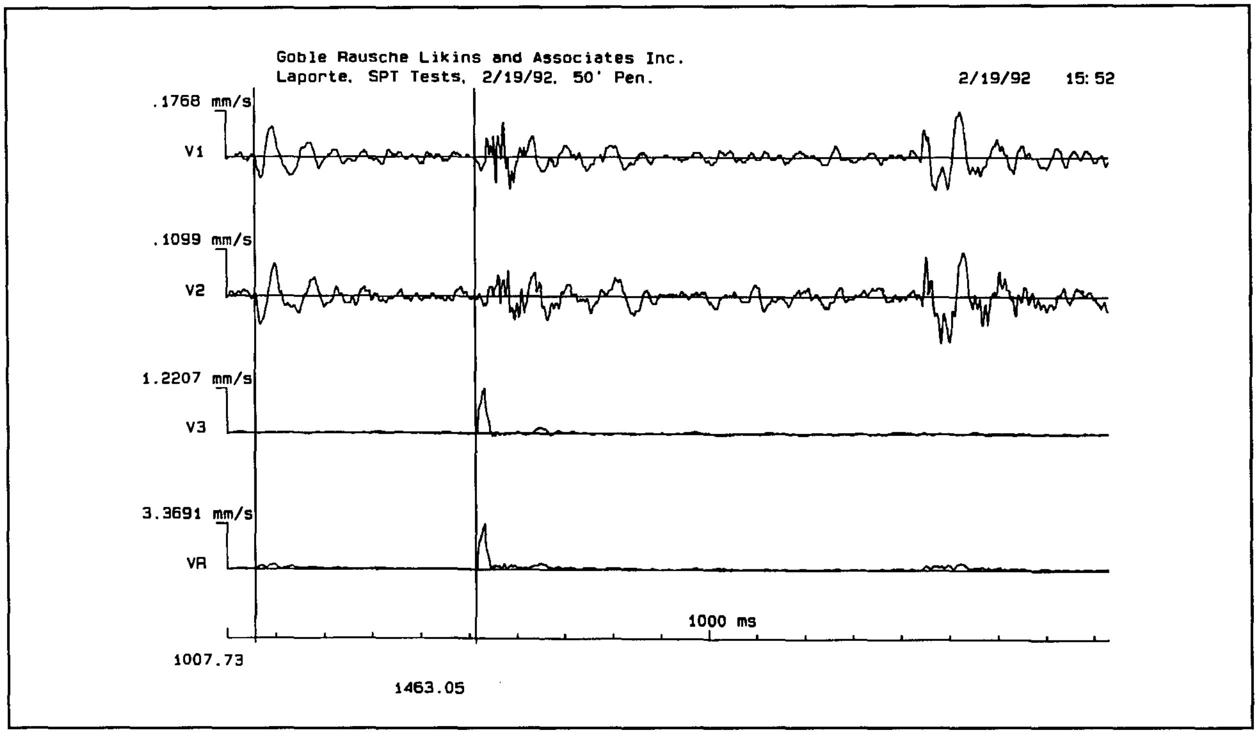

Figure E.6: SPT Results, 50 ft, 2 s

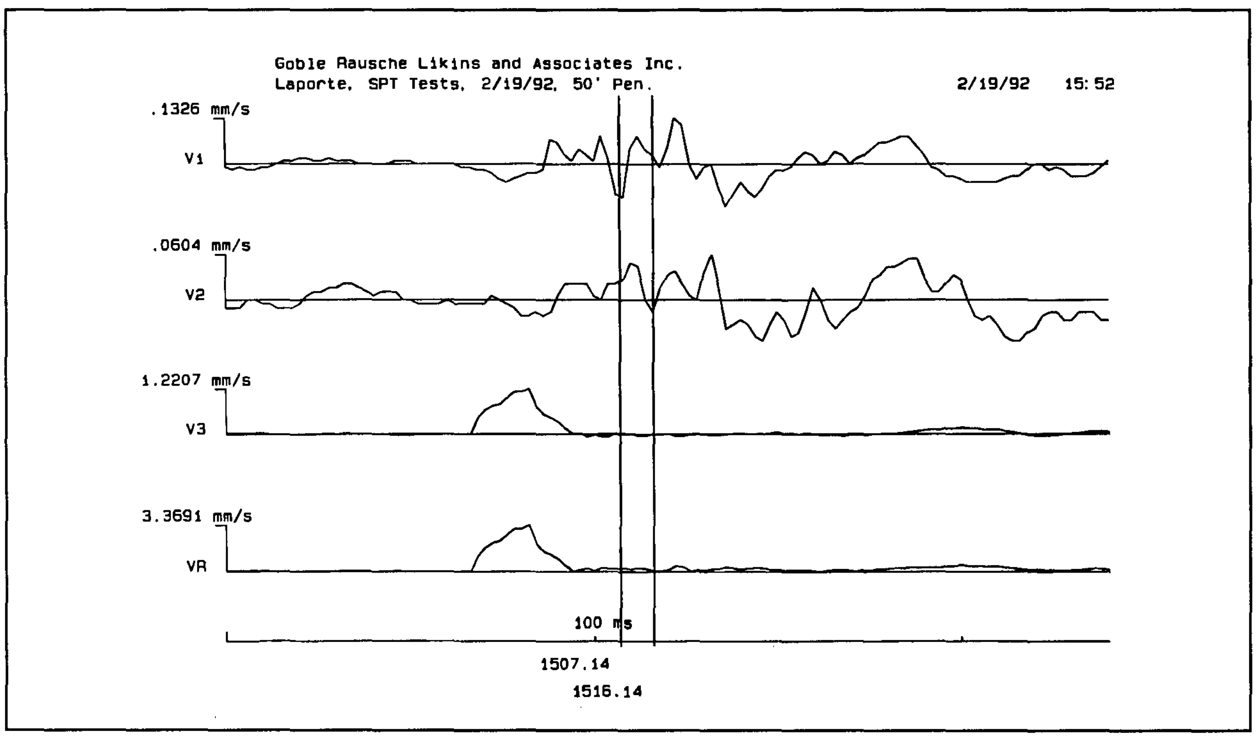

Figure E.7: SPT Results, 50 ft, 250 ms

APPENDIX F

RESULTS FROM SENSITIVITY STUDY

A wave equation study was conducted to investigate the sensitivity of the bearing graph results to changes in the four basic dynamic pile analysis parameters: shaft and toe quakes, and shaft and toe damping factors. For this first limited study, similar pile-hammer combinations were chosen with primarily different pile materials. Of course other, and maybe more meaningful combinations are possible.

(a) HP 14x117 (HP 360x174) with Delmag D36-32

(b) 24-in (610-mm) square PSC pile with Delmag D36-32

(c) 24-in (610-mm) tapered timber pile with Kobe K 35

All three analyzed situations were for relatively large piles under open end diesel hammers. These examples were chosen in order to make the analyzed situations vary only with respect to pile material. Obviously, many other configurations could and should be included in these studies.

For each value of the investigated parameter, capacities were chosen from the bearing graph at 39 and 91 blows/ft (100 and 300 blows/m) to represent both easy and hard driving cases. The results were then plotted in the form of normalized capacity as a function of the magnitude of the investigated parameter. Normalized capacity was defined as:

$$R_{un} = R_u / (V_i Z) \qquad \text{(F.1)}$$

with Z being the impedance, and V_i the ram impact velocity as indicated by the GRLWEAP program. In general, the plots show a reduction in capacity with increase in value of the investigated parameters. At higher blow counts (91 blows/ft or 300 blows/m), the reaction tends to be greater.

Table F.1 summarizes these results by showing the percentage reduction of the capacity for a 100 percent increase of the investigated parameter above the GRLWEAP recommendation. For example, the capacities were calculated for shaft dampings (shaft quakes) of 0.05 and 0.1 s/ft or 0.15 and 0.30 s/m (0.1 and 0.2 in or 2.5 and 5.0 mm). Table F.1 indicates that for these two quantities, capacity prediction would decrease by an average of 11 and 4 percent, respectively at a blow count of 30 blows/ft (100 blows/m), and by 12 and 3 percent, respectively at 91 blows/ft (300 blows/m). The greatest variation of capacity prediction occurred with toe quakes and high blow counts (up to 31 percent).

Obviously, capacity predictions are more sensitive to the change of toe parameters than shaft parameters. This is in part due to the fact that the results presented here were obtained for toe parameters whose absolute values were much greater than the corresponding shaft values. For this study, starting values for shaft and toe damping factors were 0.05 and 0.15 s/ft (0.02 and 0.49 s/m), and shaft and toe quakes of 0.1 and D/120 in (2.54 and D/120 mm). One thing is comforting, however, the relative capacity changes are in general much lower than the relative soil parameter changes causing them.

Table F.1: Summary of Sensitivity Study from Three Hammer-Pile Combinations

Blow Count blows/m	Capacity Reduction for 100 percent Parameter Increase, (%)				
		Shaft Quake	Toe Quake	Shaft Damping	Toe Damping
100	Min	0	6	8	19
	Max	11	12	13	24
	Avg	4	8	11	20
300	Min	7	7	9	12
	Max	20	31	15	21
	Avg	9	16	12	17

APPENDIX G

DOCUMENTED LARGE QUAKE CASES

G.1 INTRODUCTION

This discussion only concerns cases with excessively large toe quakes since unusually large shaft quakes, or very small shaft or toe quakes have not been described in the literature nor encountered in the authors' practice. However, several cases of large toe quakes causing installation problems or uncertain bearing capacities have been described in the literature (see chapter 2). In addition, four complete data sets with indicated large restrike toe quakes were found in the data base compiled in this research project. Other cases have been encountered during the authors' practice. Unfortunately, since no load test was performed, these additional cases did not satisfy the requirements of a complete data set and therefore could not be included in the data base. A discussion of such additional cases is included in this appendix because of its importance for driveability analyses.

G.1.1 Literature Cases

The data collected by Authier and Fellenius (1980), Likins (1983), and Hannigan (1984) has been discussed in chapter 2. Complete data sets were not presented by these authors. These cases represent piles driven into till (4 cases) and into dense sand or dense fine sand (2 cases). Hannigan suggested that the capacity determined by the wave equation analysis would have been overpredicted by 49 percent, had the large quake condition not been recognized. Hannigan presented the only case of a non-displacement pile with large toe quake. However, he also suggested that the pile actually plugged and therefore acted like a displacement pile. Hannigan showed that, in his case, a large quake existed both at end of driving and during restrike.

G.1.2 Additional Cases

G.1.2.1 Pine Bluff, Arkansas

GRL engineers tested two piles in this area. Satisfactory soil information was only available for the first pile tested and only this one will be discussed here. The pile consisted of 14 in (360 mm) square prestressed concrete of 40 ft (12 m) length. Its design toe depth was 20 ft (6.1 m) where the soil was described as a medium dense to dense, tan and gray clayey sand with sandy clay or clay pockets. The SPT N-values ranged between 28 and 39. The ultimate pile capacity calculated from dynamic records at 20 ft (6.1 m) depth was 215 kips (956 kN). At 17 ft (5.2 m) depth, a maximum capacity of 260 kips (1 156 kN) was calculated by CAPWAP with a toe quake of 0.44 in (11.2 mm). The blow count was 47 blows/ft (154 blows/m). The pile was later driven to greater depth where it encountered very stiff silty clay and an even lower bearing capacity. A restrike test was not performed.

A standard wave equation analysis yielded 310 kips (1 379 kN) capacity at 47 blows/ft (154 blows/m). A wave equation analysis with hammer performance adjustments based on dynamic measurements indicated the observed blow count and the 260-kip (1 156-kN) CAPWAP capacity, when a standard toe quake of 0.12 in (3.1 mm) was used together with standard damping factors (WEAP would not have indicated a quake problem!). The corresponding result with a 0.44-in (11.2-mm) toe quake was approximately 230 kips (1 023 kN) (12 percent underprediction), but required the toe damping factor be reduced to 0.10 s/ft (0.33 s/m) (rather than analyzing with the standard 0.15 s/ft or 0.49 s/m). The relatively low prediction error considering the nearly 4 times greater than normal toe quake must be attributed to a high energy relative to the capacity and to a relatively stiff (short) pile.

G.1.2.2 Portland, Maine (Data Base ID# 24)

The pile was an 18-in (457-mm) diameter closed ended pipe with a length of 60 ft (18.3 m) and an end of driving penetration of 50 ft (15.2 m).

The pile toe was driven into dense, medium to fine sand with varying amounts of gravel sand and silt (ablation till). The SPT N-value at the pile toe was approximately 32 to 39. Driving with the Kobelco K45 open end diesel hammer resulted in an end of driving blow count of 15 blows/ft (49 blows/m) and 36 blows/ft (118 blows/m) at the beginning of restriking. The large quake assessment was made with the restrike data.

It is particularly important to note that the ultimate capacity of this pile (static test result of 350 kips (1 557 kN) after Davisson) would be overpredicted if the standard toe quake of 0.15 in (3.81 mm) rather than the CAPWAP (restrike) toe quake of 1.0 in (25.4 mm) were used in a wave equation analysis. The standard wave equation predicted 595 kips (2 647 kN) (70 percent overprediction) and the hammer performance adjusted analysis still gave 480 kips (2 135 kN) (37 percent overprediction). The contention that large quakes are only dynamic properties and that the associated dynamically calculated bearing capacities are always unrealistically low, is therefore incorrect in at least this one case. It is correct, however, that the quake was smaller during the static load test as evidenced by the much stiffer static than dynamic load test curve (figure G.1). However, the maximum load determined by CAPWAP matches the Davisson load determined in the static test. Thus, even if the large quake is a dynamic quantity, its effect on the capacity prediction must be recognized.

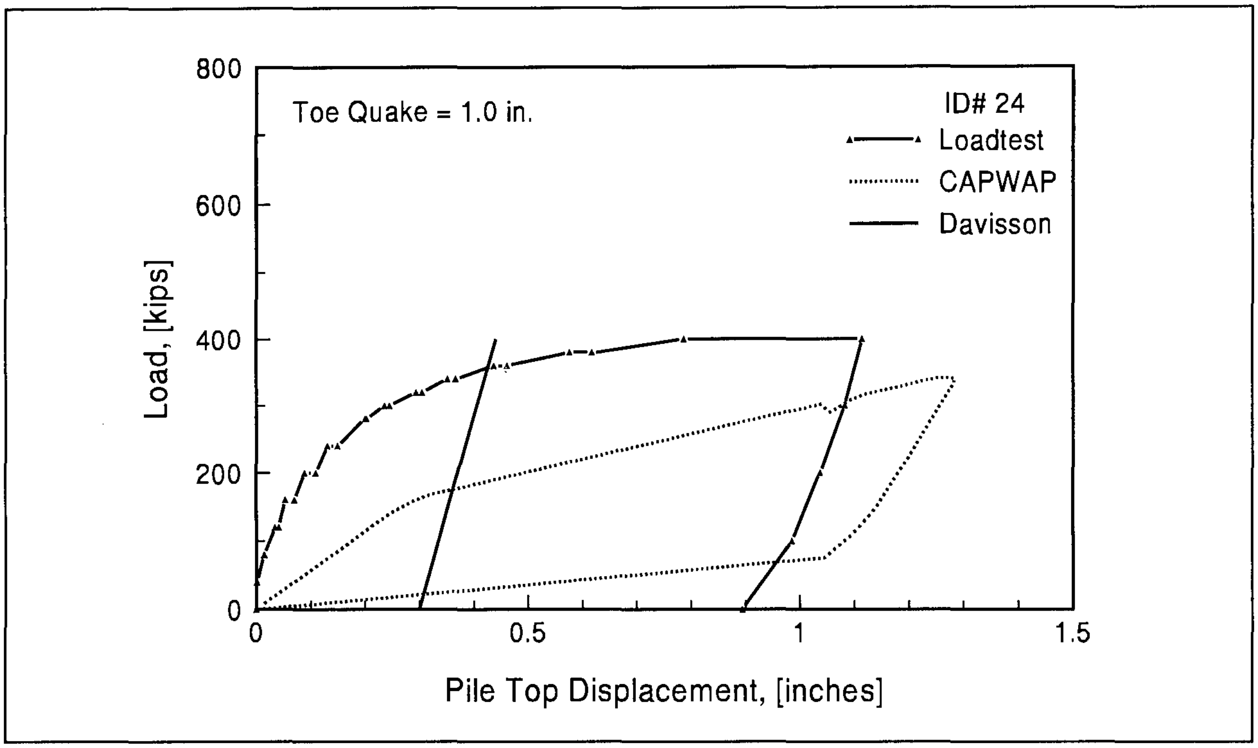

Figure G.1: Load-set Curves from Static and Dynamic Test, ID# 24

G.1.2.3. White City, Florida (Data Base ID# 63)

The 24-in (610-mm) PSC pile of 44 ft (13.4m) length was driven into a dense sand to a depth of 30 ft (9.1 m) where the SPT N-value reached 26. (Higher values were encountered at a greater depth). The soil was described as compacted gray sand.

The end of driving and restriking blow counts under the Delmag D 46-02 were 60 and 96 blows/ft (197 and 315 blows/m), respectively. As for DB ID# 25, the CAPWAP calculated load-set curve (figure G.2) was much flatter than the static load test curve. Agreement between CAPWAP ultimate (480 kips or 2 135 kN) and Davisson's static capacity (460 kips or 2 046 kN) from the static load test was again good. However, the Davisson limit applied to the CAPWAP curve would have produced a severe underprediction. Therefore, the large quake was again a dynamic and not a static parameter. However, without knowledge of the large dynamic quake, the capacity would have been overpredicted. The wave equation analyses predicted 700 and 850 kips (3 114 and 3 781 kN) before and after adjustment of hammer performance, respectively. Without recognizing better than normal hammer performance and the large quake condition, the overprediction would have been 53 percent. Had the hammer performed as normally expected, the blow counts would have been higher and the overprediction could have been even 85 percent. The ultimate capacity of 460 kips (2 046 kN) was obtained when WEAP toe quake of 1.07 in (27.2 mm) was utilized.

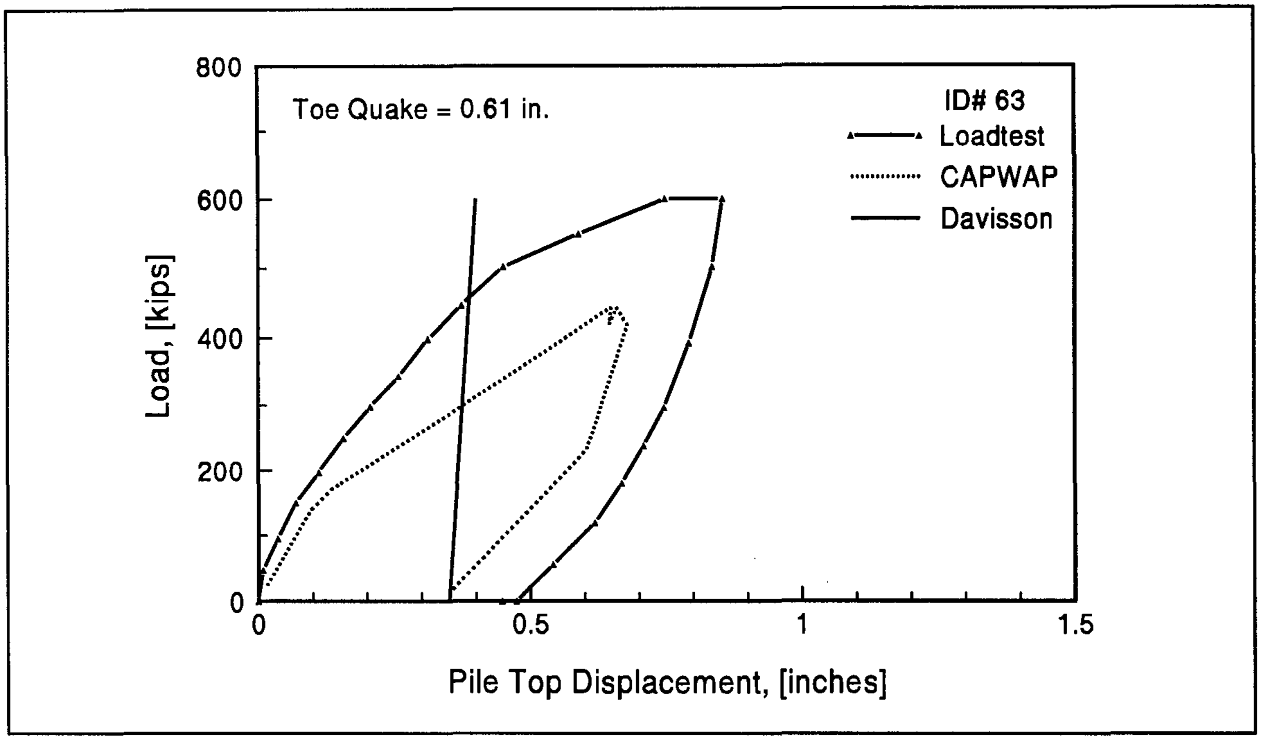

Figure G.2: Load-set Curves for Static and Dynamic Test, ID# 63

G.1.2.4 Battery Creek, South Carolina (Data Base ID# 75)

The pile consisted of a 24-in (610-mm) octagonal prestressed concrete pile with HP12x74 (HP310x110) stinger. The total pile length was 81.5 ft (24.8 m); the stinger extended 2.5 ft (0.76 m) below the concrete, *i.e.*, the concrete pile length was 79 ft (24.1 m). The soil at the pile toe (and for more than 60 ft or 18.3 m above it) consisted of calcareous sand, medium dense, fine to coarse with gravel size limestone and shell. The pile was driven to 33 blows/ft (108 blows/m) at the end of driving. During restrike with the same Vulcan 520 hammer, the blow count was 24 blows/ ft (79 blows/m).

The static load test indicated a Davisson limit load of 510 kips (2 269 kN). The standard and hammer performance adjusted capacity values from wave equation analyses were 600 and 660 kips (2 669 and 2 936 kN), respectively. The overprediction, therefore, would have been 29 percent if the large quake had not been recognized.

CAPWAP and the static load test produced nearly identical load-set curves (figure G.3), indicating that the calculated large quake (0.45 in or 11.4 mm) was both a static and a dynamic soil condition.

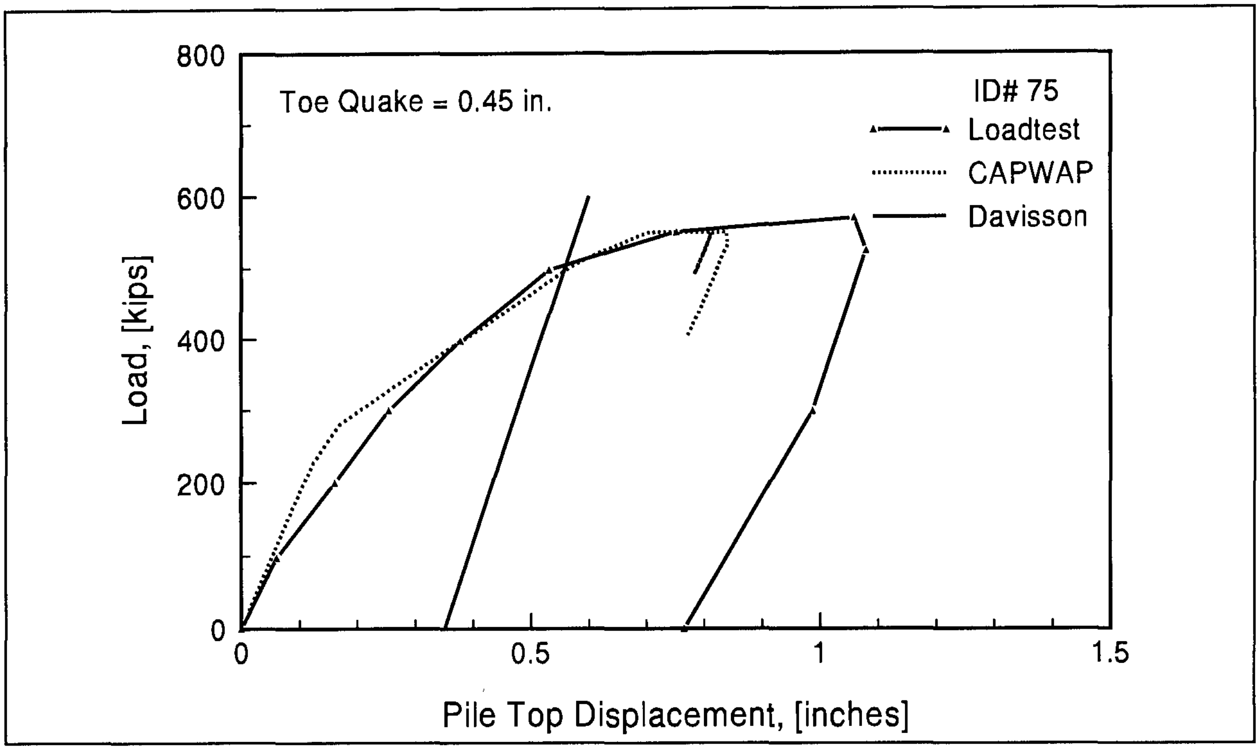

Figure G.3: Load-set Curves from Static and Dynamic Test, ID# 75

Of course, the existence of the 2.5 ft (0.76 m) long stinger sheds some doubt on these conclusions. First, the stinger could have been damaged since its impedance was rather small compared to that of the concrete pile. Secondly, the pile width at the toe is not certain. Should the concrete pile toe be considered when calculating end bearing, or the steel tip, or both together, or the steel tip filled with compacted soil (this could have been a relatively flexible material and possibly have provided an explanation for the large quake). This latter reasoning could explain why the static and dynamic quakes were similar.

G.1.2.5 Hartford Bridge, Vermont (Data Base ID# 27)

This last example is of a different nature; CAPWAP indicated a large toe quake and approximately 50 percent end bearing which means that plugging occurred on this H-pile. The load test curve (figure G.4) matched the CAPWAP simulation for low loads suggesting that the large quake occurred both during static and dynamic testing. However, the unusually large capacity underprediction by both CAPWAP and WEAP (see below) must be attributed to different failure mechanism under static and dynamic loads. This case is, therefore, not suitable for the calculation of dynamic soil parameters but was considered informative in the present context.

The pile was an HP14x73 (HP360x108) which is a non-displacement pile. The total length of the pile was 95 ft (29 m) and the end of driving penetration was 90 ft (27.4 m). The soil can be described as loose to medium dense sandy silt of approximately 20 ft (6.1 m) thick, overlying very dense sandy gravel with cobbles and boulders. The soil borings closest to this pile was terminated at 70 ft (21.3 m) depth, but other soil borings at the site indicated that the sandy gravel layer extended to at least 115 ft (35.1 m) depth. The soil at the pile toe therefore is sandy gravel with SPT N-values of approximately 60.

The pile was installed with an MKT DA-35B closed end diesel hammer with an end of driving blow count of 32 blows/ft (105 blows/m) and beginning of restriking blow count of 72 blows/ft 236 blows/m).

Unlike the four displacement piles discussed earlier, the wave equation analysis results for this non-displacement pile underpredicted the capacity. The static load test indicated a Davisson limit load of 390 kips (1 735 kN). The standard wave equation analysis predicted 275 kips or 1 223 kN (30 percent underprediction) and the hammer performance adjusted predicted 335 kips or 1 490 kN (15 percent underprediction). The load-set curve from static load test and CAPWAP simulation are presented in figure G.4. A standard toe quake used in the wave equation analysis was 0.121 in (3.1 mm). To match the Davisson limit load, the toe quake had to be reduced to values less than 0.121 in (3.1 mm). This conflicts with the 0.34 in (8.6 mm) toe quake predicted by CAPWAP.

One explanation to the capacity prediction problems might be the plugging action at the pile toe. During the static load test, the soil plug acted at the pile toe to provide the toe resistance. However, during dynamic testing, the soil plug slipped and therefore the large toe resistance was not activated. Another possibility is a severe underprediction of friction. In the dynamic situation, the full friction might only occur along the outer flanges of the H-profile while the failure surface might extend all along the pile-soil interface (3 times greater surface area) during static testing. Note also that SPT results indicate a rather substantial soil resistance which would not be apparent from the pile driving record. One therefore may be tempted to fault the SPT, even though the static test verifies significant bearing capacities.

In summary, this soil exhibited large quakes, but their effect on driveability was negligible since dynamically activated resistances were significantly lower than the static one.

G.1.3 Conclusions

The results from correlation analyses and the associated analysis input values are shown in table G.1 for the five cases discussed earlier. It would probably be relatively easy to find other test results like the Pine Bluff case with a high quake at the end of driving situations. Those case studies would be of importance for driveability analyses. However, the current phase of

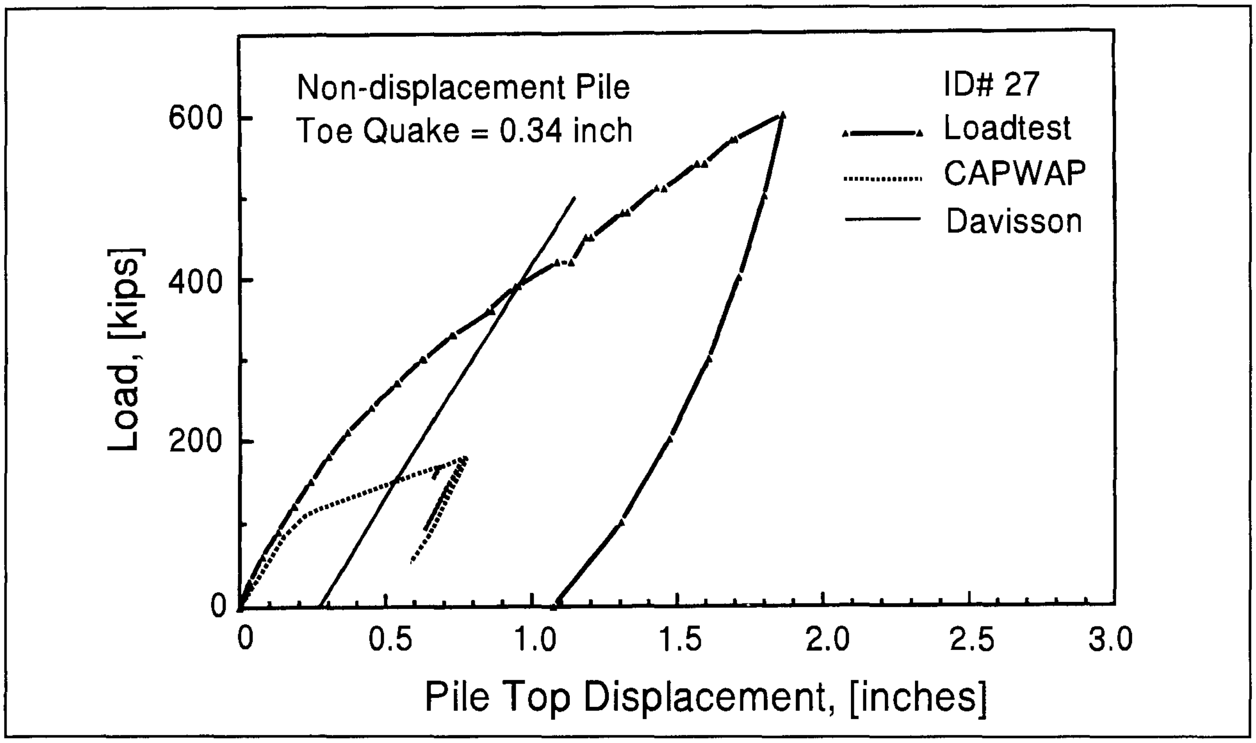

Figure G.4: Load-set Curves for Static and Dynamic Test, ID# 27

the study has primarily addressed the capacity determination aspects which must be based on restrike, not end of driving information. Including the literature cases, soils prone to large quakes primarily seem to consist of saturated sands (probably fine grained or with a significant amount of fines in them) and glacial tills (an overconsolidated conglomerate of various grain sizes). It is conceivable that large toe quake situations are often not recognized in cohesive soils because their associated capacity are negligible.

Large quakes are, with exceptions, dynamic phenomena not occurring during static loading. The exception recognized here was a calcareous sand. Large quakes may sometimes cause extremely high blow counts (and also higher tension stresses). Associated low capacities are then often a very unwelcome surprise.

Further data investigations are needed to find unusually large end of driving quakes which would affect driveability. The current study did not attempt to identify such large end of drive quakes.

Table G.1: Summary of Large Toe Quake Cases								
Pile	Pile Type	Blow/Test blows/ft	Capacity kips	WEAP(S) kips	WEAP(A) kips	Quake(S) in	Quake(A) in	Quake Ratio
Pine Bluff	14"PSC	47/EOD	260	310	260	0.12	0.44	3.67
ID# 24	18"CEP	36/BOR	350	595	480	0.15	1.00	6.67
ID# 63	24"PSC	96/BOR	460	700	850	0.20	1.07	5.35
ID# 75	24"PSC-O	15/BOR	510	600	660	0.20	0.45	2.25
ID#27	HP14x73	72/BOR	390	275	335	0.12	N/A	N/A

Notations:

Blow/Test	Blow count and test type (EOD ... End Of Drive; BOR ... Begin Of Redrive)
Capacity	Capacity from static load test, except CAPWAP for Pine Bluff
WEAP(S)	Standard WEAP result
WEAP(A)	WEAP with standard soil parameters but adjusted for measured EMX, FMX
Quake(S)	Standard quake (D/120)
Quake(A)	Quake after adjustments
Quake Ratio	Quake(A)/Quake(S)

1 kip = 4.45 kN
1 blow/ft = 328 blows/m
1 inch = 25.4 mm

APPENDIX H

DOCUMENTED HIGH SOIL DAMPING CASES

H.1 INTRODUCTION

The following section discusses cases for which high soil damping was calculated in the correlation study. A high soil damping is referred to as a damping value higher than GRLWEAP recommendations. The wave equation analysis characterizes soil shaft damping based on cohesive or cohesionless soil properties. The use of correct damping value is critical in accurately predicting the bearing capacity of the pile. For the pile toe damping factor, the recommendations are independent of soil types.

Unless the soil which requires a high damping factor for proper modeling can be identified, overprediction of the pile bearing capacity cannot be prevented. When a high soil damping case was found during the correlation study, the question as to whether to increase the shaft or toe damping factor was decided based on the soil resistance distribution on the pile which was determined from static pile capacity calculations (using Norlund and alpha method). If the statically calculated shaft resistance was equal to or greater than 70 percent of the total resistance then the shaft damping factor was increased. If the toe resistance was equal to or greater than 70 percent of the total resistance then the toe damping was increased; otherwise both shaft and toe damping were increased proportionally. Because of this procedure, resulting damping factors were dependent on the quality of prediction of the static pile capacity calculations.

H.2 HIGH TOE DAMPING CASES

Data base entries from three sites have been clearly identified as having high toe damping. All of them were located near a water front (*i.e.*, river or bay), therefore the soil is believed to be fully saturated. All piles were driven into either silty sand or clayey sand with a high SPT N-value. Fully saturated cohesionless soil therefore can be suspected to have a high toe damping.

In discussing damping factors, it must be realized that according to Smith's damping definition, damping can be high either because the static resistance is surprisingly low or because the viscous resistance effects are high. Thus, a high toe damping factor may not necessarily indicate high soil viscosity.

The problem with toe resistance is that it has two unknowns in the correlation analysis: damping factor (discussed above) and quake. The rule established for the choice of toe quake in the correlation study (as recommended by GRLWEAP manual, *i.e.*, D/120 except where CAPWAP indicated $q_t > 2D/120$) may not always yield consistent and meaningful results.

H.2.1 Apalachicola, Florida (Data Base ID# 1 to 7)

The piles tested were part of the foundation for the Apalachicola River and Bay Bridges. A total of six 24-in (610-mm) prestressed concrete piles are presented. Two of the test piles (ID's# 1 and 3) were part of the River Bridge site and the remaining 4 were located at the Bay Bridge site. The piles were driven to end of driving penetrations ranging from 55 to 105 ft (16.8 to 32.0 m). Although some of these piles had excessive blow counts (greater than 240 blows/ft or 787 blows/m), the piles were included in the data base because overprediction was indicated (underprediction would have been blamed on partial resistance mobilization).

The soil description can generally be described as loose clayey sand or very soft clay overlying a compact clayey sand or sand with the presence of shell. The top soft clay layer existed mostly at the bay sites. The toe soil for the piles was therefore clayey sand or sand with SPT N-values ranging from 30 to 50.

All piles were installed with a Vulcan 020 single acting air hammer to end of driving blow counts ranging from 37 to 63 blows/ft (121 to 207 blows/m), and beginning of restriking blow counts ranging from 96 to 672 blows/ft (315 to 2 204 blows/m).

The standard wave equation and the hammer performance adjusted analysis indicated an overprediction for all piles when compared to the static load test capacity based on Davisson's criterion. The overprediction of three piles were due to high toe damping and for the three other piles were due to both high toe and shaft damping based on the criteria discussed in section H.1. The three piles with high shaft damping were located at the bay sites where significant resistance came from the clay layer above the compact sand.

Comparing ID# 4 and ID# 5, both piles were driven in very similar soils to almost the same pile penetration and with similar transferred energies. The restrike tests for both piles were also done at a comparable time, but the beginning of restrike blow count for ID# 4 and ID# 5 were 96 and 576 blows/ft (315 and 1 889 blows/m), respectively. This blow count difference appears large, even though both blow counts are relatively high and therefore do not necessarily indicate large differences in capacity. After carefully examining the soil data near the pile toe, the only explanation to this large difference in blow count is indicated by the existence of a higher than hydrostatic piezometric pressure near the pile toe of ID# 4. The static load test results based on Davisson's criterion for ID# 4 and ID# 5, were 524 and 812 kips (2 331 and 3 612 kN), respectively, a ratio of 1.6. Corresponding respective correlation toe damping factors were 0.43 and 0.28 s/ft (1.41 and 0.92 s/m). The piezometric pressure apparently affected both the static and dynamic soil behavior but more severely the dynamic one.

The bearing capacity predicted by the standard wave equation analysis ranged between 691 and 1 086 kips (3 075 and 4 833 kN). The hammer performance adjusted bearing capacity ranged between 760 and 1 165 kips (3 382 and 5 184 kN) overpredicting between 5 and 45 percent. To match the bearing capacity from static load test, the toe damping had to be adjusted to between 0.2 and 0.6 s/ft (0.66 and 1.97 s/m). A summary is presented for each pile in table H.1.

H.2.2 Bailey Fork, Tennessee (Data Base ID# 61)

The pile was driven for a bridge abutment crossing the Bailey Fork Creek. It was a 14-in (356-mm) square PSC pile of 45 ft (13.72 m) length and had an end of driving penetration of 26 ft (7.92 m). The pile was driven with a Delmag D19-32 open end diesel hammer to an end of driving blow count of 157 blows/ft (515 blows/m) and beginning of restriking blow count of 226 blows/ft (741 blows/m).

The soil boring generally consisted of approximately 20 ft (6.1 m) of silt and 10 ft (3.05 m) of clayey sand overlying a very dense sand with SPT N-value exceeding 100. Although the driving records indicated that driving was terminated at the clayey sand layer, the pile toe was believed to be terminated in the very dense sand layer, judging from the sudden increase in blow count.

The static load test capacity based on Davisson's criterion was 300 kips (1 335 kN). The bearing capacity predicted from standard wave equation and hammer performance adjusted analysis were 425 and 350 kips (1 891 and 1 558 kN) therefore overpredicting by 42 and 17 percent, respectively. The bearing capacity predicted by wave equation analysis agreed with the Davisson limit load when a toe damping of 0.27 s/ft (0.89 s/m) was used.

H.2.3 Port of Los Angeles, California (Data Base ID# 85)

The pile was driven at the main channel of Los Angeles Harbor with a Delmag D46-02 open end diesel hammer. The pile was a 24-in (610-mm) diameter octagonal PSC with length of 95 ft (29.0 m). The pile was driven to an end of driving penetration of 84.6 ft (25.8 m) with a blow count of 238 blows/ft (781 blows/m). The beginning of restriking blow count was 240 blows/ft (787 blows/m).

Table H.1: Summary of High Toe Damping Cases Based On Restrike Tests													
Location	ID	Pile Type	Penetration ft	Blow Count blows/ft	Capacity kips	WEAP(S) kips	Capacity Ratio (S)	WEAP(A) kips	Capacity Ratio (A)	J (S) s/ft	J (A) s/ft	J Ratio
Apalachicola, FL	# 1	24"PSC	90.6	360	958	1,010	1.05	1,165	1.22	0.15	0.43	2.87
	# 3	24"PSC	55.4	240	714	952	1.33	965	1.35	0.15	0.60	4.00
	# 4	24"PSC	66.3	96	524	691	1.32	760	1.45	0.15	0.43	2.87
	# 5	24"PSC	62.1	576	812	990	1.22	885	1.09	0.15	0.28	1.87
	# 6	24"PSC	104.8	672	808	1,054	1.30	978	1.21	0.15	0.33	2.20
	# 7	24"PSC	103.0	576	976	1,086	1.11	1,025	1.05	0.15	0.22	1.47
Bailey Fork, TN	# 61	14"PSC	26	226	300	425	1.42	350	1.17	0.15	0.27	1.80
Port of LA, CA	# 85	24"PSC-O	84.6	240	1,030	1,200	1.17	1,516	1.47	0.15	0.47	3.13
Average							1.24		1.25			2.53

Notations:

Blow Count	Beginning of restriking blow count
Capacity	Capacity from static load test
WEAP(S)	Standard WEAP capacity
WEAP(A)	WEAP with standard soil parameters but adjusted for measured EMX, FMX
J (S)	Standard toe damping
J (A)	Toe damping after adjustments for hammer performance
J Ratio	J (A)/J (S)
Capacity Ratio (S)	WEAP (S) / capacity from static load test
Capacity Ratio (A)	WEAP (A) / capacity from static load test

1 kip = 4.45kN; 1 blow/ft = 3.28 blows/m; 1 in = 25.4 mm; 1 s/ft = 3.28 s/m; 1 ft = 0.3048 m

The soil description indicated an upper sand layer, a fine grained soil layer and the lower sand layer. The upper sand layer consisted of native soil and fill material. The fine grained soil layer underlying the upper sand layer consisted of high plasticity silt and clay, and also included a layer of sandy clay, sandy silt and sand. Some highly organic soil was also encountered. The lower sand layer consisted of very dense sand and silty sand with the SPT N-value generally exceeding 100.

The static load test capacity based on Davisson criterion was 1 030 kips (4 584 kN). The standard wave equation analysis predicted 1 200 kips or 5 340 kN (17-percent overprediction) capacity and the hammer performance adjusted analysis predicted 1 516 kips (6 746 kN) capacity (47-percent overprediction). A toe damping of 0.47 s/ft (1.54 s/m) was required in the wave equation analysis to match the Davisson limit load.

H.3 HIGH SHAFT DAMPING CASES

Four sites from the data base have been identified with a high shaft damping. All sites seem to be associated with piles driven into cohesive soils, occasionally with low SPT N-value.

H.3.1 St. Mary Cement, Cleveland, Ohio (Data Base ID# 43)

The project consisted of the foundation work for a silo on the bank of Cuyahoga River. The pile was an HP12x53 profile of 166 ft (50.6 m) length. The pile was first driven to an end of driving penetration of 105 ft (32 m). The soil description indicated primarily silt and some loose silty sand for the upper 45 ft (13.7 m). Beneath the 45-ft (13.7-m) layer is silty clay with some occasional gravel and cobble. The SPT N-values of the clay layer ranged from 20 to 30. A stiffer clay layer was indicated at 100 to 110 ft (30.5 to 33.5 m) depth with SPT N-values ranging from 50 to 66.

The pile was installed with a Vulcan 506 single acting air hammer to an end of driving blow count of 52 blows/ft (171 blows/m) and beginning of restriking blow count of 240 blows/ft (787 blows/m).

The static load test capacity based on Davisson criteria was 315 kips (1 402 kN). The bearing capacity predicted by standard wave equation analysis and after hammer performance adjustment were 350 and 345 kips (1 558 and 1 535 kN), an overprediction of 11 and 9 percent, respectively. This overprediction would not have occurred if a shaft damping factor of 0.26 s/ft (0.85 s/m) had been utilized in the analysis.

H.3.2 Omaha, Nebraska (Data Base ID# 17, 19 and 20)

The project was located at the median of interstate I-80. A total of four piles of different types were driven at a spacing of 24 ft (7.3 m). The piles consisted of an HP10x42, a 12-in (305-mm) square PSC, a 14-in (356-mm) square PSC and a 12¾-in (324-mm) diameter closed end pipe pile. The total length of the piles ranged between 65 to 75 ft (19.8 to 22.9 m). The piles were driven to end of driving penetration of 56 to 72 ft (17.1 to 21.9 m).

In our study, the 12-in (305-mm) square PSC (ID#18) was omitted due to the lack of dynamic information caused by pile top damage during restriking of the pile.

The soil description indicated 53 to 61 ft (16.2 to 18.6 m) layer of silty clay (73 to 75 percent silt and 24 to 25 percent clay) overlying a clayey glacial till deposit. All the piles were driven to the glacial till deposit.

The piles were driven with a Delmag D30 open end diesel hammer to an end of driving blow count ranging from 30 to 110 blows/ft (98 to 361 blows/m) and beginning of restriking blow count ranging from 60 to 96 blows/ft (197 to 315 blows/m).

The static load test bearing capacity based on Davisson criterion ranged from 285 and 383 kips (1 268 and 1 704 kN). The static load test indicated plunging failure before the Davisson limit load was achieved. The bearing capacity determined from standard wave equation analysis ranged from 350 and 375 kips (1 558 and 1 669 kN) and from the hammer performance adjusted analysis ranged from 320 and 480 kips (1 424 and 2 136 kN). A higher shaft damping of between 0.28 and 0.35 s/ft (0.92 and 1.15 s/m) were required to match the Davisson limit capacity. The summary of each pile is presented in table H.2 which also demonstrates that high shaft damping was required irrespective of the pile type.

H.3.3 West Baton Rouge, Louisiana (Data Base ID# 28)

The test pile was located at Pier 14 of the railroad overpass structure, a 24-in (610-mm) PSC pile of 103 ft (31.4 m) length and was driven to an end of driving penetration of 84.5 ft (25.8 m).

The soil can be described as a 90 to 95-ft (27.4 to 29.0-m) layer of silty clay to clay with a trace of organic material. Underlying the silty clay layer was a silty sand with SPT N-values varying between 24 to 50.

The pile was driven with a Vulcan 020 single acting air hammer. The end of driving and beginning of restriking blow counts were 20 and 132 blows/ft (66 and 433 blows/m), respectively.

Table H.2: Summary of High Shaft Damping Cases													
Location	ID	Pile Type	Penetration ft	Blow Count blows/ft	Capacity kips	WEAP(S) kips	Capacity Ratio (S)	WEAP(A) kips	Capacity Ratio (A)	J' (S) s/ft	J' (A) s/ft	J' Ratio
St. Mary, OH	# 43	HP12x53	105	240	315	350	1.11	345	1.10	0.20	0.26	1.30
Omaha, NE	# 17	HP10x42	72	96	310	370	1.19	350	1.13	0.20	0.30	1.50
	# 19	14"PSC	56	72	383	375	0.98	480	1.25	0.20	0.35	1.75
	# 20	12¾"CEP	66	60	285	350	1.23	320	1.12	0.20	0.28	1.40
W.B. Rouge, LA	# 28	24"PSC	84.5	132	390	990	2.54	700	1.79	0.20	0.94	4.70
Socastee, SC	# 71	HP14x73	80	96	320	570	1.78	450	1.41	0.20	0.44	2.20
	# 72	24"CEP	80.5	96	620	830	1.34	880	1.42	0.20	0.30	1.50
	# 73	24"PSC	80	400	1,080	1,640	1.52	1,640	1.52	0.20	0.31	1.55
Dawhoo,SC	# 68	24"PSC	80	204	1,060	1,080	1.02	1,480	1.40	0.20	0.44	2.20
	# 69	16"PSC	88	180	610	670	1.10	765	1.25	0.20	0.48	2.40
Average							1.38		1.34			2.05

Notations:

Blow Count	Beginning of restriking blow count
Capacity	Capacity from static load test
WEAP(S)	Standard WEAP capacity
WEAP(A)	WEAP with standard soil parameters but adjusted for measured EMX, FMX
J' (S)	
J' (A)	Shaft damping after adjustments for hammer performance
J' Ratio	J' (A)/J' (S)
Capacity Ratio (S)	WEAP (S) / capacity from static load test
Capacity Ratio (A)	WEAP (A) / capacity from static load test

1 kip = 4.45kN; 1 blow/ft = 3.28 blows/m; 1 in = 25.4 mm; 1 s/ft = 3.28 s/m; 1 ft = 0.3048 m

The static load test capacity, based on Davisson's criterion, was 390 kips (1 736 kN). Again, the pile plunged before the Davisson limit load was achieved. The standard wave equation analysis and hammer performance adjusted analysis resulted in bearing capacities of 990 (254 percent) and 700 (179 percent) kips or 4 406 and 3 115 kN, respectively. A shaft damping was increased to 0.94 s/ft (3.08 s/m) to match the Davisson limit load. This was probably the most non-conservative result encountered in this study.

H.3.4 Socastee, South Carolina (Data Base ID# 71 to 73)

The soil can generally be described as interlayered of sand and highly plastic clay of varying thickness. Three piles which consisted of an HP14x73, a 24-in (610-mm) diameter closed end pipe pile and a 24-in (610-mm) square PSC were tested. All of these piles were 85 ft (25.9 m) length and were driven to an end of driving penetration of approximately 80 ft (24.4 m).

The HP14x73 and pipe piles were driven with a Vulcan 512 single acting air hammer to an end of driving blow count ranging between 14 and 45 blows/ft (46 and 148 blows/m) and the same beginning of restriking blow count for both piles of 96 blows/ft (315 blows/m). The PSC pile was driven with a Vulcan 520 single acting air hammer with the beginning of restriking blow count of 400 blows/ft (1,312 blows/m).

The Davisson load test capacity based ranged between 320 and 1 080 kips (1 424 and 4 806 m). The standard wave equation analysis and the hammer performance adjusted analysis overpredicted the Davisson limit load for all three piles. A shaft damping ranging from 0.30 to 0.44 s/ft (0.98 to 1.44 s/m) was required in the analysis to match the Davisson limit load. The summary results for each pile is presented in table H.2 which also demonstrates that high shaft damping occurred irrespective of pile type.

H.3.5 Dawhoo, South Carolina (Data Base ID# 68 to 70)

Two piles, a 24-in (610-mm) square PSC and a 16-in (406-mm) square PSC were driven with a Vulcan 520 single acting air hammer to an end of driving blow count ranging from 6 to 20 blows/ft (20 to 66 blows/m) and beginning of restriking blow count ranging from 96 to 240 blows/ft (315 to 787 blows/m). The length of the piles were between 80 to 90 ft (24.4 to 27.4 m). The end of driving penetration ranged from 77.5 to 87 ft (23.6 to 26.5 m). The HP14x73 was not included in the data base due to lack of hammer and driving information.

The soil consisted of approximately 21 ft (6.4 m) of medium dense to loose silty fine sand, overlying 16 ft (4.9 m) of soft to firm organic silty clay, very dense sand and stiff to very stiff silty clay and clayey silt. The stiff silty clay is locally known as "Cooper Marl."

The static load test bearing capacity, based on Davisson's criterion, ranged between 610 and 1 060 kips (2 715 and 4 717 kN). The standard wave equation analysis predicted capacities ranged between 670 and 1 080 kips (2 982 and 4 806 kN). The hammer performance adjusted bearing capacity ranged between 765 and 1 480 kips (3 404 and 6 586 kN) (overprediction of 25 to 40 percent). The wave equation analysis would match the Davisson limit load had the shaft damping factors been used ranging from 0.44 and 0.48 s/ft (1.44 and 1.57 s/m). The summary results for each pile are presented in table H.2.

H.4 CONCLUSION

Three sites with a high toe damping cases have been presented. All of these cases indicate displacement pile driven to very dense cohesionless toe soil with high SPT N-value. In addition, these sites are all located near marine environment therefore the soil is believed to be fully saturated. The soil boring for all of these sites indicated the presence of shell. The toe damping factors as high as 0.6 s/ft (1.97 s/m) were calculated.

Five sites with high shaft damping have also been discussed. The soil at all of these sites can be characterized as cohesive soil of silty clay and clayey silt type with high plasticity, at least in one case. Unlike the high toe damping cases, the high shaft damping occurred for a variety of pile types. The highest shaft damping factor found was 0.94 s/ft (3.08 s/m).

REFERENCES

Authier, J. and Fellenius, B. H., 1980. Quake values determined from dynamic measurements. Proceedings of the International Seminar on the Application of Stress-Wave Theory on Piles, Stockholm, pp. 197-215.

ASTM, 1986. Standard test method for stress wave energy measurement for dynamic penetrometer testing systems. D 4633-86, ASTM Philadelphia.

Batanov, V. A., 1967. (See Novak, 1977).

Beringen, F. L., and van Koten, H., 1984. Skin friction data in sands from dynamic load tests. Proceedings of the Second International Conference on the Application of Stress-Wave Theory on Piles, Stockholm, pp. 170-177.

Bosscher, P. J. and Showers, D. R., 1987. Effect of soil type on standard penetration test input energy. ASCE Journal of Geotechnical Engineering, Vol. 113, No. 4, pp. 385-389.

Briaud, J. L. and Garland, E., 1984. Influence of loading rate on axially loaded piles in clay. Research Report for the American Petroleum Institute, Civil Engineering Department, Texas A&M University, College Station, TX.

Briaud, J. L. and Garland E., 1985. Loading rate method for pile response in clay. ASCE Journal of Geotechnical Engineering, Vol. III, No. 3, pp. 319-355.

Briaud, J. L. and Tucker, L. M., 1988. Measured and predicted axial response of 98 piles. ASCE Journal of Geotechnical Engineering, Vol 114, No. 9, pp. 984-1001.

Brown, R. E., 1978. Drill rod influence on standard penetration test. Technical Note, ASCE Journal of Geotechnical Engineering Division, Vol. 103, GT11, pp. 1332-1336.

Camp, W. M. and Hussein, M., 1993. The effect of overburden on pile capacity in a calcareous marl. Deep Foundation Institute, 18th Annual Members Conference.

Campanella, R. G., Robertson, P. K. and Gillespie, D., 1986. Seismic cone penetration test. Proceedings of In Situ Specialty Conference, ASCE, Virginia Tech, pp. 116-130.

Corte, J. F. and Lepert, P., 1986. Lateral resistance during driving and dynamic pile testing. Proceedings of the Third International Conference on Numerical Methods in Offshore Piling, Nantes, France, pp. 19-33.

Coyle, H. M., Bartoskewitz, R. E. and Korb, K. W., 1972. Soil resistance parameters for wave equation analysis. Journal of Materials, JMLSA, Vol. 7, No. 4, pp. 486-495.

Coyle, H. M. and Gibson, G. C., 1970. Empirical damping constants for sands and clays. ASCE Journal of the Soil Mechanics and Foundations Division, Paper No. 7296, SM3.

Preceding page blank

d'Alembert, 1747. (See Timoshenko, 1951).

Dayal, U., and Allen, J. H., 1975. The effect of penetration rate on the strength of remolded clay and sand samples. Canadian Geotechnical Journal, Vol. 12 No. 3, pp. 336-348.

Ellstein, R. A., 1988. Dynamic cone, wave equation and microcomputers: The Mexican experience. Penetration Testing, ISOPT-1, De Ruiter editor, Balkema, Rotterdam, pp. 341-345.

Eriksson, H., 1990. Static behavior of driven piles estimated from stress wave measurements on dynamic probes. Presented at the 1990 PDA Users Day, Gothenburg, Sweden.

Fellenius, B. H., 1980. The analysis of results from routine pile load tests. Ground Engineering, Foundation Publications Ltd., Vol. 13, No. 6, pp. 19-31.

Fellenius, B. H., Riker, R. E., O'Brien, A. J., and Tracy, G. R., 1989. Dynamic and static testing in soil exhibiting set-up. ASCE Journal of Geotechnical Engineering, Vol. 115, No. 7, pp. 984-1001.

Forehand, P. W. and Reese, J. L., Jr., 1964. Prediction of pile capacity by the wave equation. ASCE Journal of the Soil Mechanics and Foundations Division, Paper No. 3820, SM 2.

Gazetas, G., 1991. Foundation vibrations. Foundation Engineering Handbook, 2nd edition, H-Y Fang editor, Van Nostrand Reinhold, New York, pp. 553-593.

Goble, G. G. and Rausche, F., 1976. Wave equation analysis of pile driving - WEAP program. Vol. 1 to 4, FHWA IP-76-14.1 through FHWA IP-76-14.4.

Goble, G. G. and Rausche, F., 1980. Pile driveability predictions by CAPWAP. Institution of Civil Engineers, Numerical Methods in Offshore Piling, ICE, London, pp. 29-36.

Goble Rausche Likins and Associates, Inc., 1995 CAPWAP Manual. 4535 Emery Industrial Parkway, Cleveland, Ohio.

Goble Rausche Likins and Associates, Inc., 1995 GRLWEAP Manual. 4535 Emery Industrial Parkway, Cleveland, Ohio.

Hannigan, P. J., 1984. Large quakes developed during driving of low displacement piles. Proceedings of the Second International Conference on the Application of Stress-Wave Theory on Piles, Stockholm, pp. 118-125.

Heerema, E. P., 1979. Relationships between wall friction, displacement velocity and horizontal stress in clay and in sand, for pile driveability analysis. Ground Engineering.

Heerema, E. P., 1981. Dynamic point resistance in sand and in clay, for pile driveability analysis. Ground Engineering.

Hirsch, T. J., Jr., Carr, L. and Lowery, L. L., Jr., 1976. Pile driving analysis wave equation user's manual - TTI program. Vol. 1 to 4, FHWA IP-76-13.1 through IP-76-13.4.

Holeyman, A., 1988. Modelling of dynamic behavior at the pile base. Proceedings of the Third International Conference on the Application of Stress-Wave Theory to Piles, Ottawa, Canada, pp. 174-185.

Kovacs, W. D. and Salomone, L. A., 1982. SPT hammer energy measurement. ASCE Journal of the Geotechnical Engineering Division, Vol. 108, No. GT4, pp. 599-620.

Kraft, L. M., Ray, R. P., and Kagawa, T., 1981. Theoretical t-z curves. ASCE Journal of the Geotechnical Engineering Division, Vol. 107, No. GT11, pp. 1543-1561.

Lee, S. L., Chow, Y. K., Karunaratne, G. P., and Wong, K. Y., 1988. Rational wave equation model for pile-driving analysis. ASCE Journal of Geotechnical Engineering, Vol. 114, No. 3, pp. 306-325.

Liang, R. Y. and Hussein, A. I., 1992. Dynamic cone penetrometer test, part I, theory; part II, theory verification and application. University of Akron.

Liang, R. Y. and Sheng, Y., 1992. Theoretical interpretation of Smith model parameters. Proceeding of the Fourth International Conference on the Application of Stress-Wave Theory to Piles, The Hague, The Netherlands, pp. 111-116.

Likins, G. E., 1983. Pile installation difficulties in soils with large quakes. ASCE Conference Proceedings, Dynamic measurement of piles and piers, Philadelphia, Pennsylvania.

Litkouhi, S. and Poskitt, T. J., 1980. Damping constants for pile driveability calculations. Geotechnique 30, No. 1, pp. 77-86.

Matsumoto, K. and Matsubara, M., 1982. Effects of rod diameter in the standard penetration test. Proceedings of Second European Symposium on Penetration Testing, Amsterdam, pp. 107-112.

McLean, F. G., Franklin, A. G. and Dahlstrand, T. K., 1975. Influence of mechanical variables on the SPT. Proceedings ASCE Specialty Conference, Raleigh NC, Vol 1, pp. 287-318.

Meyerhof, G. G., 1976. Bearing capacity and settlement of pile foundations. ASCE, Journal of the Geotechnical Engineering Division, pp. 195-228.

Meynard, A. and Corte, J. F., 1984. Experimental study of lateral resistance during driving. Proceedings of the Second International Conference on the Application of Stress-Wave Theory on Piles, Stockholm, pp. 135-142.

Middendorp, P. and van Brederode, P. J., 1984. Skin friction models for sand from static and dynamic laboratory load test. Proceedings of the Second International Conference on the Application of Stress-Wave Theory on Piles, Stockholm, pp. 210-220.

Mitwally, H. and Novak, M., 1988. Pile driving analysis using shaft models and FEM. Proceedings of the Third International Conference on the Application of Stress-Wave Theory on Piles, Ottawa, Canada, pp. 455-466.

Mohan, D., Aggarwal, V. S. and Tolia, D. S., 1970. The correlation of cone size in the dynamic cone penetration test with the standard penetration test. Geotechnique 20, No. 3, pp. 315-319.

Morgano, C. M. and Liang, R., 1992. Energy transfer in SPT - rod length effect. Proceedings of the Fourth International Conference on the Application of Stress-Wave Theory to Piles, The Hague, The Netherlands, pp. 121-127.

Mure, J. N., Kightley, M. L., Gravare, C.-J. and Hermansson, I., 1983. CAPWAP - an economic and comprehensive alternative to traditional methods of load testing of piles. Piling and ground treatment for foundations, Thomas Telford, London, England, pp. 167-174.

Nguyen, T. T., Berggren, B. and Hansbo, S., 1988. A new soil model for pile driving and driveability analysis. Proceedings of the Third International Conference on the Application of Stress-Wave Theory to Piles, Ottawa, Canada, pp. 353-367.

Novak, M., 1977. Vertical vibration of floating piles. ASCE Journal of the Engineering Mechanics Division, Vol. 103, No. EM1, pp. 153-168.

Novak, M., Nogami, T. and Aboul-Ella, F., 1978. Dynamic soil reactions for plane strain case. ASCE Journal of Engineering Mechanics Division, Vol. 104, No. EM4, pp. 953-959.

Peck, G. M., 1962. Bearing theories related to model test on remolded clay. M. Eng. thesis, McGill University, Montreal, Canada.

Preim, M. J., March, R. and Hussein, M., 1989. Bearing capacity of piles in soils with time dependent characteristics. International Conference on Piling and Deep Foundations, London, pp. 363-370.

Randolph, M. F. and Simons, H. A., 1986. An improved soil model for one-dimensional pile driving analysis. Proceedings of the Third International Conference on Numerical Methods in Offshore Piling, Nantes, France, pp. 3-17.

Rausche, F., Moses, F. and Goble, G. G., 1972. Soil resistance predictions from pile dynamics. ASCE Journal of the Soil Mechanics and Foundations Division, Vol. 98, No. SM9, Proc. Paper 9220: pp. 917-937.

Rausche, F., 1977. Determination of wave equation constants from CAPWAP. Presented at seminar and workshop, University of Colorado, 1977.

Robertson, P. K., Campanella, R. G., Davies, M. P. and Sy, A., 1989. An evaluation of pile design in Fraser river delta using in-situ tests. Foundation Engineering: Current Principles and Practice, ASCE Proceedings of Geotechnical Engineering Division, Evanston, Illinois, pp. 92-105.

Sanglerat, G., 1972. The penetrometer and soil exploration. Elsevier Publishing Co., Amsterdam London, New York.

Schmertmann, J. H., 1978. Use the SPT to measure dynamic soil properties?-yes, but...! Dynamic Geotechnical Testing, ASTM STP 654, American Society for Testing and Materials, pp. 341-355.

Schmertmann, J. H., 1979. Statics of SPT. ASCE Journal of Geotechnical Engineering Division, Vol. 105, No. GT5, pp. 655-670.

Schmertmann, J. H. and Palacios, A., 1979. Energy dynamics of SPT. ASCE Journal of the Geotechnical Engineering Division, Vol. 105, No. GT8, pp. 909-926.

Simons, H. A. and Randolph, M. F,. 1985. A new approach to one-dimensional pile during analysis. Proceedings of the Fifth International Conference on Numerical Methods in Geomechanics, Nagoya, Japan, pp. 1457-1464.

Skempton, A. W., 1986. Standard penetration test procedures and the effects in sands of overburden pressure, relative density, particle size, ageing and overconsolidation. Geotechnique 36, No. 3, pp. 425-447.

Skov, R. and Denver, H., 1988. Time-dependence of bearing capacity of piles. Proceedings of the Third International Conference on Application of Stress-Wave Theory on Piles, Ottawa, Canada, pp. 879-888.

Smith, E. A. L., 1960. Pile-driving analysis by the wave equation. ASCE Journal of the Soil Mechanics and Foundations Division, 86(4), pp. 35-61.

Soares, M., de Mello, J. and de Matos, S., 1984. Pile driveability studies, Pile driving measurements. Proceedings of the Second International Conference on the Application of Stress-Wave Theory on Piles, Stockholm, pp. 64-71.

St. Venant, 1867. (see Timoshenko, 1951).

Tschebotarioff, G. P., 1973. Foundations, retaining and earth structures. 2nd edition, McGraw-Hill Book Company, pp. 233.

Timoshenko, S. and Goodier, J. N., 1951. Theory of Elasticity. McGraw-Hill Book Company, Inc., New York.

Thompson, C. D., 1980. Discussion of quake values determined from dynamic measurements. Proceedings of the International Seminar on the Application of Stress-Wave Theory on Piles, Stockholm, pp. 319-322.

Wrench, B. P. and Nowatzki, E. A., 1986. A relationship between deformation modulus and SPT N for gravels. Proceedings of In Situ '86 Specialty Conference, ASCE, Virginia Tech, pp. 1163-1177.

Wu, A. K. H., Kuhlemeyer, R.L. and To, C. W. S., 1989. Validity of Smith model in pile driving analysis. ASCE Journal of Geotechnical Engineering, Vol. 115, No. 9.

van Koten, H., Sandbergen, R. and Starink, T. W., 1988. Model tests on static and dynamic bearing capacity of piles. Proceedings of the Third International Conference on the Application of Stress-Wave Theory on Piles, Ottawa, Canada, pp. 368-376.

Vesic, A. S., 1967. A study of bearing capacity of deep foundations. Final Report, Project B-189, Department of Civil Engineering, Georgia Institute of Technology, Atlanta, Georgia.

☆U.S. GOVERNMENT PRINTING OFFICE:1997-418-103/75309

U.S. DEPARTMENT OF COMMERCE
Technology Administration
National Technical Information Service
Springfield, VA 22161 (703) 487-4650